



**DISCRETE AND CONTINUOUS MODELS  
AND APPLIED COMPUTATIONAL  
SCIENCE**

**Volume 27 Number 4 (2019)**

**Founded in 1993**

**Founder: PEOPLES' FRIENDSHIP UNIVERSITY OF RUSSIA**

**DOI: 10.22363/2658-4670-2019-27-4**

Edition registered by the Federal Service for Supervision of Communications,  
Information Technology and Mass Media  
**Registration Certificate: ПИ № ФС 77-76317, 19.07.2019**

ISSN 2658-7149 (online); 2658-4670 (print)

4 issues per year.

Language: English.

Publisher: Peoples' Friendship University of Russia (RUDN University).

Indexed in Ulrich's Periodicals Directory (<http://www.ulrichsweb.com>),

in Russian Science Citation Index (<https://elibrary.ru>), EBSCOhost

(<https://www.elsevier.com>), CyberLeninka (<https://cyberleninka.ru>).

### **Aim and Scope**

Discrete and Continuous Models and Applied Computational Science arose in 2019 as a continuation of RUDN Journal of Mathematics, Information Sciences and Physics. RUDN Journal of Mathematics, Information Sciences and Physics arose in 2006 as a merger and continuation of the series "Physics", "Mathematics", "Applied Mathematics and Computer Science", "Applied Mathematics and Computer Mathematics".

Discussed issues affecting modern problems of physics, mathematics, queuing theory, the Teletraffic theory, computer science, software and databases development.

It's an international journal regarding both the editorial board and contributing authors as well as research and topics of publications. Its authors are leading researchers possessing PhD and PhDr degrees, and PhD and MA students from Russia and abroad. Articles are indexed in the Russian and foreign databases. Each paper is reviewed by at least two reviewers, the composition of which includes PhDs, are well known in their circles. Author's part of the magazine includes both young scientists, graduate students and talented students, who publish their works, and famous giants of world science.

The Journal is published in accordance with the policies of COPE (Committee on Publication Ethics). The editors are open to thematic issue initiatives with guest editors. Further information regarding notes for contributors, subscription, and back volumes is available at <http://journals.rudn.ru/miph>.

E-mail: [miphj@rudn.ru](mailto:miphj@rudn.ru), [dcm@sci.pfu.edu.ru](mailto:dcm@sci.pfu.edu.ru).

# EDITORIAL BOARD

## Editor-in-Chief

**Yury P. Rybakov** — Doctor of Physical and Mathematical Sciences, professor, Honored Scientist of Russia, professor of the Institute of Physical Research & Technologies, Peoples' Friendship University of Russia (RUDN University), Russian Federation, rybakov-yup@rudn.ru

## Vice Editor-in-Chief

**Leonid A. Sevastianov** — Doctor of Physical and Mathematical Sciences, professor, professor of the Department of Applied Probability and Informatics, Peoples' Friendship University of Russia (RUDN University), Russian Federation, sevastianov-la@rudn.ru

## Members of the editorial board

**Yu. V. Gaidamaka** (Russian Federation) — Doctor of Physical and Mathematical Sciences, associate professor of the Department of Applied Probability and Informatics of Peoples' Friendship University of Russia (RUDN University)

**V. I. Il'gisonis** (Russian Federation) — Doctor of Physical and Mathematical Sciences, professor, Head of the Institute of Physical Research & Technologies of Peoples' Friendship University of Russia (RUDN University), Head of the direction of scientific and technical research and development of the State Atomic Energy Corporation ROSATOM

**K. E. Samouylov** (Russian Federation) — Doctor of Engineering Sciences, professor, Head of Department of Applied Probability and Informatics of Peoples' Friendship University of Russia (RUDN University)

**Mikhal Hnatich** (Slovakia) — DrSc., professor of Pavol Jozef Safarik University in Košice

**Datta Gupta Subhashish** (India) — PhD in Physics and Mathematics, professor of Hyderabad University

**Martikainen, Olli Erkki** (Finland) — PhD in Engineering, member of the Research Institute of the Finnish Economy (ETLA, Helsinki)

**M. V. Medvedev** (USA) — Doctor of Physical and Mathematical Sciences, professor of the Kansas University

**Raphael Orlando Ramírez Inostroza** (Spain) — PhD professor of Rovira i Virgili University (Universitat Rovira i Virgili), Spain

**Bijan Saha** (Bangladesh) — Doctor of Physical and Mathematical Sciences, leading researcher in Laboratory of Information Technologies of the Joint Institute for Nuclear Research (Dubna, Russian Federation)

**Ochbadrah Chuluunbaatar** (Mongolia) — Doctor of Physical and Mathematical Sciences, leading researcher in the Institute of Mathematics, State University of Mongolia, Head of the Department in Laboratory of Information Technologies of the Joint Institute for Nuclear Research (Dubna, Russian Federation)

---

Computer Design: *A. V. Korolkova*

**Address of editorial board:**

Ordzhonikidze St., 3, Moscow, Russia, 115419  
Tel. +7 (495) 955-07-16, e-mail: publishing@rudn.ru

**Editorial office:**

Tel. +7 (495) 952-02-50, mipjh@rudn.ru, dcm@sci.pfu.edu.ru  
site: <http://journals.rudn.ru/miph>

---

Paper size 70×100/16. Offset paper. Offset printing. Typeface "Computer Modern".  
Conventional printed sheet 7,10. Printing run 500 copies. Open price. The order 1846.

PEOPLES' FRIENDSHIP UNIVERSITY OF RUSSIA

6 Miklukho-Maklaya St., 117198 Moscow, Russia

**Printed at RUDN Publishing House:**

3 Ordzhonikidze St., 115419 Moscow, Russia,

Ph. +7 (495) 952-04-41; e-mail: publishing@rudn.ru



# Contents

## Computer Science and Computer Engineering

- Migran N. Gevorkyan, Anastasia V. Demidova, Tatiana S. Demidova, Anton A. Sobolev**, Review and comparative analysis of machine learning libraries for machine learning . . . . . 305
- Vasilii S. Duzhin**, Investigation of insertion tableau evolution in the Robinson–Schensted–Knuth correspondence . . . . . 316

## Mathematical modeling

- Dmitriy V. Divakov, Alexandre A. Egorov, Konstantin P. Lovetskiy, Leonid A. Sevastianov, Andrey S. Drevitskiy**, Leaky waves in planar dielectric waveguide . . . . . 325
- Eugeny Yu. Shchetinin**, Vine copulas structures modeling on Russian stock market . . . . . 343

## Mathematical models in Physics

- Andrey A. Novitskiy, Denis V. Chuprov, Vladislav A. Kuznetsov, Eugeny A. Shevtsov**, The features of the characteristic electromagnetic plasma bunches oscillations in the long magnetic mirror . . . . . 355
- Lê Anh Nhật, Konstantin P. Lovetskiy, Leonid A. Sevastianov, Dmitry S. Kulyabov**, Numerical modeling of stationary pseudospin waves on a graphene monoatomic films . . . . . 365
- Vladimir S. Melezhik**, Efficient computational scheme for ion dynamics in RF-field of Paul trap . . . . . 378



# Computer Science and Computer Engineering

*Research article*

UDC 519.21;51-76

DOI: 10.22363/2658-4670-2019-27-4-305-315

## Review and comparative analysis of machine learning libraries for machine learning

Migran N. Gevorkyan, Anastasia V. Demidova,  
Tatiana S. Demidova, Anton A. Sobolev

*Department of Applied Probability and Informatics  
Peoples' Friendship University of Russia  
6, Miklukho-Maklaya St., Moscow 117198, Russian Federation*

(received: December 15, 2019; accepted: December 30, 2019)

The article is an overview. We carry out the comparison of actual machine learning libraries that can be used the neural networks development. The first part of the article gives a brief description of TensorFlow, PyTorch, Theano, Keras, SciKit Learn libraries, SciPy library stack. An overview of the scope of these libraries and the main technical characteristics, such as performance, supported programming languages, the current state of development is given. In the second part of the article, a comparison of five libraries is carried out on the example of a multilayer perceptron, which is applied to the problem of handwritten digits recognizing. This problem is well known and well suited for testing different types of neural networks. The study time is compared depending on the number of epochs and the accuracy of the classifier. The results of the comparison are presented in the form of graphs of training time and accuracy depending on the number of epochs and in tabular form.

**Key words and phrases:** machine learning, neural networks, MNIST, TensorFlow, PyTorch

## 1. Introduction

Due to the vast development of machine learning and data science, it is not possible to review the diversity of available software solutions. In this section we will consider only the most popular libraries and frameworks for neural networks development and machine learning.

The most common language for building neural networks at the moment is the Python language [1]. There is a number of reasons why this language has occupied this domain.

© Gevorkyan M. N., Demidova A. V., Demidova T. S., Sobolev A. A., 2019



This work is licensed under a Creative Commons Attribution 4.0 International License

<http://creativecommons.org/licenses/by/4.0/>

- Python is easy-to-learn language actively used in the field of school and university education. Because of this, it has gained popularity not only in industrial programming, but also among professionals who use programming as a research tool.
- The standard cpython interpreter makes it easy to create bindings for C-function calls, allowing Python to be used as a convenient interface for low-level libraries.
- The community has created a wide range of tools for interactive Python code execution and data visualization (e.g. [2]–[4]). Especially it is useful for scientific research, where almost always there is no original clear algorithm of solutions and it is necessary to conduct a scientific search.

A significant disadvantage of Python is its low performance, which can be overcome by writing critical parts of software in a compiled language (it is usually C or C++) or by using cython [5] translator.

Many machine learning libraries are also written in two or more languages. The part of software, which handles main part of computations, is usually implemented in C or C++ (the *core* part or *backend*). Pure Python is used for bindings to organize a convenient and easy to use interface (*interface part* or *frontend*). So, if a library is implemented in pure Python, then in most cases:

- It is an add-on to another, lower-level library and provides a more user-friendly and easy-to-learn interface;
- It is designed for educational purposes or for prototyping.

Note also that all the libraries in this review are free open source software. Also note that Python 2 support will be discontinued from the beginning of 2020 for vast majority of python libs.

## 2. Overview of machine learning (ML) libraries

From all reviewed libraries, only TensorFlow and PyTorch directly compete with each other. Other libraries complement each other's functionality and specialize in their own area.

### 2.1. Scientific Python (SciPy)

Scientific Python libraries set is not directly related to machine learning, but many machine learning libraries rely on Scientific Python components in their work. Let us briefly describe the main components included in this set.

- NumPy [6] is the library which implements high performance arrays and tools for them. The computational core is written in C (52% of code base) with the interface part in Python (48% of code base). Linear algebra functions heavily rely on LAPACK library. NumPy implements variety of linear algebra methods for working with vectors, matrices and tensors (multidimensional arrays in this case). It also supports parallel computing by utilizing vector capabilities of modern CPUs.
- SciPy [7] is the library that implements many mathematical methods, such as algebraic equations and differential equations solvers, polynomial

interpolation, various optimization methods, etc. For a number of methods the Fortran (about 23% of the total code base) and C (20% of the code base) libraries are used.

- Pandas [8] is the library designed to work with time series and table data (DataFrame data structure). It is written almost entirely in pure Python using NumPy arrays and is often used in machine learning to organize training and test samples.

In addition to these three main libraries, the scientific Python stack also includes Matplotlib [3] for data visualization and plotting, and a set of interactive shells, such as iPython and Jupyter [2].

## 2.2. TensorFlow

TensorFlow [9], [10] is an open source library used primarily for deep machine learning. It was originally developed on by Google's divisions, but in 2015 it was released as free open source software under the Apache License 2.0. The current stable version is 2.1.0.

The computational core is written in C++ (60% of all code) using CUDA technology, which allows one to utilize graphics cards in calculations. The interface part is implemented in Python (30% of all code base). There are also unofficial bindings for other languages, but only C++ and Python interfaces are officially supported.

The library is based on the principle of *data flows* (dataflow), according to which the program is organized in the form of computational blocks associated with each other in the form of a directed graph which is called *computational graph*. Data is processed by passing from one block to another.

Such application architecture makes it easy to use parallel calculations on both multi-core CPUs and distributed cluster systems. In addition, it is well suited for building neural networks in which each neuron is presented by an independent component.

In addition to the computational graph, TensorFlow uses a data structure called *tensor*. It is similar to the tensor from differential geometry in the sense that it is a multidimensional array.

## 2.3. PyTorch

The PyTorch [11] library was created on the basis of Torch [12]. The original Torch library was developed in C and used Lua as the interface. With the growth of Python popularity in machine learning, Torch has been rewritten in C++11/CUDA (60% code) and Python (32% code). Initial development was conducted in the company of Facebook, but currently PyTorch is an OpenSource library, distributed under a BSD-like license. The current version is 1.3.1.

PyTorch, as well as TensorFlow, is built on the basis of dataflow concept. The main difference from TensorFlow is that in TensorFlow computational graph is static, then in PyTorch the graph is dynamic. This means that one can modify the graph on the fly, adding or removing nodes as needed. In TensorFlow, the entire graph must be specified before the model run.

The developers of PyTorch emphasize that Python is tightly integrated into the library (library is more pythonic). This makes it easier to use than

TensorFlow, as the user does not have to dive into low-level parts written in C++.

It is worth noting, however, that TensorFlow surpasses PyTorch in popularity, as it appeared earlier and is used in many educational courses on machine learning.

## 2.4. Theano

Theano [13] library is a Python interface for the optimizing compiler. It allows user to specify functions and after that translates them to C++. Then Theano compiles C++ code to run it on the CPU (using g++ for compilation), or on the graphics accelerator (using nvcc to utilize CUDA). In addition, automatic differentiation algorithms are built into the library.

After optimization and compilation, the functions become available as regular python functions, but have high performance. Vector, matrix, and tensor operations are supported and efficiently parallelized on available hardware (multi-core processor or graphics accelerator).

With support for multidimensional array operations and automatic differentiation, Theano is widely used as a backend for building neural networks. In particular, it can be used by the Keras library.

Theano is written almost entirely in Python, but requires NumPy, SciPy, pyCUDA and BLAS, as well as g++ or NVIDIA CUDA compilers (recommended for optimal performance).

Development of the library was suspended in 2017, but resumed in 2018. The current version is 1.0.4.

## 2.5. Keras

The Keras [14] library provides a high-level programming interface for building neural networks. It can work on top of TensorFlow, Microsoft Cognitive Toolkit (CNTK) [15] or Theano [13]. The library is written entirely in Python and is distributed under the MIT license. Current version 2.3.1

The library is based on the following principles: ease of use, modularity, extensibility.

The modularity principle allows you to separately describe the neural layers, optimizers, activator functions, etc, and then combine them into a single model. The model is fully described in Python. The created model can be saved to disk for further use and distribution.

## 2.6. SciKit Learn

SciKit Learn [16] is the library for data processing. It implements various methods of classification, regression analysis, clustering and other algorithms related to classical machine learning. It is written almost entirely in Python (98% of all code base), but uses NumPy and SciPy for algorithms implementation. Despite the fact that number of current version is 0.21.1, the project is very stable, as it has been developing since 2007.

SciKit Learn is suitable for traditional machine learning and data preprocessing tasks. This library does not support the concept of dataflow and

does not allow one to create his own models. The absence of a computational graph does not allow flexible scale of models for multi-core processors and graphics accelerators and forces to limit the degree of parallelism that is implemented in NumPy.

### 3. Comparative analysis of machine learning libraries

#### 3.1. Description and architecture of neural network

For the comparative analysis of deep machine learning libraries, we choose the problem of handwritten digit recognition from the MNIST database and the neural network [17] to solve it.

The MNIST database is contained in a CSV file, where comma-separated digits are written. In a CSV file, the first value is a marker that represents the corresponding digit. Next value is the size of the digit image in pixels, consisting of 784 values and having a dimension of square  $28 \times 28$ .

The training file consists of 60 thousand copies, and the test file of 10 thousand copies. To solve the problem we choose the MLP (multilayer perceptron) architecture. Perceptron was one of the first models of neural networks, which was supposed to simulate the neural processes in human mind. This model was proposed by Frank Rosenblatt in 1957 and first implemented in 1960 [18]. A multilayer perceptron according to Rosenblatt differs from a single layer in that it contains additional hidden layers.

The neural network (Figure 1) consists of an input layer, two hidden layers, and one output layer. The input layer contains 784 neurons, the hidden layers contain 256 neurons, and the output layer 10, according to the number of features. The activation function in hidden layers is ReLU, which has the form  $f(x) = \max(0, x)$  [19]. Stochastic gradient descent (SGD) [20] is used as the optimization algorithm.

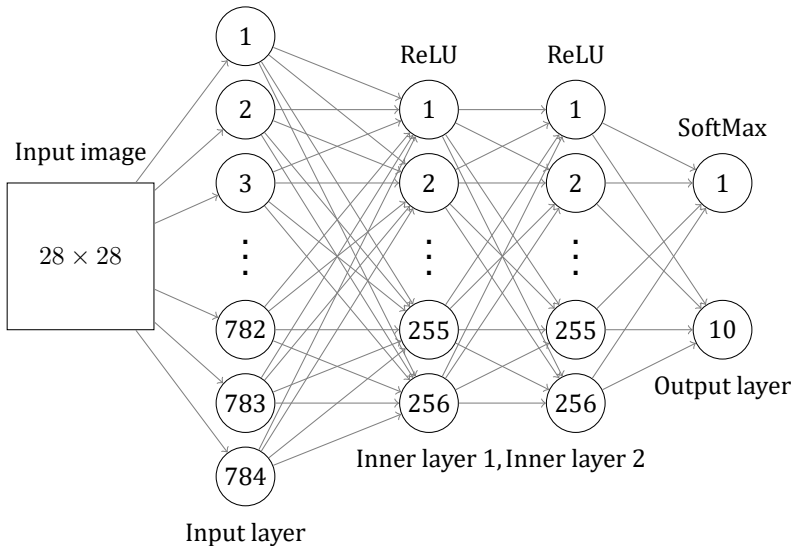


Figure 1. A multilayer perceptron for the recognition of handwritten digits

### 3.2. Software implementation of a neural network using various libraries

With each library from the overview above, we built perceptron models. Each neural network was trained, and training time and accuracy were measured for a different number of training eras. We used these measurements for comparative analysis of libraries. The constructed graphs describe the dependence of learning time and accuracy on the number of eras (Figures 2–6).

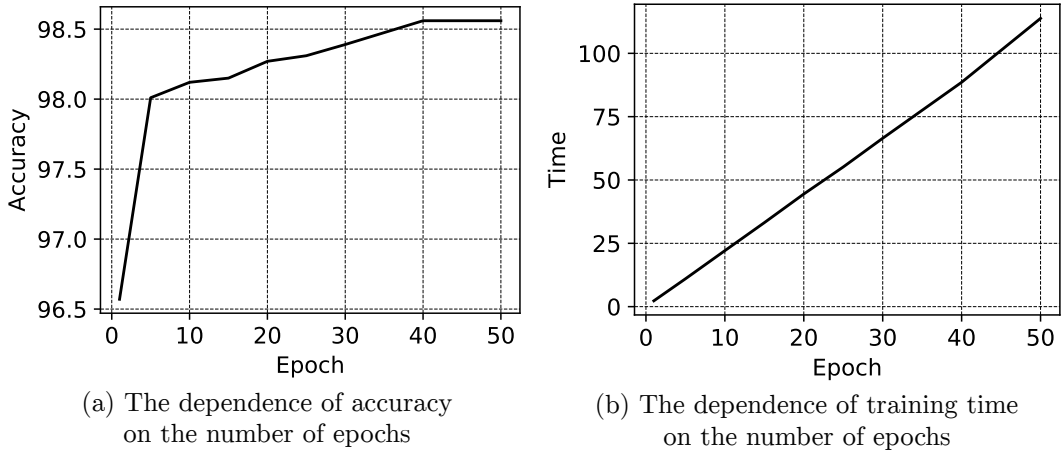


Figure 2. Results of a neural network built with the help of the Keras library

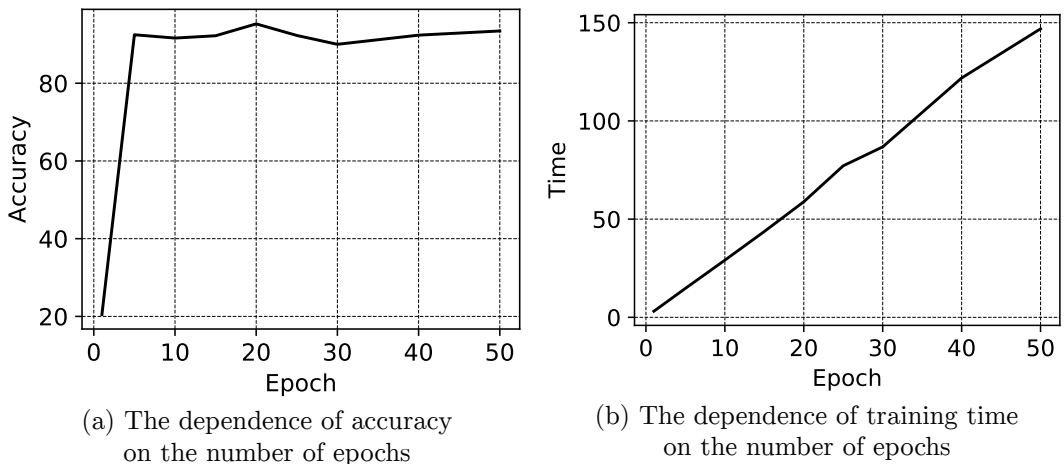
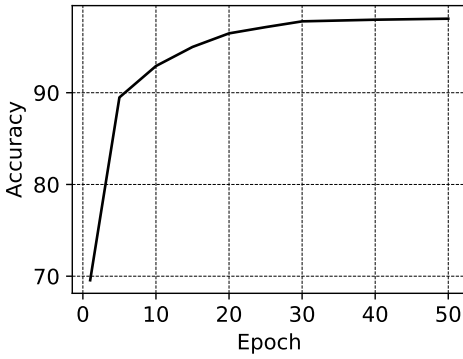


Figure 3. Results of a neural network built with the help of the SciKit Learn library

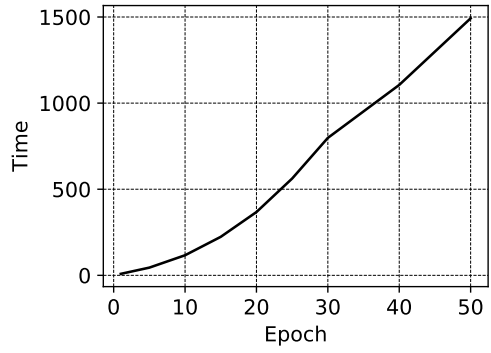
The first plot shows the dependence of time on the number of epochs. The second plot shows the dependence of accuracy on the number of epochs.

Below is the summary table of the results of neural network training at 50 epochs for different libraries (see Table 1).

On the diagram (Figure 7) the time and accuracy values are shown for the considered libraries. All values are normalized.

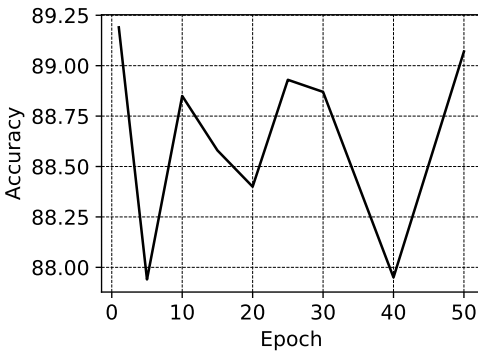


(a) The dependence of accuracy on the number of epochs

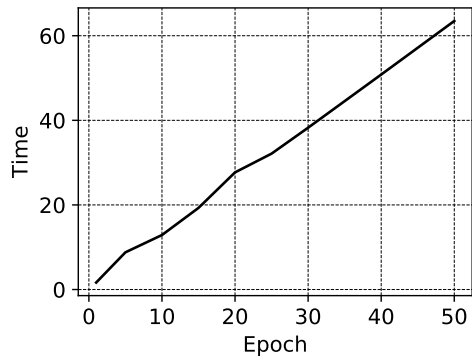


(b) The dependence of training time on the number of epochs

Figure 4. Results of a neural network built with the help of the PyTorch library

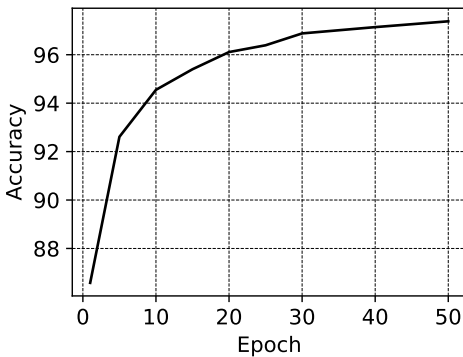


(a) The dependence of accuracy on the number of epochs

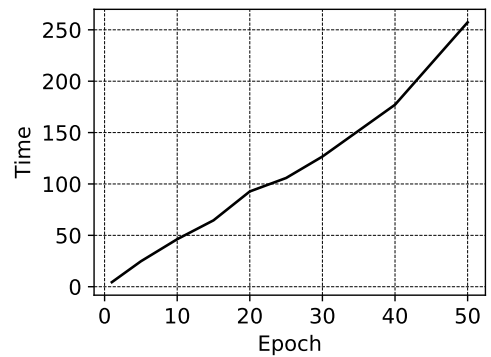


(b) The dependence of training time on the number of epochs

Figure 5. Results of a neural network built with the help of the TensorFlow library



(a) The dependence of accuracy on the number of epochs



(b) The dependence of training time on the number of epochs

Figure 6. Results of a neural network built with the help of the Theano library

Table 1

Results of comparative analysis of machine learning libraries

Library	Accuracy, %	Time, sec.
MLPClassifier	93.45	146.90
Keras	98.56	113.80
TensorFlow	89.07	63.48
Theano	97.38	257.29
PyTorch	98.07	1492.29

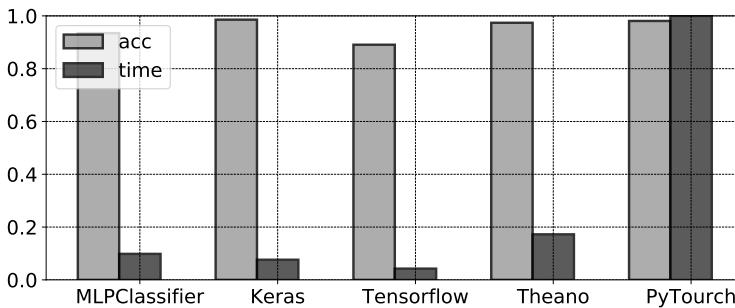


Figure 7. The time and accuracy values

In the PyTorch library, the learning time increases faster than in all other libraries with the growth of epochs, which time is approximately the same. The learning time of TensorFlow, Scikit-learn and Keras libraries varies from 1 to 3 seconds per epoch. While this indicator in PyTorch exceeds 8 seconds, which is several times higher than the training time of other libraries.

The accuracy of the TensorFlow library does not exceed 0.9, which is low compared to other libraries. Scikit-learn also showed a low accuracy result. The PyTorch library shows a good accuracy result only with a large number of epochs, but with the growth of the number of epochs, the learning time increases greatly. The minimum accuracy was 98.07. The Keras and Theano libraries are the most accurate and their accuracy is kept at 0.98.

## 4. Conclusion

Based on the comparison of different libraries, a number of conclusions can be drawn. Almost all libraries except PyTorch show approximately the same learning time. In the case of PyTorch, the longer learning time can be explained by the support of a dynamic computational graph, which apparently imposes additional computational costs. In turn, the TensorFlow library showed an average accuracy result, behind PyTorch and Theano.

## Acknowledgments

The publication was prepared with the support of the “RUDN University Program 5-100”.

## References

- [1] G. Van Rossum and F. L. Drake Jr, *Python tutorial*. Centrum voor Wiskunde en Informatica Amsterdam, The Netherlands, 1995.
- [2] T. Kluyver *et al.*, “Jupyter Notebooks — a publishing format for reproducible computational workflows,” in *Positioning and Power in Academic Publishing: Players, Agents and Agendas*, F. Loizides and B. Schmidt, Eds., IOS Press, 2016, pp. 87–90. DOI: 10.3233/978-1-61499-649-1-87.
- [3] J. D. Hunter, “Matplotlib: A 2D graphics environment,” *Computing in Science & Engineering*, vol. 9, no. 3, pp. 90–95, 2007. DOI: 10.1109/MCSE.2007.55.
- [4] F. Pérez and B. E. Granger, “IPython: a system for interactive scientific computing,” *Computing in Science and Engineering*, vol. 9, no. 3, pp. 21–29, May 2007. DOI: 10.1109/MCSE.2007.53.
- [5] S. Behnel, R. Bradshaw, C. Citro, L. Dalcin, D. S. Seljebotn, and K. Smith, “Cython: the best of both worlds,” *Computing in Science & Engineering*, vol. 13, no. 2, pp. 31–39, Mar. 2011. DOI: 10.1109/MCSE.2010.118.
- [6] S. van der Walt, S. C. Colbert, and G. Varoquaux, “The NumPy array: a structure for efficient numerical computation,” *Computing in Science Engineering*, vol. 13, no. 2, pp. 22–30, Mar. 2011. DOI: 10.1109/MCSE.2011.37.
- [7] E. Jones, T. Oliphant, P. Peterson, *et al.* (2001–). SciPy: open source scientific tools for Python, [Online]. Available: <http://www.scipy.org/>.
- [8] W. McKinney, “Data structures for statistical computing in Python,” in *Proceedings of the 9th Python in Science Conference*, S. van der Walt and J. Millman, Eds., 2010, pp. 51–56.
- [9] Martín Abadi *et al.* (2015). TensorFlow: large-scale machine learning on heterogeneous systems. Software available from [tensorflow.org](http://tensorflow.org), [Online]. Available: <http://tensorflow.org/>.
- [10] (2019). TensorFlow official repository, [Online]. Available: <https://github.com/tensorflow/tensorflow>.
- [11] A. Paszke, S. Gross, S. Chintala, G. Chanan, E. Yang, Z. DeVito, Z. Lin, A. Desmaison, L. Antiga, and A. Lerer, “Automatic differentiation in PyTorch,” in *31st Conference on Neural Information Processing Systems (NIPS 2017)*, Long Beach, CA, USA, 2017.
- [12] (2019). Torch official repository, [Online]. Available: <https://github.com/torch/torch7>.
- [13] Theano Development Team, “Theano: a Python framework for fast computation of mathematical expressions,” May 2016. eprint: [arXiv: abs/1605.02688](https://arxiv.org/abs/1605.02688).
- [14] F. Chollet. (2019). Keras, [Online]. Available: <https://keras.io/>.

- [15] (2019). CNTC official repository, [Online]. Available: <https://github.com/Microsoft/cntk>.
- [16] F. Pedregosa *et al.*, “Scikit-learn: machine learning in Python,” *Journal of Machine Learning Research*, vol. 12, pp. 2825–2830, 2011.
- [17] (2019). MNIST handwritten digit database, Yann LeCun, Corinna Cortes and Chris Burges, [Online]. Available: <http://yann.lecun.com/exdb/mnist/>.
- [18] F. Rosenblatt, “The perceptron: a probabilistic model for information storage and organization in the brain,” *Psychological review*, vol. 65, no. 6, 1958. DOI: 10.1037/h0042519.
- [19] X. Glorot, A. Bordes, and Y. Bengio, “Deep Sparse Rectifier Neural Networks,” in *Proceedings of the Fourteenth International Conference on Artificial Intelligence and Statistics*, G. Gordon, D. Dunson, and M. Dudík, Eds., ser. Proceedings of Machine Learning Research, vol. 15, Fort Lauderdale, FL, USA: PMLR, Nov. 2011, pp. 315–323.
- [20] T. Zhang, “Solving large scale linear prediction problems using stochastic gradient descent algorithms,” in *Proceedings of the Twenty-first International Conference on Machine Learning*, ser. ICML '04, Banff, Alberta, Canada: ACM, 2004. DOI: 10.1145/1015330.1015332.

#### For citation:

M. N. Gevorkyan, A. V. Demidova, T. S. Demidova, A. A. Sobolev, Review and comparative analysis of machine learning libraries for machine learning, *Discrete and Continuous Models and Applied Computational Science* 27 (4) (2019) 305–315. DOI: 10.22363/2658-4670-2019-27-4-305-315.

#### Information about the authors:

**Migran N. Gevorkyan** — Candidate of Physical and Mathematical Sciences, assistant professor of Department of Applied Probability and Informatics of Peoples' Friendship University of Russia (RUDN University) (e-mail: [gevorkyan-mn@rudn.ru](mailto:gevorkyan-mn@rudn.ru), phone: +7(495)9520250, ORCID: <https://orcid.org/0000-0002-4834-4895>, ResearcherID: E-9214-2016, Scopus Author ID: 57190004380)

**Anastasia V. Demidova** — Candidate of Physical and Mathematical Sciences, assistant professor of Department of Applied Probability and Informatics of Peoples' Friendship University of Russia (RUDN University) (e-mail: [demidova-av@rudn.ru](mailto:demidova-av@rudn.ru), phone: +7(495)9520250, ORCID: <https://orcid.org/0000-0003-1000-9650>, ResearcherID: AAD-2214-2019, Scopus Author ID: 57191952809)

**Tatiana S. Demidova** — student of Department of Applied Probability and Informatics of Peoples' Friendship University of Russia (RUDN University) (e-mail: [1032152607@pfur.ru](mailto:1032152607@pfur.ru), phone: +7(495)9520250, ORCID: <https://orcid.org/0000-0001-6076-1619>, Scopus Author ID: 57210151914)

**Anton A. Sobolev** — student of Department of Applied Probability and Informatics of Peoples' Friendship University of Russia (RUDN University) (e-mail: [1032152618@pfur.ru](mailto:1032152618@pfur.ru), phone: +7(495)9520250, ORCID: <https://orcid.org/0000-0003-1629-1378>, Scopus Author ID: 57206139419)

УДК 519.21;51-76

DOI: 10.22363/2658-4670-2019-27-4-305-315

## Обзор и сравнительный анализ библиотек машинного обучения для построения нейронных сетей

М. Н. Геворкян, А. В. Демидова, Т. С. Демидова,  
А. А. Соболев

*Кафедра прикладной информатики и теории вероятностей  
Российский университет дружбы народов  
ул. Миклухо-Маклая, д. 6, Москва, 117198, Россия*

Статья носит обзорный характер. В ней проведено сравнение актуальных библиотек машинного обучения, которые могут быть использованы для построения нейронных сетей.

В первой части статьи даётся краткое описание библиотек TensorFlow, PyTorch, Theano, Keras, SciKit Learn, стека библиотек SciPy (NumPy, SciPy, Pandas, Matplotlib, Jupyter). Делается обзор области применения перечисленных библиотек и основных технических характеристик, таких как быстродействие, поддерживаемые языки программирования, текущее состояние разработки. Среди рассматриваемых библиотек только PyTorch и TensorFlow непосредственно конкурируют друг с другом. Остальные библиотеки взаимодополняют друг друга и часто используются совместно при построении различных моделей машинного обучения.

Во второй части статьи проводится сравнение пяти библиотек на примере многослойного перцептрона, который применяется к задаче распознавания рукописных цифр. Данная задача хорошо разработана и является модельной для тестирования различных реализаций нейронных сетей. Сравняется время обучения в зависимости от количества эпох и точности работы классификатора. Результаты сравнения представлены в виде графиков времени обучения и точности в зависимости от количества эпох и в табличном виде.

**Ключевые слова:** машинное обучение, нейронные сети, MNIST, TensorFlow, PyTorch

UDC 519.165, 517.938

PACS 02.70.–c, 02.50.Ga

DOI: 10.22363/2658-4670-2019-27-4-316-324

## Investigation of insertion tableau evolution in the Robinson–Schensted–Knuth correspondence

Vasilii S. Duzhin

*Department of Algorithmic Mathematics  
Saint Petersburg Electrotechnical University “LETI”  
5, Professora Popova St., St. Petersburg 197376, Russian Federation*

(received: December 23, 2019; accepted: December 30, 2019)

Robinson–Schensted–Knuth (RSK) correspondence occurs in different contexts of algebra and combinatorics. Recently, this topic has been actively investigated by many researchers. At the same time, many investigations require conducting the computer experiments involving very large Young tableaux. The article is devoted to such experiments.

RSK algorithm establishes a bijection between sequences of elements of linearly ordered set and the pairs of Young tableaux of the same shape called insertion tableau  $P$  and recording tableau  $Q$ . In this paper we study the dynamics of tableau  $P$  and the dynamics of different concrete values in tableau  $P$  during the iterations of RSK algorithm. Particularly, we examine the paths within tableaux  $P$  called bumping routes along which the elements of an input sequence pass. The results of computer experiments with Young tableaux of sizes up to  $10^8$  were presented. These experiments were made using the software package for dealing with 2D and 3D Young diagrams and tableaux.

**Key words and phrases:** Robinson–Schensted–Knuth correspondence, Young tableaux, Young graph, Markov process, central measure, Plancherel measure, asymptotic representation theory

### 1. Introduction

Robinson–Schensted–Knuth (RSK) algorithm also known as Robinson–Schensted–Knuth correspondence which maps permutations to the pairs of Young tableaux, plays an important role into various combinatorial problems. The combinatorics of Young diagrams and Young tableaux including RSK algorithm, finds numerous applications in physics, mathematics and informatics [1]–[3].

RSK correspondence can be easily generalized from the case of permutations to the case of infinite sequences of linearly ordered set. In such instance, an insertion tableau is a semi-standard Young tableau filled by elements of this

© Duzhin V. S., 2019



This work is licensed under a Creative Commons Attribution 4.0 International License

<http://creativecommons.org/licenses/by/4.0/>

ordered set. This implies that the RSK algorithm is applicable to a sequence of random independent values uniformly distributed over the interval  $[0,1]$ , i.e. to the Bernoulli scheme. A correspondence between two dynamical systems such as Bernoulli shift and iterations of Schützenberger transformation was built in [4]. Later [5] it was proved that this correspondence is isomorphism. It was also proved there that the first element of an infinite sequence of uniformly distributed random values can be unambiguously restored only by the limit angle of inclination of Schützenberger path of a recording tableau.

In practice, we are interested in the restoration of the first element of a finite sequence. Unlike the case of infinite sequences, we also need an insertion tableau  $P$  in addition to a recording tableau  $Q$  to restore the first element. Since tableau  $P$  changes during every iteration, the investigation of tableau  $P$  evolution properties is also important for studying the algorithms of restoration of an entire sequence.

The results of computer experiments related to the estimation of the first element value in a finite segment of an infinite sequence using tableau  $Q$  are given in [6]. The subject of this article is to examine how tableau  $P$  changes during RSK insertions.

## 2. Definitions

*Young diagrams* are popular combinatorial structures which correspond to integer partitions. There are many ways to present a Young diagram. Particularly, in this paper we define it by so-called French notation as left-justified and bottom-justified finite set of square boxes (see Figure 1 (a)).

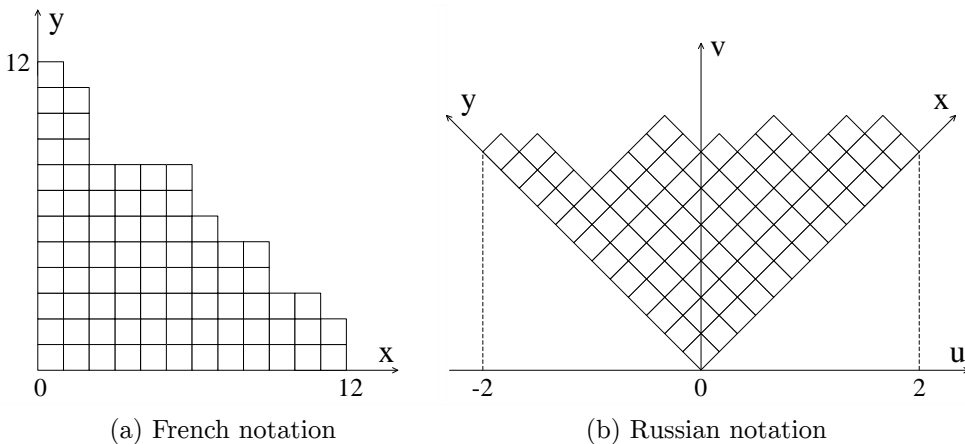


Figure 1. An example of a Young diagram

Another way of presenting Young diagrams called Russian notation is shown in Figure 1 (b). The Russian notation was proposed by Vershik and Kerov [7] and is derived from the French notation by rotating the axes 45 degrees counterclockwise. Note that the diagram in Figure 1 (b) is normalized in such a way that the total area of boxes is 1. This notation is used in many papers because it makes studying the Plancherel measure much easier.

It is convenient to consider Young diagrams as vertices of infinite oriented graded graph called the Young graph. In this graph, edges connect diagrams which differ in one box. If the edge connects a diagram  $\lambda_n$  of the size  $n$  with a diagram  $\lambda_{n+1}$  of the size  $n + 1$ , then  $\lambda_{n+1}$  can be obtained from  $\lambda_n$  by adding a single box.

If we assign to each edge a certain transition probability, a Markov process will be defined on the graph. The most important class of such processes is the class of central processes for which the probabilities of different paths between a fixed pair of diagrams are equal. A complete description of all central processes on the 2D Young graph was obtained by Vershik in [8]. The only central process on the Young graph with  $o(n)$  speed of growth along the axes is called the Plancherel process. This process and explicit formulas of its transition probabilities are described in [8].

The limit shape of the Plancherel process called the Vershik–Kerov–Logan–Schepp (VKLS) limit shape [7] is given by the formula:

$$S = \begin{cases} \frac{2}{\pi}(u \arcsin(u) + \sqrt{1 - u^2}), & |u| \leq 1, \\ |u|, & |u| \geq 1, \end{cases} \quad (1)$$

where  $u$  is a coordinate in the Russian notation.

A *Young tableau*  $\tau$  is a Young diagram  $\lambda$  filled by values increasing in rows and columns. These values can be elements of an arbitrary linearly ordered set. Wherein we say that  $\lambda$  is a shape of  $\tau$ . A *standard Young tableau* (SYT) is a Young diagram filled by integers  $[1, n]$ ,  $n > 0$  which grow strictly in rows and columns. It is easy to see that a Young tableau corresponds to a path on the Young graph. The numbers in tableau set the order of adding the boxes when walking from the root of the graph. A *semistandard Young tableau* (SSYT) is a Young tableau with values strictly increasing in columns and weakly increasing in rows.

In addition to the finite Young tableaux consisting of  $n$  boxes, infinite tableaux can be considered as well. By *infinite Young tableau* we mean a mapping  $\sigma : \mathbb{Z}_+^2 \Rightarrow \mathbb{N}$  such that for the fixed  $i, j \in \mathbb{N}$  the values  $\sigma_{i,k}$  and  $\sigma_{k,j}$ ,  $k \in \mathbb{N}$  grow strictly. These infinite tableaux are also called enumerations of the integer lattice  $\mathbb{Z}_+^2$ . For the case of SYT or SSYT, some integers may be missing, i.e. the corresponding mapping  $\mathbb{Z}_+^2 \rightarrow \mathbb{N}$  is not necessary bijective. In this research we consider SYT filled by integers and SSYT filled by real numbers belonging to the interval  $[0, 1]$ .

### 3. Robinson–Schensted–Knuth algorithm

RSK algorithm establishes a bijection between a set of permutations of  $n$  distinct integers and a set of pairs of standard Young tableaux of size  $n$  of the same shape. These tableaux are called insertion tableau  $P$  and recording tableau  $Q$ .

At the beginning, the first value of a permutation is put into the empty tableau  $P$  and 1 is inserted in the tableau  $Q$ . In each step of the algorithm, the next value  $v$  of permutation is being compared with values of the first column of  $P$ . If  $v$  exceeds all these values, it is being put on the top of the

first column. Otherwise, it replaces the closest larger value of the first column. The replaced value is being bumped in the second column and being processed in the same way. This process continues until a certain value is put on the top of a column at position  $(x, y)$ . Finally, the index of a processed value is being put into tableau  $Q$  at  $(x, y)$ . So,  $P$  and  $Q$  tableaux are supported to have the same shape. The algorithm finishes when all the values of a permutation are processed.

Note that above steps can be performed in reverse order, i.e. a permutation can be constructed from a pair of Young tableaux of the same shape. Such a procedure is called *reverse RSK algorithm*. Also, RSK algorithm is applicable to any ordered sequences such as sequences of integer or real values.

RSK algorithm defines two equivalence relations on a set of permutations. The permutations are called Knuth-equivalent if they correspond to the same tableau  $P$  and dual Knuth-equivalent if they correspond to the same tableau  $Q$ . Another Donald Knuth's definition of these equivalence classes directly in terms of permutations is given in [9]. Some interesting properties of Knuth-equivalent and dual Knuth-equivalent permutations were investigated in [6].

## 4. Visualization of Plancherel tableaux

In order to study the properties of the RSK algorithm, it is of interest to examine how the shape of tableau  $P$  changes in time. The evolution of tableau  $Q$  has a simple description: it is proved by Donald Knuth that RSK transforms an uniformly distributed random sequence in a pair of Plancherel-distributed Young tableaux. Therefore, tableau  $Q$  grows as a tableau in a Markov process which generates the Plancherel measure.

There exists an interesting way to visualize a Young tableau in the 3D space proposed by A. M. Vershik. Consider a function on the set of boxes of the corresponding Young diagram. The values of this function are the numbers within the corresponding boxes. A Young tableau can be represented as a 3D graph of this function.

For the Plancherel tableaux, with a rise of their sizes this graph tends to a surface which can be described as follows. Consider a set of positively directed rays on the 2D plane emanating from the origin. Each ray intersects with the VKLS limit shape (1) at some point  $(x', y')$ . For a point  $(t \cdot x', t \cdot y')$  which lies on this ray,  $z = t^2$ . So, this surface intersects with the planes containing axis  $z$  along parabolas which touches the coordinate plane  $x, y$  in the origin. This property completely characterizes the surface. An example of such a visualization for the tableau  $P$  of size  $10^5$  is shown in Figure 2 (a). Note that the coordinates  $(x, y)$  are divided by  $\sqrt{n}$ .

A very similar picture can be produced by generating a Markov chain of Plancherel distributed Young diagrams. Figure 2 (b) demonstrates how the number of added box divided by  $10^5$  depends on normalized coordinates of this box in a Young tableau.

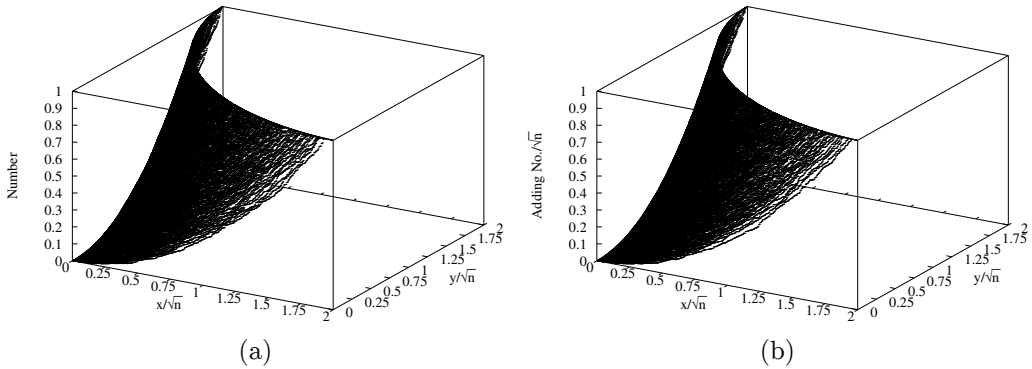


Figure 2. (a) Values of boxes in tableau  $P$  after  $10^5$  RSK iterations; (b) Positions of added boxes in Plancherel process after adding  $10^5$  boxes

## 5. Bumping forest

Each time a new value comes to the input of the RSK algorithm, it bumps a certain element in the first column of tableau  $P$  and takes its position. Then, the bumped element bumps another element in the second column and so on. A *bumping route* is a sequence of all boxes bumped in a single RSK iteration. A bumping route is defined for each position in the first column.

Bumping routes were presented in [10]. Also a problem of hydrodynamic description of bumping routes was raised there. The limit behaviour of bumping routes including explicit formula of their limit shape was described in [11]. The possible use of bumping routes to speed up the RSK algorithm was discussed in [12].

In the current research we have constructed all the bumping routes for tableau  $P$  of size  $10^8$ . Some of them are shown in Figure 3.

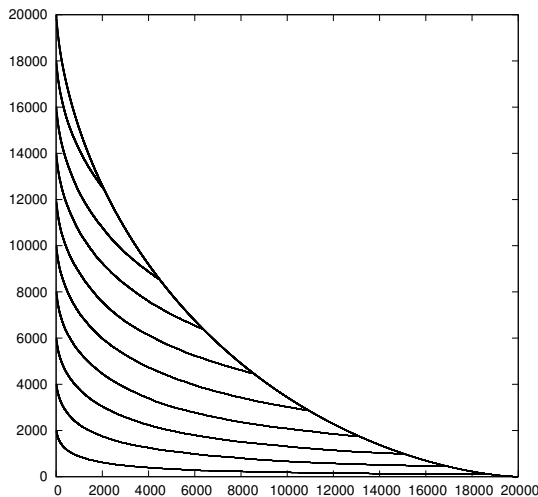


Figure 3. Some bumping routes of tableau  $P$

A *bumping tree* is a set of bumping routes converging into a single box. A *bumping forest* is a union of all bumping routes. Figure 4 (a) demonstrates an example of a Young tableau and its bumping forest. The bumping forest itself is illustrated in Figure 4 (b).

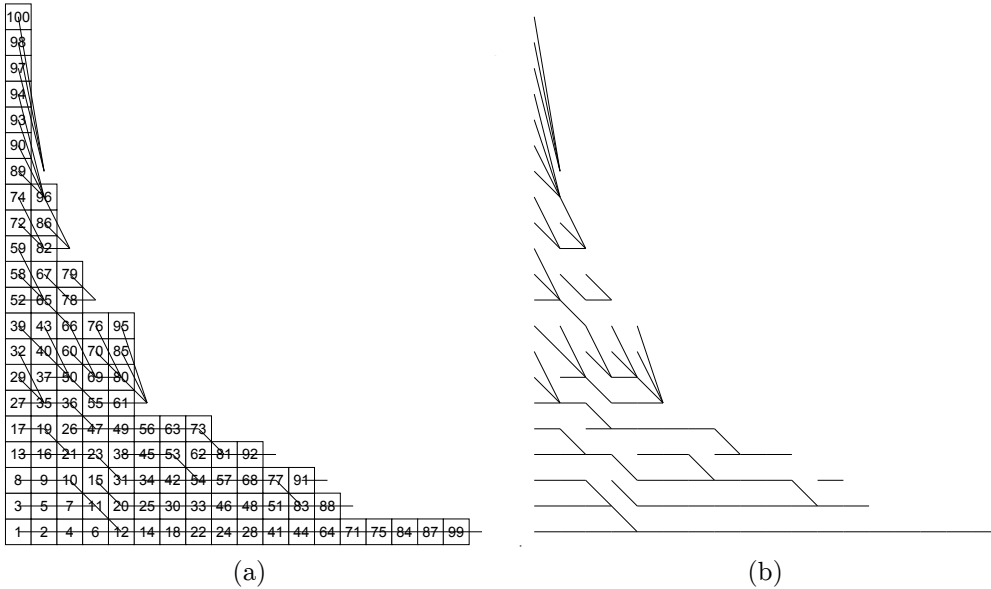


Figure 4. (a) A Young tableau and its bumping forest; (b) A bumping forest

### 6. Dynamics of insertion tableau

Along with studying the dynamics of the entire tableau, we are also interested in investigating the dynamics of concrete values in tableau  $P$ . Here we discuss the results of our computer experiment dedicated to analysis of motion of these values within a semi-standard Young table  $P$  filled by random real numbers from the interval  $[0, 1]$ . The idea of this algorithm is as follows. Firstly, we construct tableau  $P$  of size  $k$ . Next, the observed value  $z$  is fed to the input of RSK. Then, we observe how the position of  $z$  changes while RSK processes next  $n - k$  values. Each trajectory is close to a Vershik–Kerov–Logan–Schepp limit shape (1).

The results of this experiment is illustrated in Figure 5. We examined trajectories of 9 different numbers:  $z = [0.1, 0.2, \dots, 0.9]$ . The horizontal curves are trajectories of different  $z$ . Black points are the final positions of  $z$  for  $k/n = [0.1, 0.3, 0.5, 0.7, 0.9]$ ,  $n = 10^7$ .

It is easily seen from the Fig. 5 that the dynamics of motion of different values in RSK looks very similar. The average dynamics of a certain  $z$  can be obtained by rescaling the unique average motion dynamics of  $z = 1$ .

Note that, with a rise of  $n$ , the motion of these value continues until they eventually reach the coordinate plane. Unfortunately, this process often takes a really huge amount of RSK iterations what makes it hard to simulate it using available computation power.

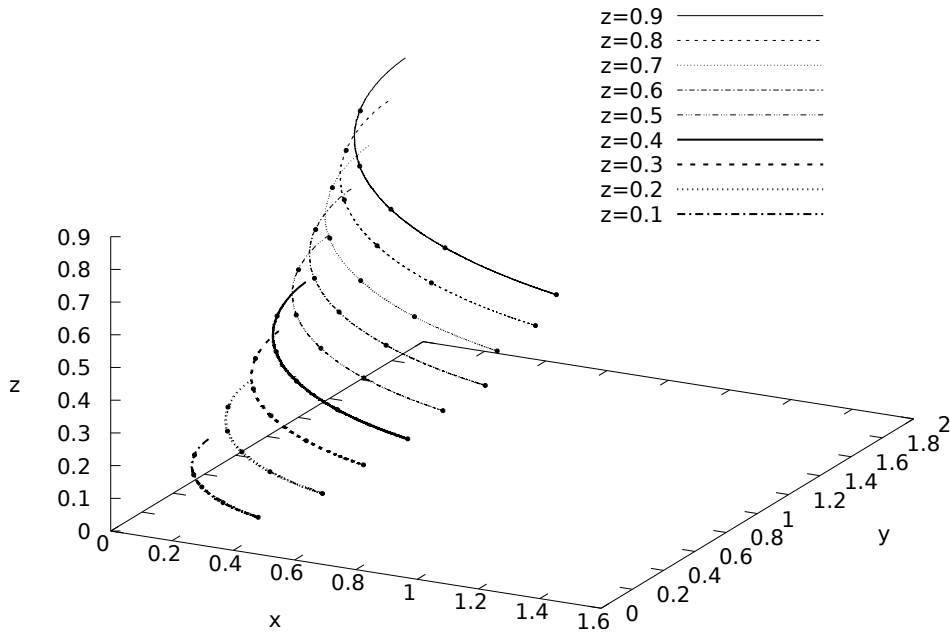


Figure 5. Evolution of random values in RSK algorithm

## 7. Conclusions

The results of numerical experiments presented in this article demonstrate two types of dynamics in an insertion tableau of the Robinson–Schensted–Knuth algorithm. The first investigated dynamics is a modification of tableau after a single RSK iteration when a new value moves along a certain path called a bumping route. The second dynamics is related to the motion of the concrete value during many RSK iterations. Numerical experiments for studying these dynamics are presented in this paper.

## References

- [1] N. O’Connell, “A path-transformation for random walks and the Robinson – Schensted correspondence,” *Transactions of the American Mathematical Society*, vol. 355, no. 9, pp. 3669–3697, 2003. eprint: [www.jstor.org/stable/1194859](http://www.jstor.org/stable/1194859).
- [2] D. Dauvergne, “The Archimedean limit of random sorting networks,” 2018. arXiv: [arXiv:abs/1802.08934](https://arxiv.org/abs/1802.08934) [math.PR].
- [3] O. Angel, A. E. Holroyd, D. Romik, and B. Virág, “Random sorting networks,” *Advances in Mathematics*, vol. 215, no. 2, pp. 839–868, 2007. DOI: [10.1016/j.aim.2007.05.019](https://doi.org/10.1016/j.aim.2007.05.019).
- [4] S. V. Kerov and A. M. Vershik, “The characters of the infinite symmetric group and probability properties of the Robinson–Schensted–Knuth algorithm,” *SIAM J. Algebraic Discrete Methods*, vol. 7, no. 1, pp. 116–124, 1986. DOI: [10.1137/0607014](https://doi.org/10.1137/0607014).

- [5] D. Romik and P. Śniady, “Jeu de taquin dynamics on infinite Young tableaux and second class particles,” *Annals of Probability: An Official Journal of the Institute of Mathematical Statistics*, vol. 43, no. 2, pp. 682–737, 2015. DOI: 10.1214/13-AOP873.
- [6] N. N. Vassiliev, V. S. Duzhin, and A. D. Kuzmin, “Investigation of properties of equivalence classes of permutations by inverse Robinson – Schensted – Knuth transformation [Issledovaniye svoystv klassov ekvivalentnosti perestanovok s pomoshch’yu obratnogo preobrazovaniya Robinsona],” *Informatsionno-upravliaiushchie sistemy [Information and Control Systems]*, no. 1, pp. 11–22, 2019, in Russian. DOI: 10.31799/1684-8853-2019-1-11-22. eprint: <https://elibrary.ru/item.asp?id=36930159>.
- [7] A. M. Vershik and S. V. Kerov, “Asymptotic of the largest and the typical dimensions of irreducible representations of a symmetric group,” *Functional Analysis and Its Applications*, vol. 19, no. 1, pp. 21–31, 1985. DOI: 10.1007/BF01086021.
- [8] A. M. Vershik and S. V. Kerov, “Asymptotic theory of characters of the symmetric group,” *Functional Analysis and Its Applications*, vol. 15, no. 4, pp. 246–255, 1981. DOI: 10.1007/BF01106153.
- [9] G. E. Andrews, *The Theory of Partitions*, ser. Encyclopedia of Mathematics and its Applications. Cambridge: Cambridge University Press, 1984. DOI: 10.1017/CB09780511608650.
- [10] C. Moore. (2006). Flows in young diagrams. online resource, [Online]. Available: <http://tuvalu.santafe.edu/~moore/gallery.html>.
- [11] D. Romik and P. Śniady, “Limit shapes of bumping routes in the Robinson–Schensted correspondence,” *Random Structures & Algorithms*, vol. 48, no. 1, pp. 171–182, Sep. 2014. DOI: 10.1002/rsa.20570.
- [12] V. Duzhin, A. Kuzmin, and N. Vassiliev, “RSK bumping trees and a fast RSK algorithm,” in *International Conference Polynomial Computer Algebra ‘2019; St. Petersburg, April 15–20, 2019 / Euler International Mathematical Institute, Ed. by N. N. Vassiliev*, VVM Publishing, 2019. eprint: <https://elibrary.ru/item.asp?id=41320890>.

#### For citation:

V. S. Duzhin, Investigation of insertion tableau evolution in the Robinson–Schensted–Knuth correspondence, *Discrete and Continuous Models and Applied Computational Science* 27 (4) (2019) 316–324. DOI: 10.22363/2658-4670-2019-27-4-316-324.

#### Information about the authors:

**Vasilii S. Duzhin** — assistant of Department of Algorithmic Mathematics of Saint Petersburg Electrotechnical University “LETI” (e-mail: [vsduzhin@etu.ru](mailto:vsduzhin@etu.ru), phone: +7(981)7648628, ORCID: <https://orcid.org/0000-0001-8399-284X>, ResearcherID: O-1730-2016, Scopus Author ID: 57189369711)

УДК 519.165, 517.938

PACS 02.70.–с, 02.50.Ga

DOI: 10.22363/2658-4670-2019-27-4-316-324

## Исследование эволюции записывающей таблицы в соответствии Робинсона–Шенстеда–Кнута

В. С. Дужин

*Кафедра алгоритмической математики*

*Санкт-Петербургский государственный электротехнический университет  
«ЛЭТИ»*

*ул. Профессора Попова, д. 5, Санкт-Петербург, 197376, Россия*

Соответствие Робинсона–Шенстеда–Кнута (RSK) встречается в различных контекстах алгебры и комбинаторики. В последнее время данная тема активно исследуется специалистами из различных областей науки. В то же время многие такие исследования требуют проведения компьютерных экспериментов с таблицами Юнга чрезвычайно больших размеров. Эта статья посвящена таким численным экспериментам.

Алгоритм RSK устанавливает биекцию между множеством последовательностей элементов из линейно упорядоченного множества и множеством пар таблиц Юнга одинаковой формы, называемых записывающей таблицей  $P$  и нумерующей таблицей  $Q$ . В настоящей работе изучается динамика таблицы  $P$ , а также динамика позиций различных значений, перемещающихся по таблице  $P$  в течение итераций алгоритма RSK. В частности, исследовались пути в таблице  $P$ , называемые путями выталкиваний, вдоль которых перемещаются значения из входной последовательности в процессе работы алгоритма RSK. Приводятся результаты компьютерных экспериментов над таблицами Юнга с размерами до  $10^8$ . Эти эксперименты были проведены с помощью программного пакета для работы с двумерными и трёхмерными диаграммами и таблицами Юнга.

**Ключевые слова:** соответствие Робинсона–Шенстеда–Кнута, таблицы Юнга, граф Юнга, марковские процессы, центральная мера, мера Планшереля, асимптотическая теория представлений

# Mathematical modeling

*Research article*

UDC 519.6

PACS 07.05.Tp

DOI: 10.22363/2658-4670-2019-27-4-325-342

## Leaky waves in planar dielectric waveguide

Dmitriy V. Divakov<sup>1</sup>, Alexandre A. Egorov<sup>2</sup>,  
Konstantin P. Lovetskiy<sup>1</sup>,  
Leonid A. Sevastianov<sup>1,3</sup>, Andrey S. Drevitskiy<sup>1</sup>

<sup>1</sup> *Department of Applied Probability and Informatics  
Peoples' Friendship University of Russia (RUDN University)  
6, Miklukho-Maklaya St., Moscow 117198, Russian Federation*

<sup>2</sup> *A. M. Prokhorov General Physics Institute  
Russian Academy of Sciences, Moscow 119991, Russian Federation*

<sup>3</sup> *Bogoliubov Laboratory of Theoretical Physics  
Joint Institute for Nuclear Research  
6, Joliot-Curie St., Dubna, Moscow region 141980, Russian Federation*

(received: December 23, 2019; accepted: December 30, 2019)

A new analytical and numerical solution of the electrodynamic waveguide problem for leaky modes of a planar dielectric symmetric waveguide is proposed. The conditions of leaky modes, corresponding to the Gamow-Siegert model, were used as asymptotic boundary conditions. The resulting initial-boundary problem allows the separation of variables. The emerging problem of the eigen-modes of open three-layer waveguides is formulated as the Sturm-Liouville problem with the corresponding boundary and asymptotic conditions. In the case of guided and radiation modes, the Sturm-Liouville problem is self-adjoint and the corresponding eigenvalues are real quantities for dielectric media. The search for eigenvalues and eigenfunctions corresponding to the leaky modes involves a number of difficulties: the problem for leaky modes is not self-adjoint, so the eigenvalues are complex quantities. The problem of finding eigenvalues and eigenfunctions is associated with finding the complex roots of the nonlinear dispersion equation. To solve this problem, we used the method of minimizing the zero order. An analysis of the calculated distributions of the electric field strength of the first three leaky modes is given, showing the possibilities and advantages of our approach to the study of leaky modes.

**Key words and phrases:** integrated optics, waveguide, Sturm-Liouville problem, dispersion relation, leaky modes, computer simulation

© Divakov D. V., Egorov A. A., Lovetskiy K. P., Sevastianov L. A., Drevitskiy A. S., 2019



This work is licensed under a Creative Commons Attribution 4.0 International License

<http://creativecommons.org/licenses/by/4.0/>

## 1. Introduction

In the books by Marcuse [1], [2], Adams [3], Snyder and Love [4], Tamir [5], and other authors the terms “leaky rays” and “leaky modes” appear when discussing the propagation of polarized light in fiber optical waveguides with the refractive index of the core smaller than that of the cladding, and in planar waveguides with plates of material optically denser than the waveguide layer itself. In this case, Marcuse writes that the outflow of light from such a waveguide is akin to tunneling through a potential barrier in quantum mechanics. The “leaky light”, in contrast to the “emitted light”, propagates for quite a long time along the axis of the optical fiber. Similarly, in a planar waveguide, the resulting electromagnetic radiation propagates for some time at some distance along the waveguide, in contrast to the emitted light.

At the initial stage of the study of “leaky” modes, T. Tamir et al. [6]–[12], A.W. Snyder et al. [13]–[18], as well as other research teams [19]–[25], investigated the dispersion equations of optical waveguides written in terms of transition matrices from the point of view of choosing one (two) roots of an analytical function. The studies were executed using the theory of residues in Cauchy integrals.

In the papers by V. Shevchenko [24], [25] the behavior of guided modes during the transition of their wave numbers beyond critical values was analyzed, their transformation into leaky modes was shown, and the choice of quadrants to which the wave numbers should shift when passing through critical values was justified. At frequencies below critical, the reflection from the waveguide walls ceases to be complete, so that the waveguide modes continue to propagate experiencing incomplete internal reflection, because of which some radiation from the waveguide occurs. Such (improper) waveguide waves with radiative damping are called leaky waves.

Open waveguides as radiating systems were first investigated by Hansen [19], who proposed an antenna structure implemented using leaky waves. However, there was no understanding of the physical mechanism of the resulting waves. After all, the leaky waveguide mode is characterized by a complex longitudinal wave number with constant attenuation due to radiation losses.

In this case, the longitudinal attenuation leads to an exponential increase in the wave amplitude in the transverse direction. This fact violates the usual radiation condition for guided modes, described by the solutions of self-adjoint problems for the Helmholtz equation. The behavior of the resulting waves that seems non-physical was clarified by Marcuvitz [23] and Oliner [6]–[9].

In the papers by Oliner et al. [6]–[12], a detailed study of the complex roots of the dispersion equation that do not correspond to the guided modes is given. The study begins with the assumption that exponentially damped waves correspond to such roots, the experimental observation of which was earlier reported in Refs. [20]–[22]. First, using ray technique, and then with the help of mode analysis, the authors analyzed the wave solutions corresponding to four different roots of the fourth-power dispersion equation. Two of these roots correspond to solutions that exponentially decrease in the direction of propagation and are located symmetrically with respect to the axes of coordinates and the origin of coordinates. The rest two roots are rejected. Many publications of that time have been devoted to the analysis of the relative position of the variety of roots [6]–[18].

In the first decades of the study of leaky waves, the method of steepest descent was used as the most common method for their numerical search. In this case, the trajectory of the fastest descent comes close to the leakage poles, they begin to make a significant contribution or even dominate in the general directional pattern of an open waveguide. The field distribution of the resulting leaky wave increases in the transverse direction. However, the field amplitude remains finite in a wedge-like region of space that allows leakage.

As shown by Marcuvitz [23], these complex poles can correspond to leaky modes. Although they do not make a direct contribution to the correct spectral solution and can therefore be characterized by non-physical growth towards infinity, they can nevertheless accurately describe the radiation field in limited spatial domains. In Ref. [26], e.g., it is noted that in most publications on leaky modes there are no plots of fields of various types for leaky modes calculated numerically (see, e.g., [4], [5], [27]–[35]). In this case, the authors of some publications (e.g., [34]) propose to replace the leaky modes with radiative ones in limited domains. Our studies have shown that this can lead, firstly, to a large error in the calculation of losses, and secondly, to an inaccurate calculation of the field profiles of leaky modes at distances exceeding several wavelengths ( $\geq 2$ ) of the electromagnetic radiation used. The replacement of one wave with another sometimes used requires serious analysis in each specific case. As a consequence, there is an urgent need to develop new algorithms for calculating the fields of both radiative and leaky modes, surpassing the standard methods, e.g., the FDTD method, in count rate and not inferior to them in accuracy.

In quantum physics, such solutions of the stationary Schrödinger equation are called Gamow resonances [36], [37] or Siegert quasi-states [38]. In recent decades, some researchers (see [39], [40]) solve boundary-value problems for the Helmholtz equations with the asymptotic conditions of Siegert leaky waves, obtaining numerical results interpreted by them as leaky waves. We propose to obtain (using a numerical method) the solutions of boundary problems for wave equations with asymptotic conditions of Siegert leaky waves. The numerical solutions obtained using this approach coincide with the solutions of Refs. [27]–[29], [33], [35], [41], but additionally allow description of the phase fronts of leaky waves and “angular outflow cones”.

In our opinion, a more rigorous justification of the model of leaky waves of open waveguide systems can be obtained by starting calculations not from the Helmholtz equation, as is traditionally done, but from the wave equation preceding the Helmholtz equation, and most importantly, more adequately reflecting the wave nature of leaky modes.

## 2. Statement of the problem of modeling leaky modes of symmetric waveguides

Consider (Figure 1) a symmetric three-layer planar waveguide consisting of a dielectric film having the height  $h$  with real refractive index  $n_f$ , surrounded by a cladding layer with real refractive index  $n_c < n_f$ .

The propagation of radiation in such structures is described by the Maxwell equations, material equations [3]–[5], and boundary conditions that distinguish

the class of solutions interesting for the researcher — in the present case, the leaky modes [6]–[12], [26], [42].

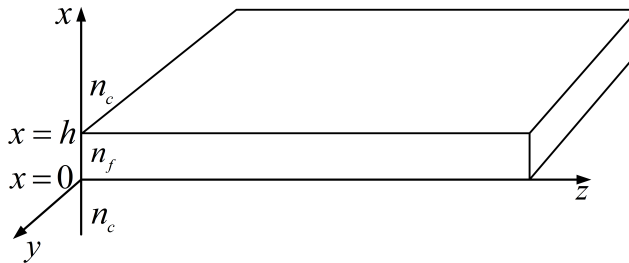


Figure 1. Symmetric three-layer dielectric waveguide

The generally accepted model of the electromagnetic field in a planar (infinitely extended along the  $Oy$ -axis) are fields that are independent of the variable  $y$ . In this case, Maxwell's equations are considerably simplified, since  $\partial E_\alpha / \partial y = \partial H_\alpha / \partial y \equiv 0$  for any  $\alpha = x, y, z$ , and they are divided into two independent subsystems — the subsystem for the so-called TE-modes and for the TM-modes. The subsystem for the TE-modes can be represented as a single wave equation for the master component  $E_y$

$$\left( \frac{\partial^2}{\partial x^2} + \frac{\partial^2}{\partial z^2} - \frac{n^2(x)}{c^2} \frac{\partial^2}{\partial t^2} \right) E_y = 0, \quad (1)$$

with the boundary conditions

$$\begin{cases} \left. \frac{\partial E_y}{\partial x} - ik_0 p_c(\beta) E_y \right|_{x=h+0} = 0, \\ \left. \frac{\partial E_y}{\partial x} + ik_0 p_c(\beta) E_y \right|_{x=-0} = 0, \end{cases} \quad (2)$$

and the initial conditions

$$E_y(x, z, t) \Big|_{\substack{z=0 \\ t=0}} = E_y^0(x), \quad (3)$$

where  $p_c(\beta) = \sqrt{n_c^2 - \beta^2}$ , and  $c$  is the electrodynamic constant,  $n(x)$  is the variable refractive index of the considered three-layer waveguide, defined below. The subsystem for the TE-mode also includes two equations for the connection of components  $H_x, H_z$  with the master component  $E_y$ .

As a model of leaky modes propagation, we will consider Eq. (1), i.e., in other words, we will consider the propagation of leaky modes in terms of a wave process. As asymptotic boundary conditions, we will consider the conditions of leaky modes corresponding to the Gamow-Siegert model [36]–[40].

In the case under consideration, the function describing the refractive index depends only on  $x$ , which makes it possible to separate the variables in Eq. (1).

As a result, we obtain solutions corresponding to leaky modes propagating in the positive direction of the  $z$ -axis:

$$E_{yj}^+ \Big|_{x>h} = A_{cj}^+ \cdot \exp \left\{ ik_0 \sqrt{n_c^2 - \beta_j^2} x + ik_0 \beta_j z - i\omega t \right\}, \tag{4}$$

$$E_{yj}^+ \Big|_{\substack{x<h \\ x>0}} = A_{fj}^+ \cdot \exp \left\{ ik_0 \sqrt{n_f^2 - \beta_j^2} x + ik_0 \beta_j z - i\omega t \right\} + \\ + B_{fj}^+ \cdot \exp \left\{ -ik_0 \sqrt{n_f^2 - \beta_j^2} x + ik_0 \beta_j z - i\omega t \right\}, \tag{5}$$

$$E_{yj}^+ \Big|_{x<0} = B_{cj}^+ \cdot \exp \left\{ -ik_0 \sqrt{n_c^2 - \beta_j^2} x + ik_0 \beta_j z - i\omega t \right\}, \tag{6}$$

where  $\omega$  is the frequency, and  $\beta_j$  are the eigenvalues of the non-self-adjoint Sturm-Liouville problem with boundary conditions that extract the leaky modes [3], [34], [41]:

$$\begin{cases} X'' + k_0^2 n^2(x) X = k_0^2 \beta^2 X, \\ X'(0) + ik_0 \sqrt{n_c^2 - \beta^2} X(0) = 0, \\ X'(h) - ik_0 \sqrt{n_c^2 - \beta^2} X(h) = 0, \end{cases} \tag{7}$$

The eigenfunctions of the problem (7) are defined as general solution of the ordinary differential equation subject to the boundary conditions of this problem, that is, they have the form

$$X(x) = \begin{cases} A_c \cdot e^{ik_0 \sqrt{n_c^2 - \beta^2} (x-h)}, & x > h, \\ A_f \cdot e^{ik_0 \sqrt{n_f^2 - \beta^2} x} + B_f \cdot e^{-ik_0 \sqrt{n_f^2 - \beta^2} x}, & 0 < x < h, \\ B_c \cdot e^{-ik_0 \sqrt{n_c^2 - \beta^2} x}, & x < 0 \end{cases} \tag{8}$$

and the constants  $A_{c,f}, B_{c,f}$  are determined from the field joining conditions at the boundaries of the waveguide layer  $x = 0$  and  $x = h$ , which with Eq. (8) taken into account constitute a homogeneous system of linear algebraic equations:

$$\begin{pmatrix} 1 & -e^{ik_0 p_f h} & -e^{-ik_0 p_f h} & 0 \\ ik_0 p_c & -ik_0 p_f e^{ik_0 p_f h} & ik_0 p_f e^{-ik_0 p_f h} & 0 \\ 0 & 1 & 1 & -1 \\ 0 & ik_0 p_f & -ik_0 p_f & ik_0 p_c \end{pmatrix} \begin{pmatrix} A_c \\ A_f \\ B_f \\ B_c \end{pmatrix} = \begin{pmatrix} 0 \\ 0 \\ 0 \\ 0 \end{pmatrix}, \tag{9}$$

where  $p_c = \sqrt{n_c^2 - \beta^2}, p_f = \sqrt{n_f^2 - \beta^2}$ .

The homogeneous system of Eqs. (9) has a nontrivial solution if and only if the determinant of the matrix of the system (9) is zero [43]. The equality to zero of the determinant of the matrix of the system (9) can be achieved

for some values of the spectral parameter  $\beta$ , which, in turn, determine the eigenvalues of the problem (7).

In each subdomain  $x > h$ ,  $0 < x < h$ , and  $x < 0$  the solution of the wave equation corresponding to the leaky modes is representable as a wave with a complex wave vector. In the case of a field corresponding to leaky modes running in the positive direction of the  $z$ -axis for  $x > h$  and  $x > h$  due to the symmetry of the waveguide, the wave vector is determined as

$$\vec{k}_j^\pm = k_0 \begin{pmatrix} \pm \sqrt{n_c^2 - \beta_j^2} \\ \beta_j \end{pmatrix} \quad (10)$$

and in the waveguide layer ( $0 < x < h$ ) there are two waves with wave vectors

$$\vec{k}_{fj}^\pm = k_0 \begin{pmatrix} \pm \sqrt{n_f^2 - \beta_j^2} \\ \beta_j \end{pmatrix} \quad (11)$$

the modules of the wave vectors being equal to the corresponding wave numbers:  $|\vec{k}_j^\pm| = k_0 n_c$  and  $|\vec{k}_{fj}^\pm| = k_0 n_f$ .

We formulate the problem of finding solutions corresponding to the leaky modes as an eigenvalue problem for a differential operator with non-self-adjoint boundary conditions (7), which we will further solve numerically.

### 3. Description of the algorithm for numerical solution of the leaky mode problem

The spectral problem for a differential operator with non-self-adjoint boundary conditions (7) is formulated numerically as a problem of approximate determination of complex solutions of the equation

$$\det M(\beta) = 0, \quad (12)$$

where  $M(\beta)$  denotes the coefficient matrix of Eqs. (9) [42]. In the case of a problem similar to (7), but with self-adjoint boundary conditions, any classical method of finding the real roots of the equation can be applied (see, e.g., [44]–[46]). Our problem (7) is not self-adjoint, therefore, the eigenvalues of this problem are generally complex and the standard methods for root search can no longer be applied.

The problem (12) can be reformulated as a problem of finding the minimum of a function of two variables as follows. The desired quantity  $\beta = \beta' + i\beta''$  is a complex number. Any solution  $\tilde{\beta} = \tilde{\beta}' + i\tilde{\beta}''$  of Eq. (12) will be also a local minimum of the non-negative function

$$F(\beta', \beta'') = |\det M(\beta' + i\beta'')|^2. \quad (13)$$

The eigenvalues corresponding to the leaky modes are localized in the first quadrant of the complex plane  $\text{Re}(\beta) > 0$ ,  $\text{Im}(\beta) > 0$ ; moreover  $0 < \text{Re}(\beta) < n_c$  (see Refs. [34], [47], as well as our papers [42]).

To find all the local minima of function (11) in this region, it is proposed to introduce a mesh in the region  $0 < \text{Re}(\beta) < n_c$ ,  $0 < \text{Im}(\beta) < B$ , where  $B$  is a constant that defines the boundary of the search for eigenvalues [42]. The nodes of the introduced mesh are used as initial approximations for the numerical method of finding the minimum of the function of two variables (13). In Refs. [42] the Hook-Jeeves method [48] was used, but there are also other efficient numerical methods for zero-order multidimensional minimization [48].

#### 4. Analysis of leaky modes in terms of inhomogeneous plane waves

Consider the complex values

$$p_{cj} = \sqrt{n_c^2 - \beta_j^2} = p'_{cj} + ip''_{cj}, \quad p_{fj} = \sqrt{n_f^2 - \beta_j^2} = p'_{fj} + ip''_{fj},$$

and  $\beta_j = \beta'_j + i\beta''_j$  in the solutions (4)–(6), explicitly distinguishing their real and imaginary parts, which will allow us to reformulate Eqs. (4)–(6) in terms of inhomogeneous waves, whose amplitude is also a function of coordinates  $x$  and  $z$ :

$$E_{yj}^+ \Big|_{x>h} = A_{cj}^+ \cdot \exp \{ -k_0 p''_{cj} x - k_0 \beta''_j z \} \cdot \exp \{ ik_0 p'_{cj} x + ik_0 \beta'_j z - i\omega t \}, \quad (14)$$

$$E_{yj}^+ \Big|_{\substack{x<h \\ x>0}} = A_{fj}^+ \cdot \exp \{ -k_0 p''_{fj} x - k_0 \beta''_j z \} \cdot \exp \{ ik_0 p'_{fj} x + ik_0 \beta'_j z - i\omega t \} + B_{fj}^+ \cdot \exp \{ k_0 p''_{fj} x - k_0 \beta''_j z \} \cdot \exp \{ -ik_0 p'_{fj} x + ik_0 \beta'_j z - i\omega t \}, \quad (15)$$

$$E_{yj}^+ \Big|_{x<0} = A_{sj}^+ \cdot \exp \{ k_0 p''_{cj} x - k_0 \beta''_j z \} \cdot \exp \{ -ik_0 p'_{cj} x + ik_0 \beta'_j z - i\omega t \}. \quad (16)$$

Consider the expression (14) in the form of an inhomogeneous wave

$$E_{yj}^+ \Big|_{x>h} = A_{cj}(x, z) \cdot \exp \{ ik_0 p'_{cj} x + ik_0 \beta'_j z - i\omega t \}, \quad (17)$$

where  $A_{cj}(x, z)$  is the amplitude of the inhomogeneous wave defined as

$$A_{cj}(x, z) = A_{cj}^+ \cdot \exp \{ -k_0 p''_{cj} x - k_0 \beta''_j z \}. \quad (18)$$

Consider in more detail the inhomogeneous wave in the form (17) with variable amplitude  $A_{cj}(x, z)$ . If such waveguide parameters exist for which the inhomogeneous wave (17) of some  $j$ -th mode propagates in the direction  $\vec{s}_j = (k_0 p'_{cj}, k_0 \beta'_j)^T$ , along which  $A_{cj}(x, z) \rightarrow 0$ , then such wave will decay (of course, if such direction exists). If a direction  $\vec{s}_j = (k_0 p'_{cj}, k_0 \beta'_j)^T$  exists, along which  $A_{cj}(x, z) = \text{Const}$ , then the wave (17) will become homogeneous and, correspondingly, if a direction  $\vec{s}_j = (k_0 p'_{cj}, k_0 \beta'_j)^T$  exists, along which

$A_{cj}(x, z) \rightarrow \infty$ , then the wave will have infinitely growing amplitude along such a direction.

Consider first the case  $A_{cj}(x, z) = \text{Const}$ . The representation (18) allows choosing a direction in the plane  $xOz$ , along which  $A_{cj}(x, z) = \text{Const}$ . This direction is described by the equation  $-k_0 p''_{cj} x - k_0 \beta''_j z = 0$ . The symmetric direction  $k_0 p''_{cj} x - k_0 \beta''_j z = 0$  will be responsible for the constant amplitude of the inhomogeneous wave, corresponding to Eq. (16). The domain above the line  $-k_0 p''_{cj} x - k_0 \beta''_j z = 0$  corresponds to the domain of the amplitude growth, as well as the domain below the line  $k_0 p''_{cj} x - k_0 \beta''_j z = 0$  (see Figure 2).

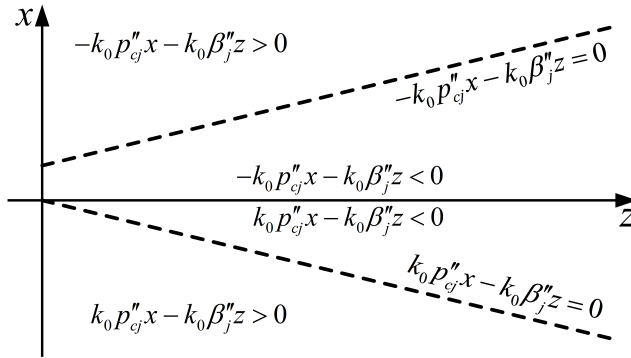


Figure 2. Amplitude growth/attenuation regions and a constant amplitude line of an inhomogeneous plane wave on  $xOz$  plane

The region of existence of leaky modes corresponding to non-uniform waves with non-increasing amplitude is shown in Figure 2 (the cone between two dashed lines). Namely, if the wave vector of the non-uniform wave is located in the cone between two dashed lines, then this leaky mode has a non-increasing amplitude and can propagate in the positive direction of the  $z$ -axis.

Let us consider the inhomogeneous wave (14) in more detail. As shown in Appendix (see (22)), in the region  $k_0 p''_{cj} x + k_0 \beta''_j z < 0$  of a non-uniform wave the amplitude will increase indefinitely, therefore we will consider the wave (14) in the region  $k_0 p''_{cj} x + k_0 \beta''_j z \geq 0$ , see Figure 2. This exponential growth is real within a limited transverse distance surrounding the origin [49]. Using conservation of energy flux, one can show [49] that any mode that decreases exponentially as it propagates must increase exponentially transverse to the direction of propagation. However, it is evident that exponential growth of the field (and mode energy) that extends to infinity is unphysical since we have a finite energy source. A more detailed analysis of this problem is beyond the scope of our paper.

## 5. Numerical analysis of leaky modes of symmetric three-layer waveguides

Let us proceed to numerical analysis of the obtained representation of the leaky modes (14)–(16). Since the structure of the waveguide under

consideration is symmetric, it is sufficient to consider only Eq. (14). We give in Figure 3 the calculated values of the complex phase deceleration coefficient calculated for a waveguide with  $n_c=1.47$ ,  $n_f=1.565$ ,  $\lambda = 0.55 \mu\text{m}$  and  $h = 1.1\lambda$ .

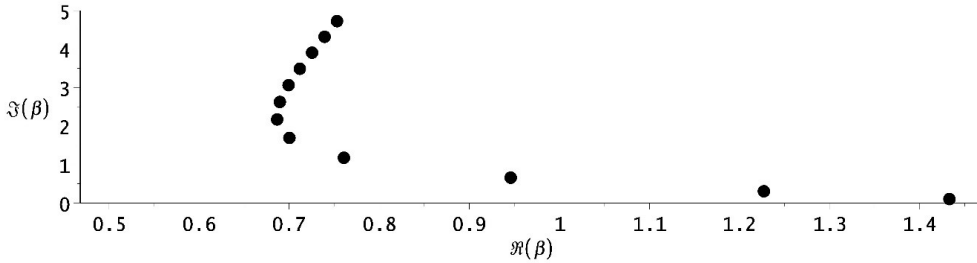


Figure 3. Complex eigenvalues corresponding to the leaky modes of a symmetric waveguide

Let us analyze the distribution of the electric field strength of the first three leaky modes at a fixed point in time.

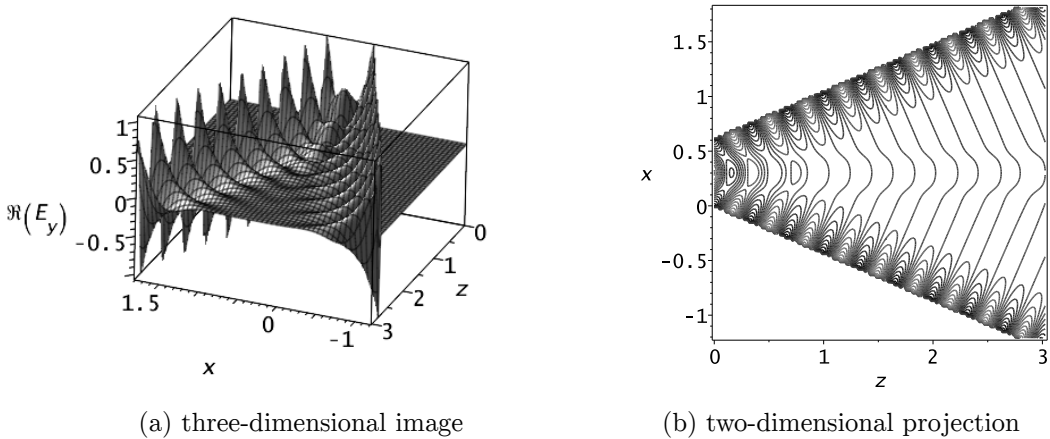


Figure 4. The real part  $E_y(x, z, t^*)$  for the first leaky mode

As seen from Figure 4, the field is concentrated in a cone formed by lines of constant amplitude, and the maximum intensity is observed at the boundaries of the cone where the amplitude is maximal. Outside the cone, there is an area of infinite growth of the amplitude of inhomogeneous waves represented by Eqs. (14)–(16); in this area the inhomogeneous waves characterizing the leaky mode in cladding layers cannot exist.

Inside the guiding layer, on the contrary, the field represented by Eqs. (14)–(16) attenuates rather rapidly and becomes almost completely damped at a distance of several wavelengths. The fields in the coating layer and the substrate are inhomogeneous waves, whose amplitudes decay exponentially the stronger, the smaller the distance to the waveguide layer. Due

to the rapid attenuation of the field in the waveguide layer and the gradual removal (escape) of inhomogeneous waves, which characterize the behavior of the leaky mode in the cladding layers, one can observe a virtual “separation” of the leaky mode from the waveguide layer. A similar “separation” is also characteristic of higher leaky modes (see Figures 5, 6).

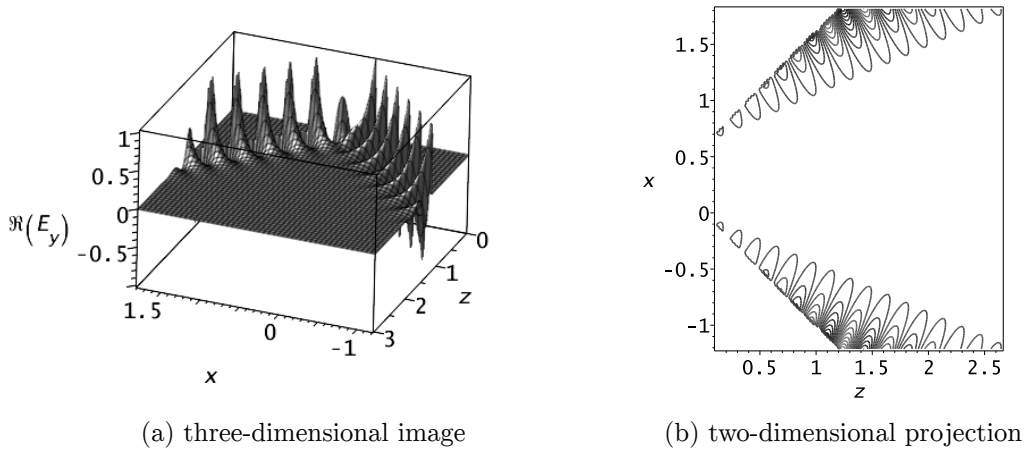


Figure 5. The real part  $E_y(x, z, t^*)$  for the second leaky mode

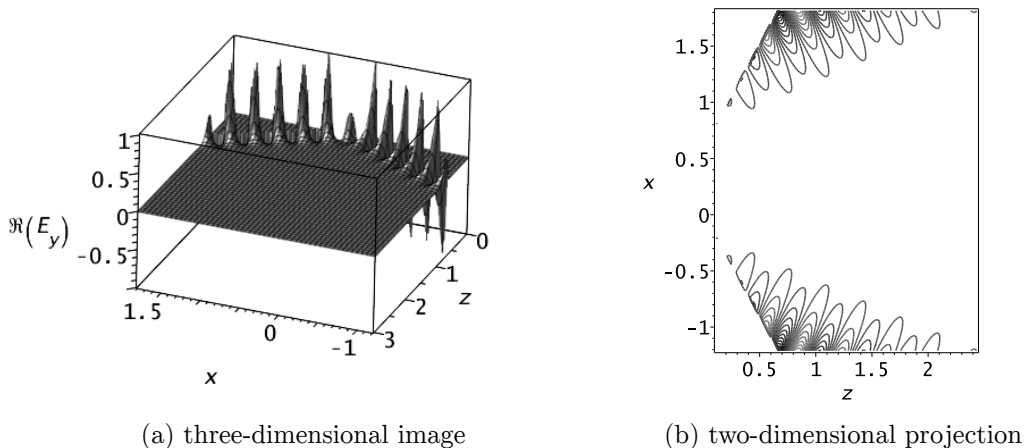


Figure 6. The real part  $E_y(x, z, t^*)$  for the third leaky mode

Further propagation of the emerging mode occurs outside the waveguide layer in the direction of the corresponding wave vectors in the upper and lower cladding layers. The leaky mode will propagate at an angle  $\theta_j =$

$\arctg\left(\frac{\operatorname{Re}(p_{cj})}{\operatorname{Re}(\beta_j)}\right)$  in the top layer and at an angle  $-\theta_j$  in the substrate in the form of two independent inhomogeneous waves.

We also note that experimental data on the propagation of leaky modes, which qualitatively agree with the results obtained by us, are given in [50] (see Figures 4(b), 5(b), 6(b)). In the experimental studies given in [50], leaky modes also propagate in a cone, and are also characterized by the presence of “separation” of the leaky mode from the waveguide layer.

It is commonly assumed that for the leaky modes the amplitude increases with the distance  $x$  from the waveguide along the vertical axis (at a fixed longitudinal distance  $z$  and in the absence of losses in the waveguide). However, as it propagates along the axis  $z$ , this mode decays due to permanent energy losses from the waveguide layer to the environment. Functionally, the fields of leaky modes (vertical profile) are identical to the fields of ordinary guided modes; however, since unlike normal guided (homogeneous) modes, the leaky modes are inhomogeneous waves. In this regard, the representation of leaky waves of planar waveguides using the solutions of the wave equation seems to be preferable for us, compared to the traditionally used representation using the solutions of the Helmholtz equation.

At the same time, some features were revealed that we plan to analyze in our further publications. It is important to emphasize that the region of existence of leaky modes corresponding to inhomogeneous waves with non-increasing amplitude is detected (the cone between two dashed lines in Figure 2). Moreover, if the wave vector of an inhomogeneous wave is located in the region of the cone between two dashed lines, then such a leaky mode has a non-increasing amplitude and can propagate for a sufficiently long distance in the waveguide without absorption.

## 6. Conclusion

As is well known, conventional guided modes that exist when the waveguide layer thickness is above the critical value are considered in the optical beam representation as plane waves propagating in a regular waveguide due to the total internal reflection of waves at the interfaces between the waveguide media. From this point of view, the leaky waves propagate due to the effect of disturbed total internal reflection: during each act of disturbed total reflection at the interfaces of the media forming the waveguide, some of the power of this guided mode is radiated, i.e. “flows out” into the space surrounding the waveguide.

It is important to emphasize that the number of leaky modes with a gradual leakage is limited, unlike the continuum of radiative modes. The resulting gradual leakage waves form a discrete spectrum and are plane inhomogeneous waves. On the contrary, the radiative modes form a continuum (their spectrum is continuous) and are plane homogeneous waves. As a result, the replacement of one kind of these waves with another kind requires serious analysis in each specific case. From this point of view, the methods developed by us are undoubtedly useful for theoretical and numerical studies of dielectric and, in particular, optical waveguides supporting leaky modes, for example, when

used as basic elements in the development of advanced sensors or various interface elements in integrated optical processors.

## Acknowledgement

The publication funded by RFBR according to the research projects no. 18-07-00567, no. 18-51-18005, and no. 19-01-00645.

## Appendix

Consider a wave similar to a plane monochromatic wave, but having a complex wave vector  $\vec{k} = \begin{pmatrix} k'_x + ik''_x \\ k'_z + k''_z \end{pmatrix}$ , that can be represented as a non-uniform plane wave:

$$U(x, z, t) = C \cdot e^{ik'_x x + ik'_z z - i\omega t} \cdot e^{-k''_x x - k''_z z}. \quad (19)$$

Lines of equal phase will be given by equations  $k'_x x + k'_z z = \text{Const}$ . Lines of equal amplitude will be given by equations  $k''_x x + k''_z z = \text{Const}$ . Lines of equal phase and equal amplitude will be orthogonal to each other in non-absorbing media due to the fact that  $k_x^2 + k_z^2 = k^2$ , where  $k$  is the wave number corresponding to the medium in which the wave propagates.

In more detail:  $k_x'^2 + k_z'^2 - k_x''^2 - k_z''^2 + 2i k'_x k''_x + 2i k'_z k''_z = k^2$  and equating the imaginary parts of the quantities in the right-hand and left-hand sides of this equality, we obtain a condition  $k'_x k''_x + k'_z k''_z = 0$  that represents the scalar product of vectors  $\vec{k}' = \text{Re}(\vec{k})$  and  $\vec{k}'' = \text{Im}(\vec{k})$ , which is zero, therefore

$$\vec{k}' \perp \vec{k}''. \quad (20)$$

### Transition to phase-ray coordinates

We introduce new coordinates attached to the lines of constant phase and constant amplitude:

$$\begin{cases} \xi = k'_x x + k'_z z \\ \eta = k''_x x + k''_z z \end{cases} \quad (21)$$

By virtue of the previously established orthogonality property (20), the introduced coordinate system will be orthogonal. In the coordinates  $\xi\eta$ , the form of the considered inhomogeneous plane wave (19) is considerably simplified:

$$U(\xi, \eta, t) = C \cdot e^{-\eta} \cdot e^{i\xi - i\omega t}. \quad (22)$$

In the new variables, according to (22), the amplitude of the inhomogeneous wave under consideration decreases along the positive direction of the axis  $O\eta$ . For each fixed  $\eta = q > 0$  the non-uniform wave is characterized by the amplitude  $C \cdot e^{-q}$  and the behavior harmonic along  $\xi$  (see Figure 7).

For each fixed  $\xi = p$ , the amplitude of the non-uniform wave decreases in the positive direction of the axis  $O\eta$  (see Figure 7).

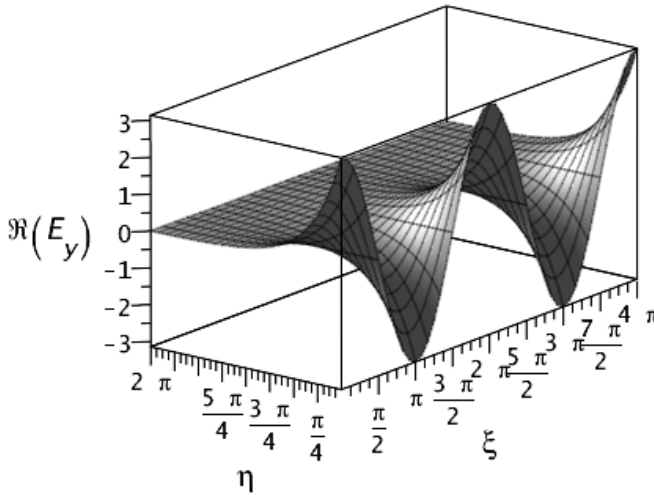


Figure 7. Profile of a leaky waveguide wave (mode) in phase-ray coordinates

In the half-plane  $\eta < 0$ , the amplitude of the non-uniform wave will increase indefinitely, therefore from the physical point of view the half-plane  $\eta < 0$  corresponds to the so-called shadow region of the non-uniform wave under consideration.

The proposed representation of a wave with a complex wave vector in the form of an inhomogeneous plane wave and the subsequent introduction of phase-ray coordinates clearly demonstrate the essential properties of such waves and will be further used to analyze leaky waves.

## References

- [1] D. Marcuse, *Light Transmission Optics*. New York: Van Nostrand Reinhold, 1972.
- [2] D. Marcuse, *Theory of Dielectric Optical Waveguides*. New York: Academic, 1973.
- [3] M. Adams, *An Introduction to Optical Waveguides*. Chichester: Wiley, 1981.
- [4] A. Snyder and J. D. Love, *Optical Waveguide Theory*. London: Chapman and Hall, 1983.
- [5] T. Tamir, *Integrated Optics*. Berlin: Springer-Verlag, 1982.
- [6] L. O. Goldstone and A. A. Oliner, "Leaky-wave antennas i: Rectangular waveguides," *IRE Transactions on Antennas and Propagation*, vol. 7, no. 4, pp. 307–319, 1959, doi: 10.1109/TAP.1959.1144702.
- [7] L. O. Goldstone and A. A. Oliner, "Leaky-wave antennas ii: Circular waveguides," *IRE Transactions on Antennas and Propagation*, vol. 9, no. 3, pp. 280–290, 1961, doi: 10.1109/TAP.1961.1144995.

- [8] T. Tamir and A. A. Oliner, “Guided complex waves, part i: Fields at an interface,” *Proc. inst. Elec. Eng.*, vol. 110, no. 2, pp. 310–324, 1963, doi: 10.1049/piee.1963.0044.
- [9] T. Tamir and A. A. Oliner, “Guided complex waves, part ii: Relation to radiation patterns,” *Proc. inst. Elec. Eng.*, vol. 110, no. 2, pp. 325–334, 1963, doi: 10.1049/piee.1963.0045.
- [10] S.-T. Peng and A. Oliner, “Guidance and leakage properties of a class of open dielectric waveguides: Part i—mathematical formulations,” *IEEE Transactions on Microwave Theory and Techniques*, vol. 29, no. 9, pp. 843–855, 1981, doi: 10.1109/TMTT.1981.1130465.
- [11] A. Oliner, S.-T. Peng, T.-I. Hsu, and A. Sanchez, “Guidance and leakage properties of a class of open dielectric waveguides: Part ii—new physical effects,” *IEEE Transactions on Microwave Theory and Techniques*, vol. 29, no. 9, pp. 855–869, 1981, doi: 10.1109/TMTT.1981.1130466.
- [12] F. Tamir and F. Y. Kou, “Varieties of leaky waves and their excitation along multilayered structures,” *IEEE Journal of Quantum Electronics*, vol. 22, no. 4, pp. 544–551, 1986, doi: 10.1109/JQE.1986.1072991.
- [13] R. Sammut and A. W. Snyder, “Leaky modes on a dielectric waveguide: Orthogonality and excitation,” *Applied optics*, vol. 15, no. 4, pp. 1040–1044, 1976, doi: 10.1364/AO.15.001040.
- [14] R. Sammut, C. Pask, and A. W. Snyder, “Excitation and power of the unbound modes within a circular dielectric waveguide,” *Proc. inst. Elec. Eng.*, vol. 122, no. 1, pp. 25–33, 1975, doi: 10.1049/piee.1975.0004.
- [15] R. Sammut and A. Snyder, “Contribution of unbound modes to light absorption in visual photoreceptors,” *J. Opt. Soc. Am.*, vol. 64, no. 12, pp. 1171–1174, 1974, doi: 10.1364/JOSA.64.001711.
- [16] A. W. Snyder, “Leaky-ray theory of optical waveguides of circular cross section,” *Appl. Phys.*, vol. 4, pp. 273–298, 1974, doi: 10.1007/BF00928381.
- [17] A. W. Snyder and D. J. Mitchell, “Leaky rays on circular optical fibers,” *J. Opt. Soc. Am.*, vol. 69, no. 5, pp. 599–607, 1974, doi: 10.1364/JOSA.64.000599.
- [18] A. W. Snyder and D. J. Mitchell, “Leaky mode analysis of circular optical waveguides,” *Optoelectronics*, vol. 6, pp. 287–296, 1974, doi: 10.1007/BF01423378.
- [19] W. W. Hansen, “Radiating electromagnetic waveguide,” [U.S. Patent No. 2 402 622], 1940.
- [20] S. Barone, “Leaky wave contributions to the field of a line source above a dielectric slab,” Microwave Research Institute, Polytechnic Institute of Brooklyn, Report R-532-546, PIB-462, 1956.
- [21] S. Barone and A. Hessel, “Leaky wave contributions to the field of a line source above a dielectric slab—part ii,” Microwave Research Institute, Polytechnic Institute of Brooklyn, Report R-698-58, PIB-626, 1958.

- [22] E. S. Cassedy and M. Cohn, "On the existence of leaky waves due to a line source above a grounded dielectric slab," *IRE Trans. Microwave Theory Tech.*, vol. 9, no. 3, pp. 243–247, 1961, doi: 10.1109/TMTT.1961.1125314.
- [23] N. Marcuvitz, "On field representations in terms of leaky modes or eigenmodes," *IRE Trans. Antennas Propag.*, vol. 4, no. 3, pp. 192–194, 1956, doi: 10.1109/TAP.1956.1144410.
- [24] V. V. Shevchenko, "On the behavior of wave numbers beyond the critical value for waves in dielectric waveguides (media with losses)," *Radiophys. Quantum Electron.*, vol. 15, pp. 194–200, 1972, doi: 10.1007/BF02209117.
- [25] V. V. Shevchenko, "The expansion of the fields of open waveguides in proper and improper modes," *Radiophys. Quantum Electron.*, vol. 14, no. 8, p. 972, 1974, doi: 10.1007/BF01029499.
- [26] A. A. Egorov, "Theoretical and numerical analysis of propagation and scattering of eigen- and non-eigenmodes of an irregular integrated-optical waveguide," *Quantum Electronics*, vol. 42, no. 4, pp. 337–344, 2012, doi: 10.1070/QE2012v042n04ABEH014809.
- [27] K. Ogusu, M. Miyag, and S. Nishida, "Leaky te modes in an asymmetric three-layered slab waveguide," *J. Opt. Soc. Am.*, vol. 70, no. 1, pp. 68–72, 1980, doi: 10.1364/JOSA.70.000048.
- [28] S. Yamaguchi, A. Shimojima, and T. Hosono, "Analysis of leaky modes supported by a slab waveguide," *Electronics and Communications in Japan*, vol. 73, no. 11, pp. 20–31, 1990, doi: 10.1002/ecjb.4420731103.
- [29] E. Anemogiannis, E. N. Glytsis, and T. K. Gaylord, "Determination of guided and leaky modes in lossless and lossy planar multilayer optical waveguides: Reflection pole method and wavevector density method," *J. Lightwave Technol.*, vol. 17, no. 5, pp. 929–941, 1999, doi: 10.1109/50.762914.
- [30] J. Petracek and K. Singh, "Determination of leaky modes in planar multilayer waveguides," *IEEE Photon. Technol. Lett.*, vol. 14, no. 6, pp. 810–812, 2002, doi: 10.1109/LPT.2002.1003101.
- [31] A. G. Rzhhanov and S. E. Grigas, "Numerical algorithm for waveguide and leaky modes determination in multilayer optical waveguides," *Technical Physics*, vol. 55, no. 11, pp. 1614–1618, 2010, doi: 10.1134/S1063784210110113.
- [32] A. B. Manenkov, "Orthogonality conditions for leaky modes," *Radiophysics and Quantum Electronics*, vol. 48, pp. 348–360, 2005, doi: 10.1007/s11141-005-0076-8.
- [33] A. A. Romanenko and A. B. Sotskii, "The solution of the dispersion relations for planar waveguides in the case of complex roots," *Tech. Phys.*, vol. 43, no. 4, pp. 427–433, 1998, doi: 10.1134/1.1258999.
- [34] E. I. Golant and K. M. Golant, "New method for calculating the spectra and radiation losses of leaky waves in multilayer optical waveguides," *Technical Physics*, vol. 51, no. 8, pp. 1060–1068, 2006, doi: 10.1134/S1063784206080160.

- [35] A. B. Sotsky, L. Steingart, J. Jackson, and et al., “Prism excitation of leaky modes of thin films,” *Tech. Phys.*, vol. 58, no. 11, pp. 1651–1660, 2013, doi: 10.1134/S106378421311025X.
- [36] G. Gamow, “Zur quantentheorie des atomkernes,” *Z. Phys.*, vol. 51, pp. 204–212, 1928, doi: 10.1007/BF01343196.
- [37] O. Civitarese and M. Gadella, “Physical and mathematical aspects of gamow states,” *Phys. Rep.*, vol. 396, no. 2, pp. 41–113, 2004, doi: 10.1016/j.physrep.2004.03.001.
- [38] A. J. F. Siegert, “On the derivation of the dispersion formula for nuclear reactions,” *Phys. Rev.*, vol. 56, pp. 750–752, 1939, doi: 10.1103/PhysRev.56.750.
- [39] O. I. Tolstikhin, V. N. Ostrovsky, and H. Nakamura, “Siegert pseudo-states as a universal tool: Resonances, s matrix, green function,” *Phys. Rev. Lett.*, vol. 79, pp. 2026–2029, 1997, doi: 10.1103/PhysRevLett.79.2026.
- [40] O. I. Tolstikhin, V. N. Ostrovsky, and H. Nakamura, “Siegert pseudostate formulation of scattering theory: One-channel case,” *Phys. Rev. A*, vol. 58, pp. 2077–2096, 1998, doi: 10.1103/PhysRevA.58.2077.
- [41] D. Stowell and J. Tausch, “Guided and leaky modes of planar waveguides: Computation via high order finite elements and iterative methods,” *PIERS Online*, vol. 6, no. 7, pp. 669–673, 2010, doi: 10.2529/PIERS091216124247.
- [42] D. Divakov, A. Tiutiunnik, and A. Sevastianov, “Symbolic-numeric computation of the eigenvalues and eigenfunctions of the leaky modes in a regular homogeneous open waveguide,” *MATEC Web of Conferences*, vol. 186, p. 01 009, 2018, doi: 10.1051/mateconf/201818601009.
- [43] R. E. Bellman, *Introduction to matrix analysis*. New York: McGraw-Hill, 1960.
- [44] J. E. Dennis and R. B. Schnabel, *Numerical Methods for Unconstrained Optimization and Nonlinear Equations*. Prentice Hall, 1983.
- [45] R. Fletcher, *Practical Methods of Optimization*, 2nd. Wiley, 1987.
- [46] J. Nocedal and S. Wright, *Numerical Optimization*, 2nd. Springer, 2006.
- [47] J. Zhu and Y. Y. Lu, “Leaky modes of slab waveguides - asymptotic solutions,” *Journal of Lightwave Technology*, vol. 24, no. 3, pp. 1619–1623, 2006, doi: 10.1109/JLT.2005.863275.
- [48] C. T. Kelley, *Iterative Methods for Optimization*. SIAM, 1999.
- [49] J. Hu and C. R. Menyuk, “Understanding leaky modes: Slab waveguide revisited,” *Advances in Optics and Photonics*, vol. 1, no. 1, pp. 58–106, 2009, doi: 10.1364/AOP.1.000058.
- [50] A. J. Martinez-Ros, J. L. Gómez-Tornero, F. J. Clemente-Fernandez, and J. Monzo-Cabrera, “Microwave near-field focusing properties of width-tapered microstrip leaky-wave antenna,” *IEEE Trans. on Antennas and Propagation*, vol. 61, no. 6, pp. 2981–2990, 2013, doi: 10.1109/TAP.2013.2252138.

**For citation:**

D. V. Divakov, A. A. Egorov, K. P. Lovetskiy, L. A. Sevastianov, A. S. Drevitskiy, Leaky waves in planar dielectric waveguide, *Discrete and Continuous Models and Applied Computational Science* 27 (4) (2019) 325–342. DOI: 10.22363/2658-4670-2019-27-4-325-342.

**Information about the authors:**

**Dmitriy V. Divakov** — Candidate of Physical and Mathematical Sciences, assistant of Department of Applied Probability and Informatics of Peoples' Friendship University of Russia (RUDN University) (e-mail: [divakov-dv@rudn.ru](mailto:divakov-dv@rudn.ru), phone: +7(495)9550783, ORCID: <https://orcid.org/0000-0001-5944-6187>, ResearcherID: N-3949-2013, Scopus Author ID: 55091105300)

**Alexandre A. Egorov** — Doctor of Physical and Mathematical Sciences, Chief Researcher of Department of Oscillations of A. M. Prokhorov General Physics Institute (e-mail: [yegorov@kapella.gpi.ru](mailto:yegorov@kapella.gpi.ru), phone: +7(499)1350210, ORCID: <https://orcid.org/0000-0002-1999-3810>, ResearcherID: F-4681-2012, Scopus Author ID: 7202362326)

**Konstantin P. Lovetskiy** (Russian Federation) — Associate Professor, Ph.D., Associate Professor of Department of Applied Probability and Informatics of Peoples' Friendship University of Russia (RUDN University) (e-mail: [lovetskiy-kp@rudn.ru](mailto:lovetskiy-kp@rudn.ru), phone: +7(495)9522572, ORCID: <https://orcid.org/0000-0002-3645-1060>, ResearcherID: A-5725-2017, Scopus Author ID: 18634692900)

**Leonid A. Sevastianov** (Russian Federation) — professor, Doctor of Physical and Mathematical Sciences, professor of Department of Applied Probability and Informatics of Peoples' Friendship University of Russia (RUDN University); leading researcher of the Bogoliubov Laboratory of Theoretical Physics (e-mail: [sevastianov-la@rudn.ru](mailto:sevastianov-la@rudn.ru), phone: +7(495)9522572, ORCID: <https://orcid.org/0000-0002-1856-4643>, ResearcherID: B-8497-2016, Scopus Author ID: 8783969400)

**Andrey S. Drevitskiy** — PhD student of Department of Applied Probability and Informatics of Peoples' Friendship University of Russia (RUDN University) (e-mail: [drevitskiy-as@rudn.ru](mailto:drevitskiy-as@rudn.ru), phone: +7(495)9550783, Scopus Author ID: 57198778786)

УДК 519.6

PACS 07.05.Tr

DOI: 10.22363/2658-4670-2019-27-4-325-342

## Вытекающие моды в планарных диэлектрических волноводах

Д. В. Диваков<sup>1</sup>, А. А. Егоров<sup>2</sup>, К. П. Ловецкий<sup>1</sup>,  
Л. А. Севастьянов<sup>1,3</sup>, А. С. Древицкий<sup>1</sup>

<sup>1</sup> Кафедра прикладной информатики и теории вероятностей  
Российский университет дружбы народов  
ул. Миклухо-Маклая, д. 6, Москва, 117198, Россия

<sup>2</sup> Институт общей физики имени А.М. Прохорова Российской академии наук  
ул. Вавилова, д. 38, Москва, 119991, Россия

<sup>3</sup> Лаборатория теоретической физики  
Объединённый институт ядерных исследований  
ул. Жолио-Кюри, д. 6, г. Дубна, Московская область, 141980, Россия

В работе предложено новое аналитическое и численное решение волноводной задачи для вытекающих мод планарного диэлектрического симметричного волновода. В качестве асимптотических граничных условий использовались граничные условия, соответствующие модели Гамова–Зигерта. Поставленная начально-краевая задача допускает разделение переменных. Возникающая в результате разделения переменных задача отыскания собственных мод открытых трёхслойных волноводов формулируется как задача Штурма–Лиувилля с соответствующими граничными и асимптотическими условиями. В случае направляемых и излучательных мод задача Штурма–Лиувилля является самосопряжённой, поэтому её собственные значения — действительные величины для диэлектрических сред. Поиск собственных значений и собственных функций, соответствующих вытекающим модам, сопряжён с рядом трудностей: задача на собственные значения и собственные функции не является самосопряжённой, поэтому собственные значения являются комплексными величинами, таким образом, задача нахождения собственных значений и собственных функций связана с нахождением комплексных корней нелинейного дисперсионного уравнения. В работе для решения этой задачи использовался метод минимизации нулевого порядка. В работе дан анализ рассчитанных распределений напряжённости электрического поля первых трёх вытекающих мод, показывающий возможности и преимущества предложенного подхода.

**Ключевые слова:** интегральная оптика, волновод, задача Штурма–Лиувилля, дисперсионное соотношение, вытекающие моды, компьютерное моделирование

UDC 519.7, 338.67

DOI: 10.22363/2658-4670-2019-27-4-343-354

# Vine copulas structures modeling on Russian stock market

Eugeny Yu. Shchetinin

*Department of Data Analysis, Decision Making and Financial Technologies  
Financial University under the Government of Russian Federation  
49, Leningradsky Prospect, Moscow 125993, Russian Federation*

(received: March 5, 2019; accepted: December 30, 2019)

Pair-copula constructions have proven to be a useful tool in statistical modeling, particularly in the field of finance. The copula-based approach can be used to choose a model that describes the dependence structure and marginal behaviour of the data in efficient way, but is usually applied to pairs of securities. In contrast, vine copulas provide greater flexibility and permit the modeling of complex dependency patterns using the rich variety of bivariate copulas which may be arranged and analysed in a tree structure. However, the number of possible configurations of a vine copula grows exponentially as the number of variables increases, making model selection a major challenge in development. So, to learn the best possible model, one has to identify the best possible structure, which necessitates identifying the connections between the variables and selecting between the multiple bivariate copulas for each pair in the structure.

This paper features the use of regular vine copulas in analysis of the co-dependencies of four major Russian Stock Market securities such as Gazprom, Sberbank, Rosneft and FGC UES, represented by the RTS index. For these stocks the D-vine structures of bivariate copulas were constructed, which models are described by Gumbel, Student, BB1 and BB7 copulas, and estimates of their parameters were obtained. Computer simulations showed a high accuracy of the approximation of the explored data by D-vine structure of bivariate copulas and the effectiveness of our approach in general.

**Key words and phrases:** copula, multivariate models, dependence structure, vines, securities

## 1. Introduction

In the field of financial analysis, finding new useful models and improving the existing ones is a constant struggle. Finding an appropriate multivariate model that efficiently describes the dependence structure as well as marginal behavior of the data being analyzed can be a very challenging task, especially in the case of higher dimensions. The approach that relies on copulas tends to outperform other methods when it comes to financial analysis, for example modeling financial returns.

© Shchetinin E. Y., 2019



This work is licensed under a Creative Commons Attribution 4.0 International License

<http://creativecommons.org/licenses/by/4.0/>

Usually the Student  $n$ -dimensional copula is a good choice for financial data of various kinds [1], and as such deserves special attention. Of course, generally speaking, thorough analysis is needed for the best results – especially if the data being analysed has different behaviour in the tails, in which case the Student copula might not capture the dependence structure very well.

We will be discussing pairwise model into bivariate copulas as laid out by Aas [2]. This approach will let us easily track the parameters relevant to the tail dependence. In order to find the most appropriate approach for our specific case, we will rely on the detailed comparison and overview of different approaches by Berg [3].

The relatively recent concept of vines, introduced by T. Bedford and R. M. Cooke [4], is very relevant to pairwise decomposition of multivariate distributions. Vines essentially a subclass of trees that can be used to efficiently represent a pairwise decomposition. We will focus primarily on  $D$ -vines and canonical vines [5], [6]. Our main source for the elements of copula theory is R. B. Nelsen, H. Joe [7]–[9].

## 2. Basics of copula theory

### Definition (pair-copula)

A *pair-copula* or simply *copula* is a function  $C : [0, 1]^2 \rightarrow [0, 1]$  that satisfies the following properties:

For any  $u, v \in [0, 1]$

- 1)  $C(u, 0) = C(0, v) = 0$ ;
- 2)  $C(u, 1) = u, C(1, v) = v$ .

For any  $u_1, u_2, v_1, v_2 \in [0, 1]$  such that  $u_1 \leq u_2$  and  $v_1 \leq v_2$

- 3)  $C(u_1, v_1) - C(u_1, v_2) - C(u_2, v_1) + C(u_2, v_2) \geq 0$ .

One of the most important theorems of copula theory is Sklar's Theorem. In terms of probability theory, it states that any joint distribution function can be written in terms of marginal (univariate) distribution functions and a copula function that can describe the dependence structure between the random variables.

### Sklar's Theorem.

Let  $X$  and  $Y$  be random variables with distribution functions  $F$  and  $G$ , respectively, and let  $H$  be their joint distribution function. Then there exists a copula  $C : [0, 1]^2 \rightarrow [0, 1]$  such that for any  $x, y \in \overline{\mathbb{R}}$  the following equation is true:

$$H(x, y) = C(F(x), G(y)). \quad (1)$$

If  $F$  and  $G$  are continuous, then  $C$  is unique. If not, then  $C$  is unique only on  $\text{Ran}F \times \text{Ran}G$  (here  $\text{Ran}F$  is the range of  $F$  and  $\text{Ran}G$  is the range of  $G$ ). Conversely, if  $C$  is a copula and  $F$  and  $G$  are distribution functions of  $X$  and  $Y$ , respectively, then  $H$ , defined by (1), is a joint distribution function for the random variables  $X$  and  $Y$ , and  $F$  and  $G$  are marginal distribution functions for  $X$  and  $Y$ , respectively.

It is not hard to describe the  $n$ -dimensional case, as well. But first, we have to define the notions of  $n$ -Box and the  $H$ -volume of an  $n$ -Box and discuss notation.

Let us use the following notation:

$$\mathbf{a} = (a_1, a_2, \dots, a_n) \in \overline{\mathbb{R}}^n, \quad \mathbf{b} = (b_1, b_2, \dots, b_n) \in \overline{\mathbb{R}}^n,$$

$\mathbf{a} \leq \mathbf{b}$  means  $a_k \leq b_k$  for all  $k$  from 1 to  $n$ .

When  $\mathbf{a} \leq \mathbf{b}$  we will use the following notation:

$$[\mathbf{a}, \mathbf{b}] = [a_1, b_1] \times [a_2, b_2] \times \dots \times [a_n, b_n].$$

The construction above is called the  $n$ -box. The vectors of the type  $\mathbf{c} = (c_1, c_2, \dots, c_n)$  where  $c_k$  equals  $a_k$  or  $b_k$  for all  $k$  are called the vertices of the  $n$ -box.

The notion of the  $C$ -volume of the  $n$ -box,  $V[\mathbf{a}, \mathbf{b}]_C$ , is discussed in [10], [11].

**Definition (n-copula)**

An  $n$ -copula is a function  $C : [0, 1]^n \rightarrow [0, 1]$  that satisfies the following properties:

For any  $\mathbf{u} = (u_1, u_2, \dots, u_n)$  in  $[0, 1]^n$

- 1)  $C(\mathbf{u}) = 0$  if any  $u_k = 0$ .
- 2)  $C(\mathbf{u}) = u_k$  if all the coordinates except  $u_k$  are equal to 0.

For any  $\mathbf{a}, \mathbf{b} \in [0, 1]^n$  such that  $\mathbf{a} \leq \mathbf{b}$

- 3)  $V_C[\mathbf{a}, \mathbf{b}] \geq 0$ .

The  $n$ -dimensional version of Sklar’s theorem is discussed in Nelsen [7], and conditional copulas are discussed in Patton [12].

### 3. Decomposition of a multivariate distribution function using pair-copula constructions

The general product rule (also called the chain rule of probability) allows us to decompose a multivariate density function in the following, non-unique way:

$$f_{12\dots n} = f_1 f_{2|1} f_{3|12} \dots f_{n|12\dots n-1}. \tag{2}$$

If we assume that  $F$  is strictly continuous and use the definition of a copula and Sklar’s Theorem, we get

$$f_{12\dots n} = c_{12\dots n} f_1 f_2 \dots f_n. \tag{3}$$

To get to the pair-copula decomposition we will also have to use the useful factorizations of this type:

$$f_{2|1} = \frac{f_1 f_2 c_{12}}{f_1} = c_{12} f_2. \tag{4}$$

$$f_{3|12} = \frac{f_{123}}{f_{12}} = \frac{f_1 f_{23|1}}{f_{2|1} f_1} = \frac{f_{23|1}}{f_{2|1}} = \frac{f_{2|1} f_{3|1} c_{23|1}}{f_{2|1}} = c_{23|1} f_{3|1} = c_{23|1} c_{13} f_3. \tag{5}$$

Now let’s apply (2), (3), (4) and (5) to a 3-dimensional density function to get a pair-copula decomposition:

$$f_{123} = f_1 f_{2|1} f_{3|12} = f_1 c_{12} f_2 c_{23|1} c_{13} f_3 = c_{12} c_{13} c_{23|1} \prod_{i=1}^3 f_i. \tag{6}$$

If we pick another conditioning variable we get another decomposition, for example

$$f_{123} = f_1 f_{2|1} f_{3|12} = f_1 c_{12} f_2 c_{13|2} c_{23} f_3 = c_{12} c_{13|2} c_{23} \prod_{i=1}^3 f_i. \tag{7}$$

The number of possible pair-copula decompositions for a 3-variable density function is 24 [13], [14] and this number rises rapidly with the number of dimensions, which makes it very complicated to find the decomposition that best preserves the known information about the dependence structure. The concept of *vines* is very useful in this regard.

### 4. The concept of vines

Vines are a concept first introduced by Bedford and Cooke [4]. A vine is a sequence of trees  $\{T_i\}$  in which the edges of  $T_i$  are the nodes of  $T_{i+1}$ . Each vine is a representation of a particular way of decomposing a multivariate distribution. The two kinds of common vines that we will use in our work are canonical vines and *D*-vines. Different types of vines represent different types of dependency structures. A canonical vine corresponds to the case where one “main” variable “interacts” with all the others, while in the case of a *D*-vine there is no such “main” variable. This idea is represented in the illustrations provided in Figures 1 and 2.

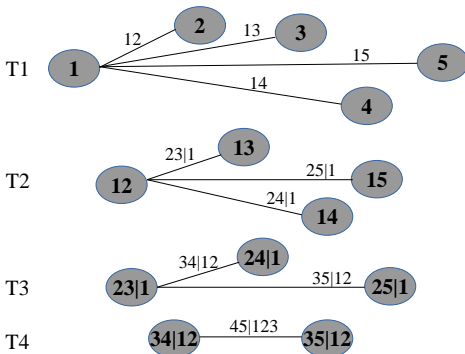


Figure 1. C-vine

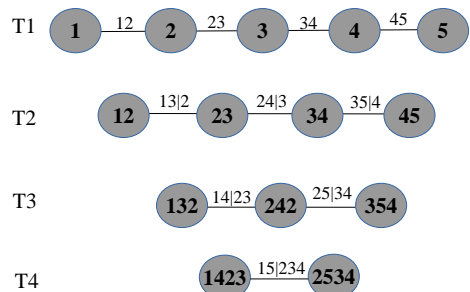


Figure 2. D-vine

The following general formulas give us the expressions for the decomposition of an *n*-dimensional density function using the *D*-vine and the canonical vine:

$$\text{D-vine: } f_{12\dots n} = \prod_{k=1}^n f_k \prod_{j=1}^{n-1} \prod_{i=1}^{n-j} c_{i,i+j|i+1,\dots,i+j-1}. \tag{8}$$

$$\text{Canonical vine: } f_{12\dots n} = \prod_{k=1}^n f_k \prod_{j=1}^{n-1} \prod_{i=1}^{n-j} c_{j,j+i|1,\dots,j-1}. \tag{9}$$

Each edge in each of the trees corresponds to a pair-copula, the density of which is used as one of the multipliers of the pair-copula construction, as we can see in (8) and (9). The first tree,  $T_1$ , should be constructed in a way that best represents the supposed dependence structure of the variables.

Alternative constructions may involve using the copula parameter estimations to get insight into the dependence structure — for example, we could assign a Student-t topula to all the pairs and, knowing that a low number of df indicates strong dependence, could construct a tree that represents that dependence structure.

**Algorithm 1.** Sequential algorithm

**Input:** Data  $(x_{l1}, \dots, x_{ln}, l = 1, \dots, N$  (realization of i.i.d. random vectors).

**Output:** R-vine copula specification, i.e.,  $\mathcal{V}, B$ .

- 1: Calculate the empirical Kendall’s tau  $\hat{\tau}_{j,k}$  for all possible variable pairs  $\{j, k\}, 1 \leq j < k \leq n$ .
- 2: Select the spanning tree that maximizes the sum of absolute empirical Kendall’s taus, i.e.,

$$\max_{e=\{j,k\} \text{ in spanning tree}} \sum \|\hat{\tau}_{j,k}\|.$$

- 3: For each edge  $\{j, k\}$  in the selected spanning tree, select a copula and estimate the corresponding parameter(s). Then transform  $\hat{F}_{j|k}(x_{lj}|x_{lk})$  and  $\hat{F}_{k|j}(x_{lk}|x_{lj}), l = 1, \dots, N$ , using the fitted copula  $\hat{C}_{jk}$  (see (2)).
- 4: **for**  $i = 2, \dots, n - 1$  **do** {Iteration over the trees}
- 5: Calculate the empirical Kendall’s tau  $\hat{\tau}_{j,k|D}$  for all conditional variable pairs  $\{j, k|D\}$  that can be part of tree  $T_i$ , i.e. all edges fulfilling the proximity condition (see Definition 2.1).
- 6: Among these edges, select the spanning tree that maximizes the sum of absolute empirical Kendall’s taus, i.e.,

$$\max_{e=\{j,k|D\} \text{ in spanning tree}} \sum |\hat{\tau}_{j,k|D}|.$$

- 7: For each edge  $\{j, k|D\}$  in the selected spanning tree, select a conditional copula and estimate the corresponding parameter(s). Then transform  $\hat{F}_{j|k \cup D}(x_{lj}|x_{lk}, \mathbf{x}_{lD})$  and  $\hat{F}_{k|j \cup D}(x_{lk}|x_{lj}, \mathbf{x}_{lD}), l = 1, \dots, N$ , using the fitted copula  $\hat{C}_{jk|d}$  (see (2)).
- 8: **end for**

## 5. Numerical experiment: choosing the right vine structure

We will now apply the theory and methods discussed above to the analysis, modeling and visualization of the returns of four major Russian companies. Our data-set consists of the log-returns of Gazprom, Sberbank, Rosneft and FGC UES from 06.06.2014 to 06.06.2018.

We will use the VineCopula package for the R programming language for most of our computational needs [15].

Our main goal is to build a model that best represents core features of our data's dependency structure. We will use the sequential method [13] with Akaike's criterion [11], [16]–[18] (to determine the most appropriate copula families) and one of the versions of Prim's algorithm (to determine maximum spanning trees [19], [20]) to ultimately determine and specify the most appropriate vine structure. We have provided the results below.

Figure 3 illustrates the D-vine structure of our model.

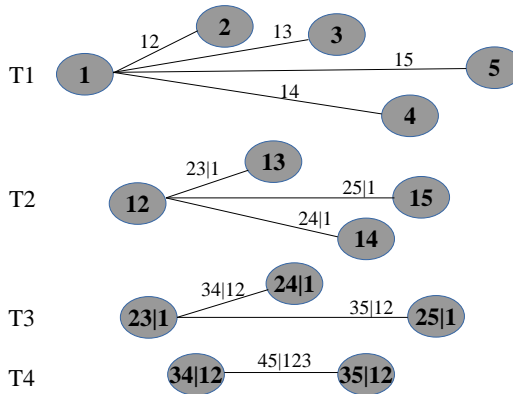


Figure 3. D-vine structure of our model

We also need to verify our model. The verification process involves drawing observations from the vine and comparing the empirical values of Spearman's Rho and some of the plots for the original observations and the sampled observations. In other words, we must observe how well the dependence structure was preserved.

For the sake of brevity, let us denote Rosneft by  $R$ , Gazprom by  $G$ , FGC UES by  $F$  and Sberbank by  $S$ .

Using AIC and MLE we have determined that:

1.  $c_{SF}$  is a rotated BB1 copula with  $\theta = 0.1980236$  and  $\delta = 1.421392$ .
2.  $c_{SG}$  is a rotated BB7 copula with  $\theta = 1.920555$  and  $\delta = 0.7580773$ .
3.  $c_{GR}$  is a rotated BB7 copula with  $\theta = 2.025809$  and  $\delta = 0.9424809$ .
4.  $c_{GR|S}$  is a rotated Gumbel copula with  $\theta = 1.2104850$ .
5.  $c_{SR|G}$  is a t-copula with  $\rho = 0.3746501$  and  $\nu = 6.7874375$ .
6.  $c_{FR|SG}$  is a rotated BB8 copula with  $\theta = 1.4269045$  and  $\delta = 0.8675492$ .

The D-vine tree structure for our model is presented on Fig. 4–6. Corresponding graphs of bivariate copula density models with estimated parameters are shown in Fig. 7.

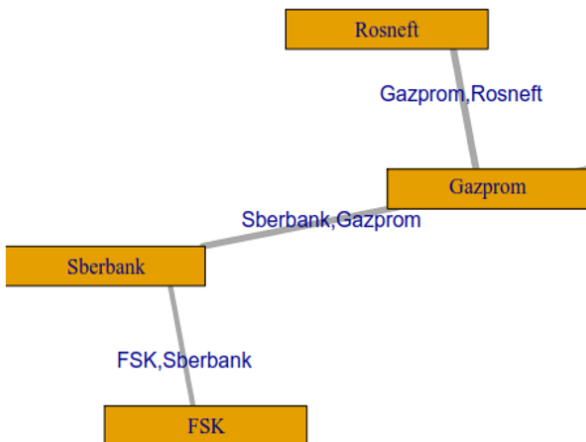


Figure 4. First tree

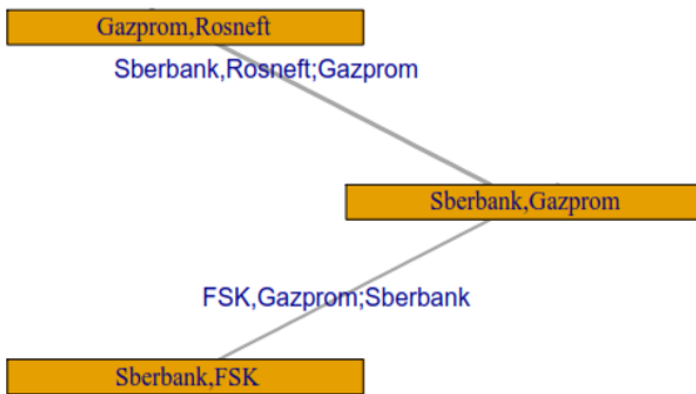


Figure 5. Second tree

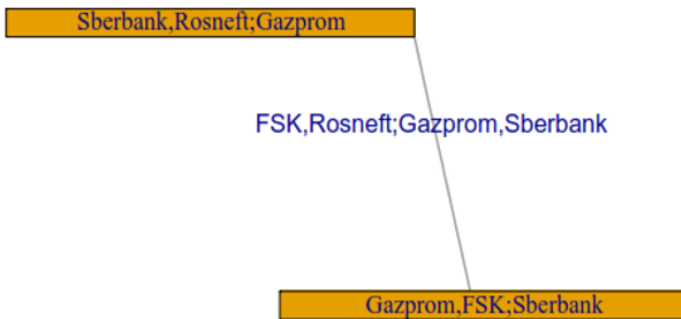


Figure 6. Final tree

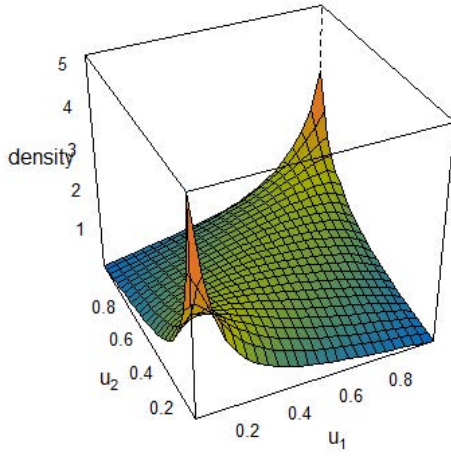
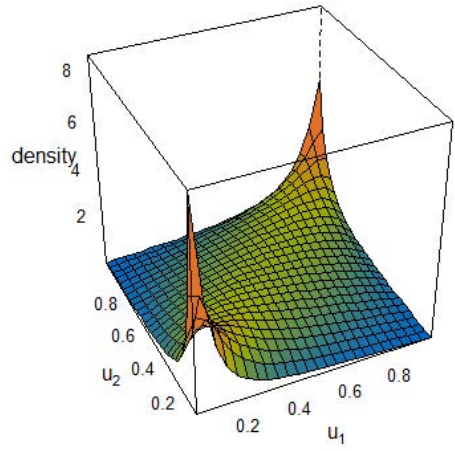
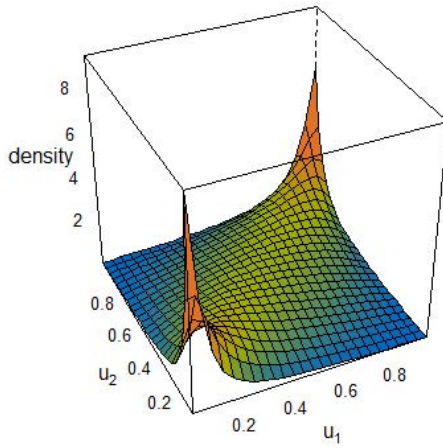
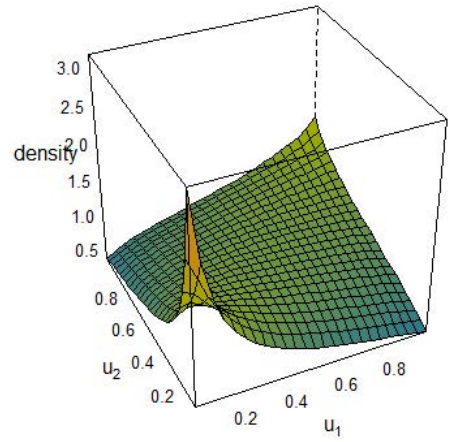
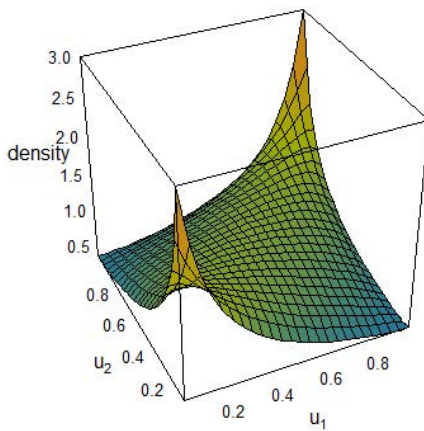
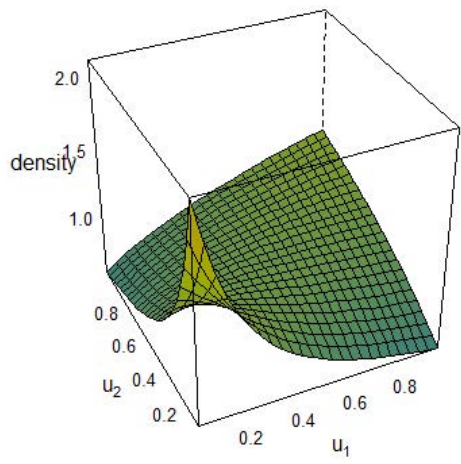
(a)  $c_{SF}$ (b)  $c_{SG}$ (c)  $c_{GR}$ (d)  $c_{GF|S}$ (e)  $c_{SR|G}$ (f)  $c_{FR|SG}$ 

Figure 7. Bivariate copula densities for the vine structure of our model

We drew 1003 observations from our D-vine — the same number as in our real-world dataset and calculated Spearman's rho values, shown below in Table 2. Judging from Table 2 and the overlaid plots, the modeled dependencies were captured in a satisfactory way. Graphical comparison of empirical and simulated data with their scatterplots is presented on Fig. 8.

Table 1  
Empirical Spearman's Rho values  
for the original observations

	G	F	R
S	<b>0.64</b>	<b>0.5</b>	0.63
G	-	0.49	<b>0.67</b>
F		-	0.49

Table 2  
Empirical Spearman's Rho values  
for the observations from sampling

	G	F	R
S	0.6	0.54	0.65
G	-	0.5	0.65
F		-	0.53

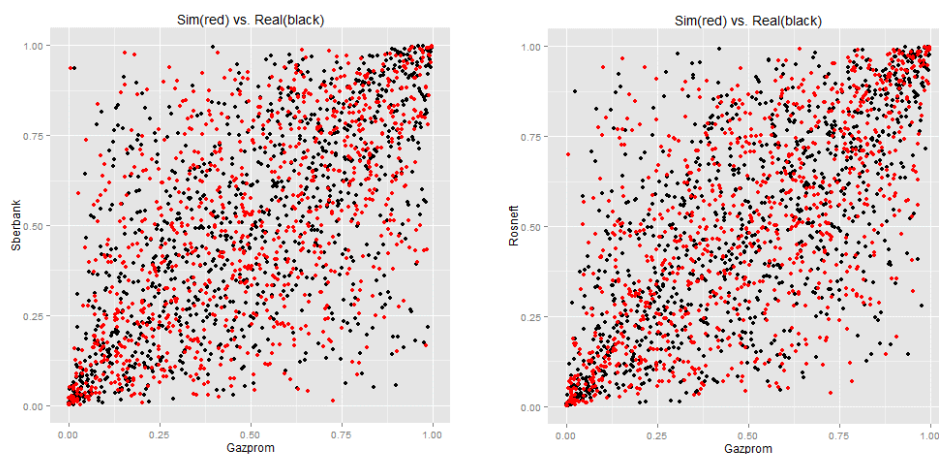


Figure 8. Real and simulated data comparison

## 6. Conclusions

In this paper we have demonstrated the usefulness of the vine copula-based approach to modeling a real-world dataset with a complex dependence structure. We have successfully specified a model that captures some of the essential dependencies that characterize our dataset. In a sense, by focusing, for the sake of brevity, exclusively on C-vines and D-vines and specific methods of copula selection and parameter estimations, we were forced to neglect other approaches which could provide additional insights. Extensive functionality provided by the VineCopula package for the R programming language let us circumvent many computational difficulties, allowing for faster and more efficient analysis.

## References

- [1] K. Aas and I. Hobaek Haff, “The generalized hyperbolic skew Student’s t-distribution,” *Journal of Financial Econometrics*, vol. 4, pp. 275–309, Jan. 2006. DOI: 10.1093/jjfinec/nbj006.
- [2] K. Aas, C. Czado, A. Frigessi, and H. Bakken, “Pair-copula constructions of multiple dependence,” *Insurance: Mathematics and Economics*, vol. 44, no. 2, pp. 182–198, 2009.
- [3] D. Berg, “Copula goodness-of-fit testing: an overview and power comparison,” *European Journal of Finance*, vol. 15, pp. 675–701, 2009. DOI: 10.1080/13518470802697428.
- [4] T. Bedford and R. M. Cooke, “Vines—a new graphical model for dependent random variables,” *The Annals of Statistics*, vol. 30, no. 4, pp. 1031–1068, 2002. DOI: 10.1214/aos/1031689016.
- [5] A. Panagiotelis, C. Czado, H. Joe, and J. Stöber, “Model selection for discrete regular vine copulas,” *Comput. Stat. Data Anal.*, vol. 106, pp. 138–152, 2017. DOI: 10.1016/j.csda.2016.09.007.
- [6] J.-D. Fermanian, “Recent developments in copula models,” *Econometrics*, vol. 5, no. 34, 2017. DOI: 10.3390/econometrics5030034.
- [7] R. B. Nelsen, *An introduction to copulas*. New York: Springer, 1999.
- [8] H. Joe, H. Li, and A. K. Nikoloulopoulos, “Tail dependence functions and vine copulas,” *Journal of Multivariate Analysis*, vol. 101, pp. 252–270, 2010. DOI: 10.1016/j.jmva.2009.08.002.
- [9] H. Joe, “Dependence comparisons of vine copulae with four or more variables,” in *D. Kurowicka and H. Joe (Eds.), Dependence Modeling*. Singapore: World Scientific, 2010.
- [10] A. K. Nikoloulopoulos, H. Joe, and H. Li, “Vine copulas with asymmetric tail dependence and applications to financial return data,” *Computational Statistics and Data Analysis*, vol. 56, no. 11, pp. 3659–3673, 2012.
- [11] *Modeling dependence in econometrics*. Berlin, Heidelberg: Springer Verlag, 2014. DOI: 10.1007/978-3-319-03395-2.
- [12] A. J. Patton, “Modelling asymmetric exchange rate dependence,” *International Economic Review*, vol. 47, no. 2, pp. 527–556, 2006. DOI: 10.1111/j.1468-2354.2006.00387.x.
- [13] E. C. Brechmann, C. Czado, and K. Aas, “Truncated regular vines in high dimensions with application to financial data,” *Canadian Journal of Statistics*, vol. 40, no. 1, pp. 68–85, 2012. DOI: 10.1002/cjs.10141.
- [14] J. Di’smann, E. Brechmann, C. Czado, and D. Kurowicka, “Selecting and estimating regular vine copulae and application to financial returns,” *Computational Statistics & Data Analysis*, vol. 59, pp. 52–69, 2013. DOI: 10.1016/j.csda.2012.09.01.
- [15] E. C. Brechmann and U. Schepsmeier, “Modeling dependence with C- and D-vine copulas: the R package CDVine,” *Journal of Statistical Software*, vol. 52, no. 3, pp. 1–27, 2013. DOI: 10.18637/jss.v052.i03.

- [16] S. Konishi and G. Kitagawa, *Information criteria and statistical modeling*. 2007. DOI: 10.1007/978-0-387-71887-3.
- [17] H. Manner and O. Reznikova, “A survey on time-varying copulas: specification, simulations and application,” *Econometric Reviews*, vol. 31, no. 6, pp. 654–687, 2012. DOI: 10.1080/07474938.2011.608042.
- [18] L. Chollete, A. Heinen, and A. Valdesogo, “Modeling international financial returns with a multivariate regime switching copula,” *J. Financ. Econ.*, vol. 7, pp. 437–480, 2009. DOI: 10.2139/ssrn.1102632.
- [19] T. H. Cormen, C. E. Leiserson, R. L. Rivest, and C. Stein, *Introduction to algorithms, 2nd Edition*. MIT Press, 2001.
- [20] D. E. Allen, M. A. Ashraf, M. McAleer, R. J. Powell, and A. K. Singh, “Financial dependence analysis: applications of vine copulas,” *Statistica Neerlandica*, vol. 67, no. 4, pp. 403–435, 2013. DOI: 10.1111/stan.12015.

**For citation:**

E. Y. Shchetinin, Vine copulas structures modeling on Russian stock market, *Discrete and Continuous Models and Applied Computational Science* 27 (4) (2019) 343–354. DOI: 10.22363/2658-4670-2019-27-4-343-354.

**Information about the authors:**

**Eugeny Yu. Shchetinin** — Doctor of Physical and Mathematical Sciences, lecturer of Department of Data Analysis, Decision Making and Financial Technologies of Financial University under the Government of Russian Federation (e-mail: [riviera-molto@mail.ru](mailto:riviera-molto@mail.ru), phone: +7(917)5390698, ORCID: <https://orcid.org/0000-0003-3651-7629>, ResearcherID: O-8287-2017, Scopus Author ID: 16408533100)

УДК 519.7, 338.67

DOI: 10.22363/2658-4670-2019-27-4-343-354

## Моделирование многомерных структур статистической зависимости на российском фондовом рынке

Е. Ю. Щетинин

*Департамент анализа данных, принятия решений и финансовых технологий  
Финансовый университет при Правительстве Российской Федерации  
Ленинградский проспект, д. 49, Москва, 125993, Россия*

Модели копул являются эффективным инструментом в статистическом моделировании, в частности в области финансового анализа. Подход к моделированию многомерных структур с их использованием позволяет описать как структуру статистической зависимости, так и маргинальные свойства данных, но обычно применяется к парам ценных бумаг. Наряду с этим, модели вьющихся копул обеспечивают большую гибкость и позволяют моделировать сложные структуры зависимостей, используя большое разнообразие двумерных копул, которые могут быть организованы в древовидную структуру. Однако число возможных конфигураций вьющихся копул растёт экспоненциально по мере увеличения числа ценных бумаг, что делает выбор модели основной научной проблемой. Таким образом, чтобы построить модель многомерных структур ценных бумаг, нужно определить наилучшую возможную структуру, которая требует выявления связей между её переменными, а также выбора между несколькими двумерными копулами для каждой пары в структуре.

В данной работе продемонстрировано применение регулярных вьющихся копул в финансовом анализе статистических связей крупнейших российских ценных бумаг, таких как Газпром, Сбербанк, Роснефть и ФСК ЕЭС, представленных в индексе РТС. Для этих ценных бумаг были построены D-vine структуры попарных копул, включающих модели Гумбеля, Стьюдента, BV1 и BV7, а также получены оценки их параметров. Компьютерное моделирование показало высокую точность аппроксимации исследуемых данных и эффективность предложенного подхода в целом.

**Ключевые слова:** финансовый анализ, ценные бумаги, многомерные структуры статистических связей, копулы, вьющиеся копулы

# Mathematical models in Physics

UDC 533.9

DOI: 10.22363/2658-4670-2019-27-4-355-364

## The features of the characteristic electromagnetic plasma bunches oscillations in the long magnetic mirror

Andrey A. Novitskiy, Denis V. Chuprov,  
Vladislav A. Kuznetsov, Eugeniy A. Shevtsov

*Institute of Physical Research and Technologies  
Peoples' Friendship University of Russia (RUDN university)  
6, Miklukho-Maklaya St., Moscow 117198, Russian Federation*

(received: December 20, 2019; accepted: December 30, 2019)

The aim of this work was to study the spectrum of LF and HF oscillations generated by plasma bunches created and confined in the volume of a microwave cavity immersed in the magnetic field of a mirror trap. The registration of electrostatic oscillations in the plasma was carried out using two flat electrodes mounted diametrically opposite in the central part of the cavity close to its wall. This diagnostic showed the presence of low-frequency oscillations with frequencies of 130 kHz and 450 kHz. The oscillation spectrum in the microwave range was recorded at the minimum of the magnetic trap using a real-time spectrometer and a loosely coupled loop antenna. The registration of the spectra in the 40 MHz band revealed a regular change in the frequency of the fundamental oscillation mode of the cavity and the presence of two harmonics of the synchrotron radiation of the plasma bunch at frequencies of 2.25 GHz and 4.52 GHz, respectively. According to the obtained data, the parameters of the formed bunch (density, shape, volume, energy spectra of plasma components) can be restored.

**Key words and phrases:** gyromagnetic autoresonance, plasma bunches, long magnetic mirror trap, electrostatic and electromagnetic oscillations, spectral analysis

## 1. Introduction

The possibility of generating long-lived plasma bunches with an energetic electronic component under conditions of gyromagnetic autoresonance (GA) in the magnetic field of mirror trap in the regime of a reverse magnetic field has been shown previously [1], [2]. In this mode the reverse pulsed magnetic field is created by coils located at the maxima of the electric component of the microwave field of a standing wave and reduced static magnetic strength to a value that corresponds to the classical electron cyclotron resonance (ECR). Then, the current in the pulse coils decreases, resulting in restoration of the initial profile of the magnetic field produced by the stationary magnetic

© Novitskiy A. A., Chuprov D. V., Kuznetsov V. A., Shevtsov E. A., 2019



This work is licensed under a Creative Commons Attribution 4.0 International License

<http://creativecommons.org/licenses/by/4.0/>

coils, and the electrons of the produced ECR plasma become trapped in the autoresonant acceleration mode.

The aim of this work was to study the spectrum of LF and HF oscillations generated by plasma bunches created and confined in the mirror trap within microwave cavity.

## 2. Experimental setup

The experimental setup is a cylindrical microwave cavity placed in an axisymmetric magnetic field of a long mirror trap configuration ( $R = 1.2$ ,  $L = 80$  cm) with magnetic field induction at a trap minimum of 1200 G. A stationary magnetic field is created by three pairs of coaxial coils fed by three DC sources.

The pulsed magnetic field required for the implementation of the GA regime is generated by the pulsed current flowing through a pair of coils axisymmetric with the cavity and the coils of the stationary magnetic field. The coils of the pulsed magnetic field are placed symmetrically with respect to the position of the minimum of the magnetic field in the trap in antinodes of the electric field of a standing wave  $TE_{118}$ -mode. The 3D-design of the experimental setup, together with the axial distribution of the induction of the resulting magnetic field at different times of the current rise time in the reversing coils of the pulsed field, are presented in Figure 1(a).

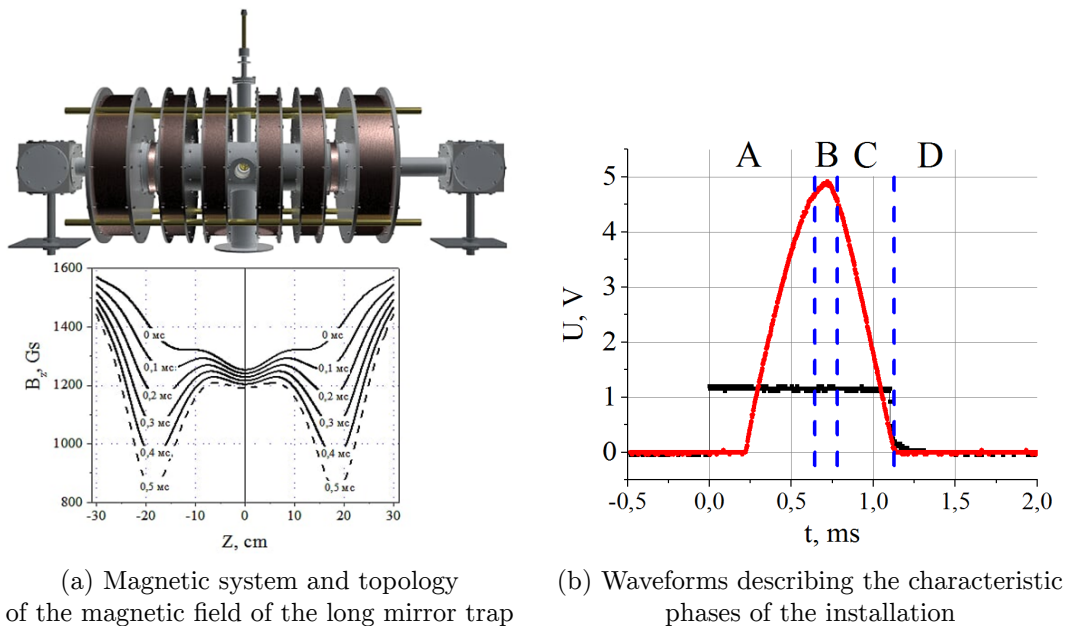


Figure 1. Microwave cavity

The direction of the current in the pulsed coils provides the creation of a pulsed magnetic field with direction of the induction opposite to the induction of the stationary field, thus reducing locally the resulting magnetic field to a level corresponding to the ECR value for the operating frequency.

The reduction of the current in the pulse coils and the restoration of the initial profile of the stationary magnetic field in the presence of the microwave field ensure the trapping and acceleration of the initial plasma electrons into the GA regime and the generation of plasma bunches in two symmetrical zones of the setup. The operating cycle of the setup is a current pulse in pulsed magnetic coils with a duration of  $900 \mu\text{s}$ , synchronized with the forward front of the microwave pulse with a duration of 1.1 ms. The duty cycle of the setup is shown in Figure 1(b): phase A — reduction of the resulting magnetic field to values of the ECR within the two zones of the trap, the phase B — formation of initial plasma under ECR in two local zones of the trap, phase C — mode of GA-effect, stage D — confinement mode of the produced plasma bunch in a stationary field of the mirror trap. The restoration of the initial profile of a stationary magnetic field with small gradients leads to the movement of produced bunches to the region of the minimum of the trap and their accumulation. The unit operates in a pulse-periodic mode with a variable duty of GA-cycle. More detailed information about experimental setup and diagnostic methods can be founded from [3], [4].

Registration of electrostatic oscillations in the plasma was carried out using two flat electrodes flush-mounted with the side wall of the cavity at the midplane. The electrodes are made of the metal disks with a diameter of 12 mm and fixed in the camera ports located in the midplane of the trap, and were oriented parallel to the cavity walls.

The motion of the bunch within the cavity leads to a change in time of the charge induced on the electrostatic probe. The charge distribution in the bunch and its motion dynamics determine the time dependence of the charge induced on the probe. Therefore, by the current taken from the probe through a load resistor of 500 Ohms, one can conclude about the bunch parameters and dynamics.

The oscillation spectrum in the microwave range was obtained at the minimum of the magnetic trap using a loop microwave probe. The time and parametric dependences of the frequencies and amplitudes of the recorded oscillations on various discharge conditions were recorded. Microwave signal processing was performed using a Tektronix RSA-6114A spectrum analyzer.

### 3. Experimental results

Processing the voltage waveforms on the load resistance of the wall electrodes using the fast Fourier transform method showed the presence of low-frequency oscillations with frequencies of 130 kHz and 450 kHz at a pressure of  $P = 1 \cdot 10^{-5}$  Torr, which are observed in the final stage of autoresonance acceleration (delay of  $400 \mu\text{s}$ ) (Figure 2).

The motion of an azimuthal and radially asymmetric plasma bunch in the cavity is accompanied by a complex redistribution of its space charge along all three coordinates. An electrostatic probe registers the integrated picture of the distribution of charge density in the near-probe region. The detected oscillations can be due to both the azimuthal and radial inhomogeneity of the bunch, and its axial displacements [5], [6].

Oscillations in the microwave range were recorded synchronously with the signal from the electrostatic probe. The loop microwave probe was introduced into the resonator port, which is at the minimum of the electric

component of the working mode, which is a transverse circular waveguide located perpendicular to the cavity axis at an angle of  $45^\circ$  to the oscillation plane of the high-frequency field vector  $\mathbf{E}$ .

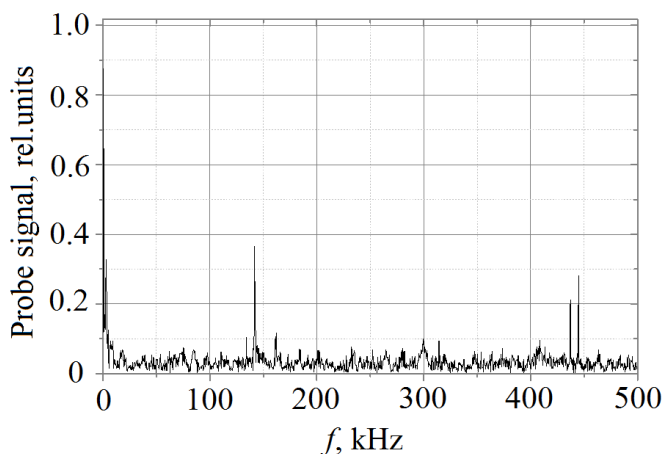
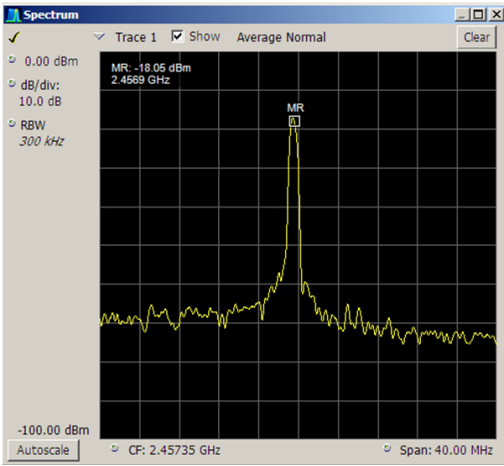


Figure 2. Spectrum of low-frequency oscillations recorded by electrostatic probe placed near the side wall of the cavity in the median plane of the trap

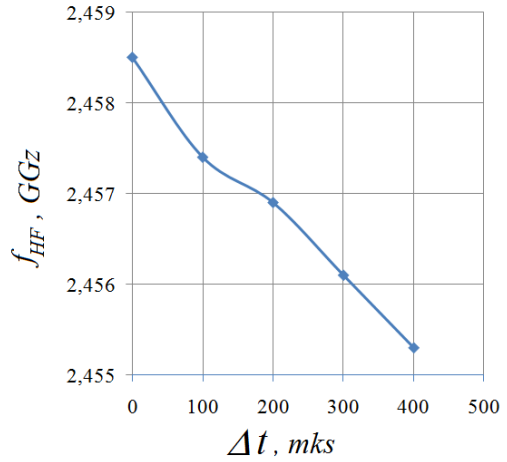
A series of experiments was carried out to obtain high-frequency spectra in the range of the fundamental frequency of oscillations. The measurement results are shown in Figure 3.

A typical spectrogram of high-frequency oscillations at the fundamental frequency of the cavity (Figure 3(a)) illustrates the relatively small magnetron generation bandwidth of the order of 1.5 MHz. The central frequency —  $f_{HF}$  of the recorded spectral range does not remain constant over time. Figure 3(b) shows the dependence of the frequency corresponding to the distribution maximum on the delay  $\Delta t$ . GA process starts when the pulsed magnetic field achieves its maximum value. The delay  $\Delta t$  is the time interval between the moment of maximum value of pulsed magnetic field and the start trigger of spectrum analyzer. The central frequency of the recorded spectral range decreases quasilinearly with increasing delay. It should be noted that this decrease cannot be due to the delay of the magnetron generation frequency when the complex conductivity of the plasma-loaded resonator changes, since the high-frequency channel uses a standard circuit with an insulator based on a circulator with a matched load that absorbs the reflected power.

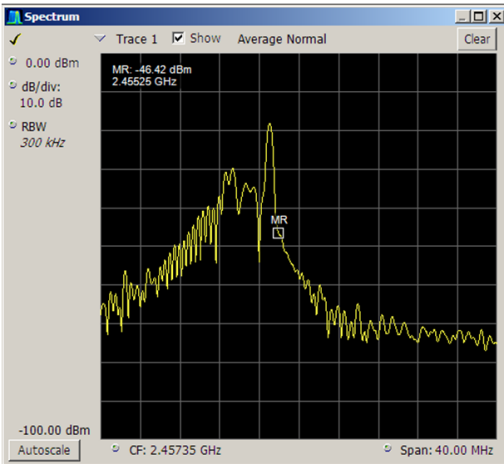
Special attention is required to the spectra obtained under the same conditions near the end of the microwave pump pulse. Figure 3(c) shows the spectrogram obtained with a delay  $\Delta t = 500 \mu s$  — this moment corresponds to the simultaneous end of microwave and magnetic field pulses (the end of phase C in Figure 1(b)). It can be seen that in addition to the magnetron generation line, the spectrum contains many other components whose level is 10 or more dB lower than the signal at the fundamental frequency. This, apparently, is due to the interaction of the standing wave field with bunch particles, which by this time have almost completely formed and begin to shift to the midplane of the mirror trap.



(a) Spectrogram of high-frequency oscillations at the fundamental frequency of the cavity



(b) Dependence of the central distribution frequency  $f_{HF}$  on the duration  $\Delta t$  of the registration delay relative to the maximum of the pulsed magnetic field



(c) Spectrogram of high-frequency oscillations at the fundamental frequency at  $\Delta t = 500 \mu s$



(d) Spectrogram of high-frequency oscillations at  $\Delta t = 510 \mu s$

Figure 3. Typical spectrograms of high-frequency oscillations and dependence of the central distribution frequency  $f_{HF}$  on the duration  $\Delta t$  of the registration delay relative to the maximum of the pulsed magnetic field

Figure 3(d) shows the spectrogram of the signal from the cavity at the moment of  $\Delta t = 510 \mu s$ . In other words, it is  $10 \mu s$  after the end of the pulse of the magnetron generator. It can be seen that the generation of electromagnetic oscillations at frequencies close to the magnetron frequency continues with a finite attenuation rate.

Of particular interest are electromagnetic waves due to the collective motion of the particles of the bunch. In fact, this is synchrotron radiation of the bunch electrons accelerated by autoresonance. However, in contrast to classical synchrotrons and wigglers, in which electrons move along strictly defined trajectories, in the discussed plasma storage synchrotron, the bunch particles participate in complex motion along highly non-trivial trajectories. This, of course, affects the spectral composition of the synchrotron radiation of the bunches and its radiation pattern. In the present work, synchrotron radiation was recorded using the same loop microwave probe, which was described above and was used to measure the spectra of microwave oscillations of the cavity at the pump frequency. In Figure 4 the corresponding experimental results are presented.

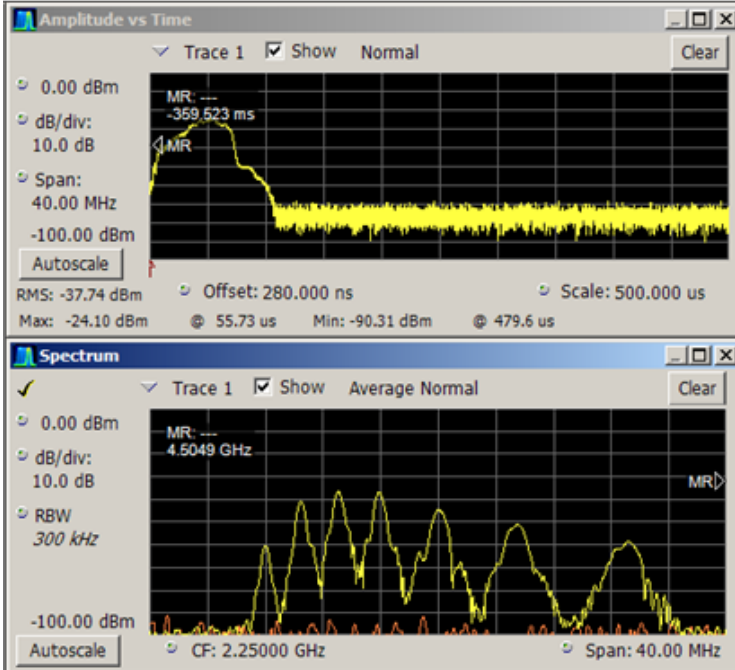
The upper curve in Figure 4(a) is the integral of the signal recorded from the loop microwave probe in the vicinity of 2.25 GHz in the 40 MHz band by the Tektronix RSA-6114A real-time spectrum analyzer. The lower curve corresponds to the spectral distribution of synchrotron radiation energy in this frequency range. The recorded spectrum has a very complex shape in which several peaks of different widths and degrees of overlap can be distinguished. As a result of this, it would not be right to talk about harmonics of synchrotron radiation, as is done in its classical consideration [7], [8], however, for brevity and definiteness of the present work, we will call radiation recorded in this spectral region the “first harmonic” of synchrotron radiation. It can be assumed that individual peaks in the recorded spectrum correspond to several spatially separated parts of plasma bunches coming from their generation regions near the pulsed-field coils to the confinement region at the midplane of the trap. Interpretation of these results requires additional studies and comparison of their results with the results of measurements of bremsstrahlung and recombination radiation of bunches, as well as data of corpuscular probes in both the radial and axial directions of observation.

The power integral and spectral distribution shown in Figure 4(b) correspond to the “second harmonic” of the synchrotron radiation of a plasma bunch. A spectrogram with a central frequency of 4.52 GHz in the 40 MHz band was obtained with the parameters of the setup and spectrum acquisition unchanged. Nonlinear changes in the spectral composition of synchrotron radiation at the “second harmonic” should be noted.

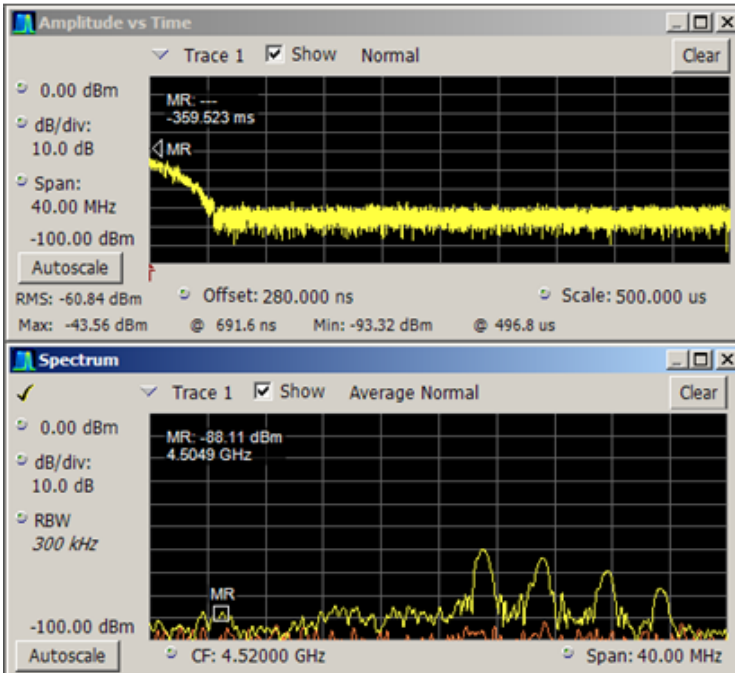
A series of experiments was carried out with a variation in the working gas pressure, which showed a broadening of the spectrum with increasing pressure.

## 4. Conclusion

Processing waveforms from electrodes using the fast Fourier transform method showed the presence of low-frequency oscillations with frequencies of 130 kHz and 450 kHz at a pressure of  $P = 1 \cdot 10^{-5}$  Torr, which are observed in the final stage of autoresonant acceleration. The low-frequency components in the emission spectrum of a relativistic bunch arise as a result of complex nonlinear interaction of the bunch particles with external and internal fields, similar to how it happens in a beam discharge [6], in betatrons [7] and in plasma engines [9].



(a) The “first harmonic” 2.25 GHz



(b) The “second harmonic” 4.52 GHz

Figure 4. Spectra of synchrotron radiation

A comparison of the low-frequency oscillations with the fluctuations in the intensity of the bremsstrahlung detected in the transverse direction, as well as the signals of the PMTs recorded in the region of the trap minimum, shows that they are interconnected and are observed synchronously when the bunches are shifted to the detection region. Microwave signals (at 2.25 GHz and 4.52 GHz) are also obtained at a given point in time, and a broadening of the spectrum is observed with increasing working gas pressure. Radiation at a frequency of 4.52 GHz was obtained in a trap at the end of a microwave pump pulse.

## Acknowledgments

The authors appreciate the support of the “RUDN University Program 5-100”, which allowed to prepare the section 2 of the paper. For the results described in the sections 3 and 4, some of us (AAN, DVC) also appreciate the financial support from the Ministry of Education and Science of the Russian Federation (agreement 3.2223.2017.4.6).

## References

- [1] V. V. Andreev, A. A. Novitsky, and A. M. Umnov, “Spectral changes of bremsstrahlung plasma bunch generated under autoresonance in a long mirror,” *IOP Conf. Series: Journal of Physics: Conf. Series*, vol. 1094, no. 9, p. 012 013, 2018. DOI: 10.1088/1742-6596/1094/1/012013.
- [2] V. V. Andreev, A. A. Novitsky, and D. V. Chuprov, “The Use of Streak Photography, X-Ray Radiography, and Radiometric and Spectrometric Measurements to Study Plasma Bunches Generated under Gyroresonant Interactions,” *Physics of Atomic Nuclei*, vol. 82, no. 10, pp. 1–10, 2019. DOI: 10.1134/S1063778819100016.
- [3] V. V. Andreev and A. M. Umnov, “Relativistic plasma and electron bunches in plasma synchrotrons of GYRAC,” *Plasma Sources Science and Technology*, vol. 8, no. 3, pp. 479–487, Jan. 1999. DOI: 10.1088/0963-0252/8/3/318.
- [4] V. V. Andreev, D. V. Chuprov, V. I. Ilgisonis, A. A. Novitsky, and A. M. Umnov, “Gyromagnetic autoresonance plasma bunches in a magnetic mirror,” *Physics of Plasmas*, vol. 24, no. 9, p. 093 518, 2017. DOI: 10.1063/1.4986009.
- [5] R. W. Gould, “Dynamics of Non-Neutral Plasmas,” *Physics of plasmas*, vol. 2, no. 6, pp. 2151–2163, 1995. DOI: 10.1063/1.871302.
- [6] S. M. Krivoruchko and E. A. Kornilov, “Excitation of Low-frequency Oscillations and Control of Two-stream Instability Spectra,” *JETP Letters*, vol. 10, no. 10, pp. 299–301, 1969.
- [7] T. J. Smith, J. Golden, and C. A. Kapetanacos, “Studies of synchrotron radiation emission from the modified betatron accelerator,” *Journal of Applied Physics*, vol. 69, no. 10, pp. 6836–6843, 1991. DOI: 10.1063/1.347673.

- [8] R. C. Davidson and S. M. Mahajan, “Synchrotron Radiation Spectrum for an Intense Relativistic E-Layer,” *Physics of Fluids*, vol. 17, pp. 2267–2274, 1974. DOI: 10.1063/1.1694702.
- [9] K. P. Kirdyashev, A. I. Bugrova, A. V. Desyatkov, and V. K. Kharchevnikov, “Low-frequency spectra of electron oscillations in an SPD-ATON stationary plasma thruster,” *Technical Physics Letters*, vol. 35, no. 2, pp. 158–161, 2009. DOI: 10.1134/S1063785009020187.

**For citation:**

A. A. Novitskiy, D. V. Chuprov, V. A. Kuznetsov, E. A. Shevtsov, The features of the characteristic electromagnetic plasma bunches oscillations in the long magnetic mirror, *Discrete and Continuous Models and Applied Computational Science* 27 (4) (2019) 355–364. DOI: 10.22363/2658-4670-2019-27-4-355-364.

**Information about the authors:**

**Andrey A. Novitskiy** (Russian Federation) — Head of Laboratory of the Institute of Physical Research and Technologies, Peoples’ Friendship University of Russia (RUDN University) (e-mail: novitskiy-aa@rudn.ru, phone: +7(915)4013703, ORCID: <https://orcid.org/0000-0002-0248-1640>, ResearcherID: O-8773-2017, Scopus Author ID: 56763990400)

**Denis V. Chuprov** (Russian Federation) — Senior Lecturer of the Institute of Physical Research and Technologies, Peoples’ Friendship University of Russia (RUDN University) (e-mail: chuprov-dv@rudn.ru, phone: +7(926)1342628, ORCID: <https://orcid.org/0000-0002-6768-6196>, ResearcherID: O-3193-2013, Scopus Author ID: 6508067157)

**Vladislav A. Kuznetsov** (Russian Federation) — Student of the Institute of Physical Research and Technologies, Peoples’ Friendship University of Russia (RUDN University) (e-mail: 1032162058@rudn.ru, phone: +7(985)8318472, ORCID: <https://orcid.org/0000-0002-3707-157X>)

**Eugeny A. Shevtsov** (Russian Federation) — Student of the Institute of Physical Research and Technologies, Peoples’ Friendship University of Russia (RUDN University) (e-mail: 1032162067@rudn.ru, phone: +7(968)9201311, ORCID: <https://orcid.org/0000-0001-7685-3630>)

УДК 533.9

DOI: 10.22363/2658-4670-2019-27-4-355-364

## Особенности характерных электромагнитных колебаний плазменных сгустков в длинном пробкотроне

А. А. Новицкий, Д. В. Чупров, В. А. Кузнецов, Е. А. Шевцов

*Институт физических исследований и технологий  
Российский университет дружбы народов  
ул. Миклухо-Маклая, д. 6, Москва, 117198, Россия*

Целью данной работы являлось изучение спектра НЧ и ВЧ колебаний генерируемых плазменными сгустками, создаваемыми и удерживаемыми в рабочем объеме высокочастотного резонатора, находящегося в магнитном поле зеркальной ловушки. Регистрация электростатических колебаний в плазме осуществлялось при помощи двух плоских электродов установленных диаметрально противоположно в центральной части резонатора в его пристеночной области. Эта диагностика показала наличие низкочастотных колебаний с частотами 130 кГц и 450 кГц. Спектр колебаний в СВЧ диапазоне регистрировался в минимуме магнитной ловушки при помощи спектрометра реально времени и слабо связанной петлевой антенны. Регистрация спектров в полосе 40 МГц позволила выявить закономерное изменение частоты основной моды колебаний резонатора и наличие двух гармоник синхротронного излучения плазменного сгустка на частотах 2.25 ГГц и 4.52 ГГц соответственно. По полученным данным могут быть восстановлены параметры сформированного сгустка (плотность, форма, объем, энергетические спектры компонент плазмы).

**Ключевые слова:** гиромагнитный авторезонанс, плазменные сгустки, протяженный пробкотрон, электростатические и электромагнитные колебания, спектральный анализ

UDC 004.021:530.182.1

DOI: 10.22363/2658-4670-2019-27-4-365-377

# Numerical modeling of stationary pseudospin waves on a graphene monoatomic films

Lê Anh Nhật<sup>1</sup>, Konstantin P. Lovetskiy<sup>1</sup>,  
Leonid A. Sevastianov<sup>1,2</sup>, Dmitry S. Kulyabov<sup>1,3</sup>

<sup>1</sup> *Department of Applied Probability and Informatics  
Peoples' Friendship University of Russia (RUDN University)  
6, Miklukho-Maklaya St., Moscow 117198, Russian Federation*

<sup>2</sup> *Bogoliubov Laboratory of Theoretical Physics  
Joint Institute for Nuclear Research  
6, Joliot-Curie St., Dubna, Moscow region 141980, Russia*

<sup>3</sup> *Laboratory of Information Technologies  
Joint Institute for Nuclear Research  
6, Joliot-Curie St., Dubna, Moscow region 141980, Russian Federation*

(received: December 23, 2019; accepted: December 30, 2019)

For the first time, the theoretical model of the spin-electron structure of a single-layer graphene film was proposed by Wallace. The literature also describes ferromagnetism generated by none of the three common causes: impurities, defects, boundaries. We believe that the source of ferromagnetism is the spontaneous breaking of spin symmetry in a graphene film. The classical field model describing spontaneously broken symmetry is necessarily non-linear. Among non-linear models, the simplest is the well-known  $\lambda\varphi^4$  model. We believe that, as a first approximation, we can describe with its help all the characteristics of spin waves that interest us, their spectra, and the domain structure of ferromagnetism in graphene. The model admits kink and anti-kink exact solutions and a quasiparticle breather, which we modeled numerically. We use the kink-anti-kink interaction energy obtained numerically to solve the Schrödinger equation, which simulates the quantum dynamics of breathers, which underlies the description of spin waves. The solution of the Schrödinger equation by the Ritz method leads to a generalized problem of eigenvalues and eigenvectors, the solution of which is mainly devoted to this work.

**Key words and phrases:** graphene, solitons, kinks, breathers, nonlinear models

## 1. Introduction

One of the main areas of the theoretical and experimental research is the study of the properties of graphene, an obvious candidate for the formation on its basis of the elemental base of future nanoelectronics and spintronics,

© Nhật L. A., Lovetskiy K. P., Sevastianov L. A., Kulyabov D. S., 2019



This work is licensed under a Creative Commons Attribution 4.0 International License

<http://creativecommons.org/licenses/by/4.0/>

which provides a gain by orders of magnitude in the field of speed, size and power consumption of devices for storing, transmitting and processing information. Significant successes were achieved in this area [1]–[7], however, a number of very unusual for carbon structures properties of graphenes, which are observed experimentally, have not yet found their adequate theoretical description. In particular, it was found [2], [3] that in graphene systems there is a ferromagnetic effect that present right up to room temperatures and above (Curie temperature exceeds 500 K). Consequently, samples of graphene films can have their own magnetization due to the presence of a nonzero spin density of valence electrons distributed in some way on the two-dimensional carbon lattice. According to researchers, these experimentally observed ferromagnetic properties of graphene structures require theoretical justification and the construction of an appropriate mathematical model.

For the first time, the theoretical model of the spin-electron structure of the single-layer graphene film was proposed by Wallace. After it was published an extensive bibliography, which we will not concern. The ferromagnetic properties of graphene structures observed experimentally by different researchers, by their own admission, require proper justification and construction of the appropriate theoretical model. We believe that the source of ferromagnetism is the spontaneous breaking of spin symmetry in a graphene film. Quantum-chemical calculations show that the Wallace model can serve only as a first approximation, and subsequent approximations allow violation of the well-known Wallace symmetry.

Quantum-chemical simulation of electron density in a monoatomic graphene film by the extended functional density method and the advanced Hartree–Fock method has demonstrated the possibility of the existence of unpaired electrons, which gives rise to spontaneous violation of spin symmetry in it, i.e., a nontrivial distribution of spin density. Experimentally it was found that such a non-trivial distribution does not have a traditional source: impurities, defects, boundaries [2].

Being caused by spontaneous symmetry breaking, such a distribution of spin density must satisfy the nonlinear phenomenological equation of the classical gauge field [8]–[14]. There can be many such fields and equations, and they all supposedly give results that coincide in a first approximation. Therefore, the scalar field on the two-dimensional continuum  $\lambda\varphi^4$  was chosen as the first object of study as a mathematical model of spin density. Here we made a transition from a discrete set of nodes of a double hexagonal lattice, in which unpaired electrons and the corresponding electron and spin densities can be localized.

The nonlinear field model proposed for the distribution of the spin density of valence electrons in a graphene film makes it possible to describe the experimentally observed ferromagnetic properties of such films. It is shown that these solutions (kinks, breathers) allow the formation of some spatially localized magnetization density configurations on the surface of a graphene film. The specified scalar field allows localized solutions: kinks and anti-kinks. The combination of kink and anti-kink is a quasiparticle, i.e. an approximate solution of the nonlinear equation for a  $\varphi^4$  scalar field. Quantitative estimates are obtained for the energy and spatial dimensions of such a configuration. Their characteristic size was tens of nanometers. It is also shown that such configurations can constitute groups of discrete spectra.

The problem of the interaction of kinks and anti-kinks with each other is considered. We also find it interesting to further consider the interaction of breathers with each other and with other physical fields, as well as the dynamics of spinons on graphene (fullerene, nanotube) nonplanar surfaces of various topologies. This work is devoted to a numerical study of the model  $\lambda\varphi^4$  [15], [16]. Within the framework of the proposed model, the problems of approximate calculation of potential fields, approximate solution of the Schrödinger equations and simulation of control of the external field of population levels [8] are solved.

## 2. Model description

In this work, we study a theoretical model that describes the properties of graphene monoatomic layers that form some two-dimensional surfaces associated with the presence of a nonzero spin density distribution function on these surfaces formed as a result of spontaneous violation of the spin symmetry of valence electrons of carbon atoms on these surfaces. Since the spin density is proportional to the magnetization density, this model allows us to describe the ferromagnetic properties of graphene structures.

In the framework of the proposed model, a transition is made from the consideration of a discrete two-dimensional carbon lattice forming a graphene film to a continuous two-dimensional surface stretched over this lattice. The indicated two-dimensional surface is the configuration space of the model. Thus, we are making the transition to a continuum field model.

In the model under consideration, a trivial, identically equal to zero, spin density configuration is admissible. However, it was experimentally established that this symmetric field configuration can be spontaneously disturbed to some physically observable.

Within the framework of the two-dimensional field model under study, there is an analogue of the Goldstone theorem, known in quantum field theory, according to which an each broken generator of the initial symmetry of the field system must correspond to a massless scalar uncharged boson, which in our case is appropriate to call as a spinon.

In this case, the spontaneous breaking of spin symmetry within the framework of the proposed model should lead to the presence on the graphene surfaces of quasiparticle spinons, which are vector bosons in 3-dimensional physical space and scalar pseudo-Goldstone bosons in the two-dimensional configuration space of the model, since the projection of the quasiparticle spin on the configuration space is equal to zero.

It is significant that the presence of collective magnetic interactions of spinons, due to the influence of the total magnetic field, created by all spinons, on each spinon individually, leads to nonlinearity of the corresponding field equations and, as a consequence, the possibility of the existence of soliton configurations on graphene surfaces, which depend, inter alia, on shape and surface topology.

In addition, the presence of collective interactions in the ensemble of spinons should lead to the appearance of an effective mass for a spinon, which should also affect the observed physical consequences, although due to the smallness of spin-spin interactions large values of this mass can hardly be expected.

Based on the foregoing, it is clear that the equations for the desired scalar field given on a certain two-dimensional surface must be nonlinear and defined on this surface of an arbitrary, generally speaking, shape and topology. The form and topology in this case determine the boundary conditions for the field function. The indicated function determines the conditions for the existence, configuration and dynamics of quasiparticles of this field on a given two-dimensional surface.

The indicated properties, in particular, are possessed by the field equations known in quantum theory, which describe, among other things, massless nonlinear scalar excitations.

Thus, to describe spinon excitations on graphene surfaces, we use one of the variants of the nonlinear field model, which allows us to calculate the eigen solutions, effective masses, topological invariants, energy spectra, the dynamics of various nonlinear spinon configurations, as well as relaxation properties, Curie temperature, and other characteristics of statistical ensembles of spinons.

### 3. Interaction model

Consider a model of a nonlinear one-component scalar field  $\varphi$  on a two-dimensional surface, the surface density of the Lagrangian of which is set in the form:

$$L(\varphi) = \frac{1}{2}(\partial_\nu\varphi\partial^\nu\varphi) - \frac{\lambda}{4}(\varphi^2 - \varphi_0^2)^2, \quad (1)$$

where  $\varphi_0$  and  $\lambda$  are the model parameters. In this case, the field equation has the form:

$$[\partial_\nu\partial^\nu - \lambda\varphi_0^2]\varphi - \lambda\varphi^3 = 0 \quad (2)$$

In the case when  $\varphi$  depends only on one coordinate  $x$  and does not depend on time, in other words:  $\varphi = \varphi(x)$ , and the equations of the form (2) have a set of static solutions, as well as kink and anti-kink solutions:

$$\varphi_\pm(x) = \pm\varphi_0 \tanh\left(\sqrt{\lambda\varphi_0^2/2x}\right). \quad (3)$$

In the vicinity of zero, kinks (anti-kinks) have a domain wall separating regions with magnetization of different signs.

The kink energy per unit length in the coordinate  $y$  is calculated by the formula:

$$E(\varphi) = \int_{-\infty}^{\infty} dx \left[ \frac{1}{2}(\partial_x\varphi)^2 + \frac{\lambda}{4}(\varphi^2 - \varphi_0^2)^2 \right] = \frac{\sqrt{3}}{8}\varphi_0^3\sqrt{\lambda}. \quad (4)$$

The kink energy density along the  $x$  coordinate is proportional to  $\left[1 - \tanh^2\left(\sqrt{\lambda\varphi_0^2/2x}\right)\right]$  and, therefore, is concentrated near zero on the domain wall.

As in any ferromagnet, in the system under consideration there is a Curie temperature [1], [2], at which the system of interacting spins is disordered due to thermal motion. This leads to the decay of the kink and the destruction of the domain structure. In other words, this is the situation when the energy of

the thermal motion of an elementary magnetic moment becomes comparable with its energy in the kink field. This allows a quantitative assessment of the model parameters.

The substitution of the numerical values gives  $d \approx 15\text{--}30$  nm, which looks quite plausible. The scatter of values for the domain wall thickness is related to the scatter of the available experimental data on measuring the Curie temperature. In any case, we see that the calculated domain wall thickness is tens of bond lengths in the cell. This confirms the correctness of the use of the proposed continuum model for the graphene lattice.

Consider the case when the solutions for the field function are explicitly time-dependent. Then we obtain stable single kink and anti-kink solutions propagating along the coordinate  $x$  with a constant velocity  $V_0$ .

The stable spatially localized field configurations (not only kinks) (in particular, which are solutions of equations of the form (2)) are of interest for many practical applications. For qualitative estimates we propose to use some approximate solutions of equations of the form (4), by using combinations of existing exact solutions.

+In particular, we can consider the system of kink and +anti-kink interaction. In the simplest case, this can be a kink and an anti-kink located at some distance  $a(t)$  from each other. Moreover, it is very important that kink and anti-kink interact with each other even at an infinitely large distance from each other. This is due precisely to the fact that their asymptotics at spatial infinity are nonzero. In addition, it should be noted that, due to the nonlinearity of the problem, the sum of exact solutions, generally speaking, is not an exact solution.

Nevertheless, we choose the field function of the system of interacting kink and anti-kink in the simple form:

$$\varphi(x, a) = [\varphi_+(x + a) + \varphi_-(x - a) - \varphi_0], \quad a > 0. \quad (5)$$

A function of the form (5) for small values of  $a$  is spatially localized near the point  $x = 0$ . Kink and anti-kink at (5), spatially separated by a sufficiently large (compared to the thickness of the kink itself) distance, interact with each other, but, however, steadily maintain their own shape.

We numerically look for such  $a(t)$  to satisfy the equation (2). The obtained solutions will correspond to breathers, that is, stable kink – anti-kink configurations, known, for example, for equations like sine-Gordon, Korteweg–de Vries, and some others, both in discrete and continuous cases.

Consider the Hamiltonian of a system whose field function of the form (5) satisfies the equation of type 2:

$$H(\varphi) = \int_{-\infty}^{\infty} dx \left[ \partial_\nu \varphi(x) \partial^\nu \varphi(x) + \frac{\lambda}{2} (\varphi(x)^2 - \varphi_0^2)^2 \right]. \quad (6)$$

This function can be considered as the total energy of the kink in the anti-kink field (or vice versa), and its dependence on the parameter  $a$  may be formally investigated. Then the dependence of the Hamiltonian of the form (6) on the parameter  $a$  corresponds to the dependence of the potential interaction energy of the kink and anti-kink on the distance between them. If

there are minima in this function, one should expect the presence of bound states in the kink–anti-kink system. These will be the desired breathers.

We will search for the bound states of the kink–anti-kink in the minima of potential energy:

$$\begin{aligned}\frac{\partial}{\partial a}H(\varphi, a_m) &= 0, \\ \frac{\partial^2}{\partial a^2}H(\varphi, a_m) &> 0.\end{aligned}\tag{7}$$

You can get the estimate:  $a_0 \approx 0.8d$ . Thus, the ratio of the distance between the kink and the anti-kink to the size of the kink itself (anti-kink) is less than unity, which again confirms the correctness of the assumptions used.

### 3.1. Numerical implementation

Since we consider functions  $\varphi(x, a)$  of the form (5), depending on the parameter  $a$ , where  $\varphi_{\pm}(x) = \pm\varphi_0 \tanh\left(\sqrt{\lambda\varphi_0^2/2x}\right)$  depends on the parameter  $\varphi_0$ , the calculation of the functional  $H(\varphi, a)$  was performed as follows. First, the partial derivative  $\frac{\partial\varphi}{\partial x}$  was calculated (the other partial derivatives of  $\varphi$  are identically equal to zero due to the choice of the form of the function  $\varphi$  (5)), then for given  $\varphi_0$ ,  $\lambda$  and  $a$  the numerical integral (6) is calculated. Thus, with the fixed parameter  $\varphi_0 = 1.0$  selected, we obtain a numerical dependence of the potential interaction energy  $U(a, \lambda)$ . The calculations were performed for various  $\lambda = 0.01 \dots 100.0$ . Moreover, for each value of  $\lambda$  the dependence is  $U_{\lambda}(a) \equiv U(a, \lambda)$  was calculated for the values of  $a$  from  $a = +0.0$  to the value of  $a(\lambda)$  for which the values of  $U_{\lambda}(a(\lambda))$  and  $U_{\lambda}(2a(\lambda))$  coincide with up to the 5th digit.

Since the dynamics of the breather in the model of spontaneous symmetry breaking [8], [9] is described by quantum nonrelativistic equations, we model the dynamics of the pulsation of stationary states of the breather by the Schrödinger equation.

## 4. Dynamics model

For the quantum-mechanical stationary wave function of the breather  $\psi_b(a)$ , the Schrödinger equation in the standard form is written:

$$\left[ -\frac{\hbar^2}{2m_b} \frac{\partial^2}{\partial a^2} U(\varphi, a) \right] \psi_b(a) = E\psi_b(a),\tag{8}$$

where  $m_b$  is the effective mass of the breather, which is equal in this case to the sum of the masses of the free kink and anti-kink, and  $U(\varphi, a)$  is the potential part of the total energy of the breather, depending on  $a$ ,  $E$  is the energy of the corresponding stationary state. The movement of the breather along the generalized coordinate  $a$  physically corresponds to a change in the distance between the kink and the anti-kink, while the center of the breather is fixed along the coordinate  $x$ , only the effective width of the breather changes (the breather “breathes”).

#### 4.1. Numerical implementation

The dynamics of the breather is described by the Schrödinger equation:

$$-\frac{d^2\varphi}{dx^2} + U(x)\varphi(x) = E\varphi(x). \quad (9)$$

We will seek a numerical solution of the equation (9) by using the Ritz–Galerkin method. Namely, under the assumption that the Schrödinger operator  $\hat{H}$  is strictly positive, we can construct the Ritz functional and the energy space in which it reaches its minimum. The local minima of the Ritz functional uniquely correspond to the eigenvectors of the operator  $\hat{H}$ . The finite-dimensional approximation of the functional over some complete system of coordinate functions  $\varphi_k(x)$  minimizes the function of several variables. The minimum of this function corresponds to the solution of the system of linear algebraic equations with the Ritz matrix  $(\hat{H}\varphi_k, \varphi_l)$ . The application of the Galerkin method to this problem leads to the eigenvalue and eigenvector problem, as does the Ritz method.

You can use an arbitrary orthonormal basis in the space  $L_2$  of quadratically integrable functions on the axis as a complete system of coordinate functions. Moreover, convergence may turn out to be slow, which will lead to the need to solve systems of linear algebraic equations of large dimension. In order to build a well-conditioned Ritz matrix, one should choose a strongly minimal or almost orthogonal complete system of functions with respect to  $\hat{H}$ . By the way, one should note that the potential energy in the equation (9) is a grid function, which complicates the analytical study of the known bases in  $L_2$ .

At the same time, the quantum operator of a nonlinear oscillator from [17] has a complete system of eigenvectors. The eigenfunctions of a nonlinear oscillator form a numerically strongly minimal system of functions for the operator  $\hat{H}$ . These functions, however, are not orthonormal in the space  $L_2$ . This fact complicates the finite-dimensional approximating problem and, more precisely, leads to the generalized eigenvalue problem and eigenvectors  $\hat{A}\vec{c} = E\hat{B}\vec{c}$ .

Then, in the general case, the solution will look like this:

$$\varphi_j(x) = \sum_{k=1}^{\infty} c_{j,k} \varphi_k(x),$$

where  $\varphi_k(x)$  are basic functions. Therefore, in order to find the solution (9), it is necessary to specify some kind of functions  $\varphi_k(x)$  and find the values of the coefficients  $c_{j,k}$  and  $E$ . From the obtained numerical values of  $V(x)$  it is clear that the form of the potential is similar to the potential of a nonlinear oscillator, so we take the eigenfunctions  $\varphi_k(x)$  for it.

Consider the case  $k = 0, 1, 2$ . Choose  $\lambda = 1$ . In this case,  $n = 3$ , but for a smaller calculation error, you can choose a value of  $n$  more than 3. Let  $n = 10$ . For  $\lambda > 0$  the condition must be satisfied:  $\frac{2\beta_0}{\lambda} \geq n$ . It follows from this inequality that in our case  $\beta_0 \geq 5$ . Consider  $\beta_0 = 6$ . Subsequent  $\beta_i$  are calculated using the formula  $\beta_i = \beta_{i-1} - \lambda$ . Therefore,  $\beta_1 = 5$ ,  $\beta_2 = 4$ . Also,

to find the form of the functions  $\varphi_k(x)$  we need the values  $r_i = \frac{\beta_i}{2\lambda}$ . In our case,  $r_0 = 3$ ,  $r_1 = \frac{5}{2}$ ,  $r_2 = 2$ .

We look for the form of the functions  $\varphi_k(x)$  using formulas:

$$\begin{cases} \varphi_0(x) = \frac{1}{(1 + \lambda x^2)^{r_0}}, \\ \varphi_1(x) = A^+(\beta_0) \varphi_0(\beta_1), \\ \varphi_2(x) = A^+(\beta_0) A^+(\beta_1) \varphi_0(\beta_2). \end{cases} \quad (10)$$

where

$$A^+ = \frac{1}{\sqrt{2}} \left( -\sqrt{1 + \lambda x^2} \frac{d}{dx} + \frac{\beta_i x}{\sqrt{1 + \lambda x^2}} \right).$$

+After substitution of the +values  $\lambda$ ,  $\beta_i$ ,  $r_i$  and simplification of the results, the functions  $\varphi_k(x)$ ,  $k = 0, 1, 2$  will take the form:

$$\begin{cases} \varphi_0(x) = \frac{1}{(1 + x^2)^3}, \\ \varphi_1(x) = \frac{11x}{\sqrt{2}(1 + x^2)^3}, \\ \varphi_2(x) = \frac{9(10x^2 - 1)}{2(1 + x^2)^3}. \end{cases} \quad (11)$$

The Ritz system takes form:

$$\sum_{k=0}^2 c_k (A\varphi_k, \varphi_j) = E \sum_{k=0}^2 c_k (\varphi_k, \varphi_j), \quad j = \overline{0, 2}, \quad (12)$$

where the operator  $A = -dv[2]x + V(x)$ .

Having written the scalar products  $(A\varphi_k, \varphi_j)$  and  $(\varphi_k, \varphi_j)$ , we get:

$$\begin{aligned} - \int_0^\infty \frac{d^2}{dx^2} \left( \sum_{k=0}^2 c_k \varphi_k(x) \right) \varphi_j(x) + \sum_{k=0}^2 c_k \int_0^\infty V(x) \varphi_k(x) \varphi_j(x) dx - \\ - E \sum_{k=0}^2 c_k \int_0^\infty \varphi_k(x) \varphi_j(x) dx = 0. \end{aligned}$$

The same equation can be written in the matrix form:

$$(D^T + B^T - EA^T) \vec{c} = \vec{0}, \quad (13)$$

where

$$D = (d_{kj}), \quad k, j = \overline{0, 2},$$

$$d_{kj} = \left( -\frac{d^2\varphi_k(x)}{dx^2}, \varphi_j(x) \right) = - \int_0^\infty \frac{d^2\varphi_k(x)}{dx^2} \varphi_j(x) dx,$$

$$A = (a_{kj}), \quad k, j = \overline{0, 2}, \quad a_{kj} = (\varphi_k(x), \varphi_j(x)) = \int_0^\infty \varphi_k(x) \varphi_j(x) dx,$$

$$B = (b_{kj}), \quad k, j = \overline{0, 2}, \quad b_{kj} = (V(x)\varphi_k(x), \varphi_j(x)) = \int_0^\infty V(x)\varphi_k(x)\varphi_j(x) dx,$$

$$\vec{c} = (c_0, c_1, c_2)^T.$$

There are four unknowns in the resulting system of equations:  $E$  and coordinates  $\vec{c} = (c_0, c_1, c_2)^T$ . In order for the system to be compatible, it is necessary that  $|D^T + B^T - EA^T| = 0$ .

The expanded form:

$$\begin{vmatrix} d_{00} + b_{00} - Ea_{00} & d_{10} + b_{10} - Ea_{10} & d_{20} + b_{20} - Ea_{20} \\ d_{01} + b_{01} - Ea_{01} & d_{11} + b_{11} - Ea_{11} & d_{21} + b_{21} - Ea_{21} \\ d_{02} + b_{02} - Ea_{02} & d_{12} + b_{12} - Ea_{12} & d_{22} + b_{22} - Ea_{22} \end{vmatrix} = 0. \quad (14)$$

We introduce the following replacements:

$$\begin{aligned} t_1 &= d_{00} + b_{00}, & t_2 &= d_{11} + b_{11}, & t_3 &= d_{22} + b_{22}, \\ t_4 &= d_{02} + b_{02}, & t_5 &= d_{10} + b_{10}, & t_6 &= d_{21} + b_{21}, \\ t_7 &= d_{20} + b_{20}, & t_8 &= d_{01} + b_{01}, & t_9 &= d_{12} + b_{12}. \end{aligned} \quad (15)$$

We get the equation:

$$\begin{aligned} &(t_1 - Ea_{00})(t_2 - Ea_{11})(t_3 - Ea_{22}) + (t_4 - Ea_{02})(t_5 - Ea_{10})(t_6 - Ea_{21}) + \\ &+ (t_7 - Ea_{20})(t_8 - Ea_{01})(t_9 - Ea_{12}) - (t_7 - Ea_{20})(t_2 - Ea_{11})(t_4 - Ea_{02}) - \\ &- (t_1 - Ea_{00})(t_2 - Ea_{12})(t_6 - Ea_{21}) - (t_3 - Ea_{22})(t_5 - Ea_{10})(t_8 - Ea_{01}) = 0. \end{aligned}$$

Opening the brackets, we obtain the equation of the third degree with respect to  $E$ .

The resulting numerical values are:

$$E = (0.6362135, -10.452091, 24.544966). \quad (16)$$

### 5. Conclusion

Thus, we see that the kink plus anti-kink system can form bound states, that is, breathers which make up some groups corresponding to different minima of the interaction energy of the kink and anti-kink. These groups of breathers should noticeably differ in spatial dimensions. It is very likely that the energy spectra of breathers from various groups can overlap. This, in turn, allows us to pose the problem of tunneling breathers from one minimum

to another, the lifetimes in each of these minima, the behavior in external fields, inverse populations, and other physical features of another, as well as the problem of the lifetimes in each of these minima and of the behavior in external fields, inverse populations, and some other physical features of the system under consideration.

We also note that under certain conditions, the interaction of kinks and breathers with each other, as well as with external fields (note, not only electromagnetic, but also, for example, acoustic), should lead to the birth-destruction of particles, which, in principle, we can describe within the framework of the proposed model by secondary quantization of the considered system and calculating the matrix elements of the corresponding scattering matrix.

Thus, in some sense, we are closing the circle, moving from a general quantum-field approach to a classical field, then to a quantum-mechanical model, and again to a quantum-field consideration through second quantization.

It seems that the proposed approach will allow us to continue to make the necessary quantitative estimates even before the numerical simulation of the problem. We also find it interesting to further consider the dynamics of spinons on graphene (fullerene, nanotube) non-planar surfaces of various topologies.

## Acknowledgments

The reported study was funded by Russian Foundation for Basic Research (RFBR), project number 18-07-00567. The reported study was funded by Russian Foundation for Basic Research (RFBR), project number 19-01-00645.

## References

- [1] J. Červenka, M. I. Katsnelson, and C. F. Flipse, “Room-temperature ferromagnetism in graphite driven by two-dimensional networks of pointdefects,” *Nature Physics*, vol. 5, no. 11, pp. 840–844, 2009. DOI: 10.1038/nphys1399.
- [2] Y. Wang, Y. Hoang, Y. Song, X. Zhang, Y. Ma, J. Liang, and Y. Chen, “Room-temperature ferromagnetism of graphene,” *Nano Letters*, vol. 9, no. 1, pp. 220–224, 2009. DOI: 10.1021/nl802810g.
- [3] P. Esquinazi, A. Setzer, R. Höhne, C. Semmelhack, Y. Kopelevich, D. Spemann, T. Butz, B. Kohlstrunk, and M. Lösche, “Ferromagnetism in oriented graphite samples,” *Physical Review B - Condensed Matter and Materials Physics*, vol. 66, no. 2, pp. 1–10, 2002. DOI: 10.1103/PhysRevB.66.024429. arXiv: 0203153 [cond-mat].
- [4] K. S. Novoselov, A. K. Geim, S. V. Morozov, D. Jiang, M. I. Katsnelson, I. V. Grigorieva, S. V. Dubonos, and A. A. Firsov, “Two-dimensional gas of massless Dirac fermions in graphene,” *Nature*, vol. 438, no. 7065, pp. 197–200, Nov. 2005. DOI: 10.1038/nature04233.

- [5] Y. Zhang, Y.-W. Tan, H. L. Stormer, and P. Kim, “Experimental observation of the quantum Hall effect and Berry’s phase in graphene,” *Nature*, vol. 438, no. 7065, pp. 201–204, Nov. 2005. DOI: 10.1038/nature04235.
- [6] N. M. R. Peres, F. Guinea, and A. H. Castro Neto, “Coulomb interactions and ferromagnetism in pure and doped graphene,” *Physical Review B*, vol. 72, no. 17, p. 174406, Nov. 2005. DOI: 10.1103/PhysRevB.72.174406. arXiv: 0507061 [cond-mat].
- [7] N. M. R. Peres, F. Guinea, and A. H. Castro Neto, “Electronic properties of disordered two-dimensional carbon,” *Physical Review B*, vol. 73, no. 12, p. 125411, Mar. 2006. DOI: 10.1103/PhysRevB.73.125411. arXiv: 0512091 [cond-mat].
- [8] D. D. Grachev, Y. P. Rybakov, L. A. Sevastianov, and E. F. Sheka, “Ferromagnetism in graphene and fullerene nanostructures. Theory, modeling, experiment,” *Bulletin of PFUR. Series “Mathematics. Information Sciences. Physics”*, no. 1, pp. 20–27, 2010.
- [9] D. D. Grachev and L. A. Sevastyanov, “The Quantum Field Model of the Ferromagnetism in Graphene Films,” *Nanostructures, Mathematical Physics and Modelling.*, vol. 4, pp. 5–15, 2011.
- [10] Y. P. Rybakov, M. Iskandar, and A. Ahmed, “Magnetic Excitations of Graphene in 8-Spinor Realization of Chiral Model,” *RUDN Journal of Mathematics, Information Sciences and Physics*, vol. 25, no. 3, pp. 266–275, 2017. DOI: 10.22363/2312-9735-2017-25-3-266-275.
- [11] Y. P. Rybakov, “Spin Excitations in Chiral Model of Graphene,” *Solid State Phenomena*, vol. 233-234, pp. 16–19, Jul. 2015. DOI: 10.4028/www.scientific.net/SSP.233-234.16.
- [12] Y. P. Rybakov, “On Chiral Model of Graphene,” *Solid State Phenomena*, vol. 190, pp. 59–62, Jun. 2012. DOI: 10.4028/www.scientific.net/SSP.190.59.
- [13] D. V. Kolesnikov and V. A. Osipov, “The continuum gauge field-theory model for low-energy electronic states of icosahedral fullerenes,” *The European Physical Journal B*, vol. 49, no. 4, pp. 465–470, Feb. 2006. DOI: 10.1140/epjb/e2006-00087-y. arXiv: 0510636 [cond-mat].
- [14] H. Watanabe and H. Murayama, “Unified Description of Non-Relativistic Nambu-Goldstone bosons,” *Physical Review Letters*, vol. 108, p. 251602, 2012. DOI: 10.1103/PhysRevLett.108.251602.
- [15] D. S. Kulyabov, K. P. Lovetskiy, and L. A. Nhat, “Simple Model of Nonlinear Spin Waves in Graphene Structures,” *RUDN Journal of Mathematics, Information Sciences and Physics*, vol. 26, no. 3, pp. 244–251, 2018. DOI: 10.22363/2312-9735-2018-26-3-244-251.
- [16] L. A. Nhat, K. P. Lovetskiy, and D. S. Kulyabov, “A new algorithm used the Chebyshev pseudospectral method to solve the nonlinear second-order Lienard differential equations,” *Journal of Physics: Conference Series*, vol. 1368, pp. 042036.1–8, Nov. 2019. DOI: 10.1088/1742-6596/1368/4/042036.

- [17] J. F. Cariñena, M. F. Rañada, and M. Santander, “One-dimensional model of a quantum nonlinear harmonic oscillator,” *Reports on Mathematical Physics*, vol. 54, no. 2, pp. 285–293, Oct. 2004. DOI: 10.1016/S0034-4877(04)80020-X. arXiv: 0501106 [hep-th].

**For citation:**

L. A. Nhật, K. P. Lovetskiy, L. A. Sevastianov, D. S. Kulyabov, Numerical modeling of stationary pseudospin waves on a graphene monoatomic films, *Discrete and Continuous Models and Applied Computational Science* 27 (4) (2019) 365–377. DOI: 10.22363/2658-4670-2019-27-4-365-377.

**Information about the authors:**

**Lê Anh Nhật** (Vietnam) — PhD student of Department of Applied Probability and Informatics of Peoples’ Friendship University of Russia (RUDN University) (e-mail: leanhnhat@tuyenquang.edu.vn, ORCID: <https://orcid.org/0000-0003-4882-6680>, ResearcherID: Q-6055-2018, Scopus Author ID: 57207191808)

**Konstantin P. Lovetskiy** (Russian Federation) — Docent, PhD in Physics and Mathematics, Associate Professor at the Department of Applied Probability and Informatics of Peoples’ Friendship University of Russia (RUDN University) (e-mail: lovetskiy-kp@rudn.ru, phone: +7(495)9550783, ORCID: <https://orcid.org/0000-0002-3645-1060>, ResearcherID: A-5725-2017, Scopus Author ID: 18634692900)

**Leonid A. Sevastianov** (Russian Federation) — Professor, Doctor of Sciences in Physics and Mathematics, Professor at the Department of Applied Probability and Informatics of Peoples’ Friendship University of Russia (RUDN University) (e-mail: sevastianov-la@rudn.ru, phone: +7(495)9550783, ORCID: <https://orcid.org/0000-0002-1856-4643>, ResearcherID: B-8497-2016, Scopus Author ID: 8783969400)

**Dmitry S. Kulyabov** (Russian Federation) — Docent, Doctor of Sciences in Physics and Mathematics, Professor at the Department of Applied Probability and Informatics of Peoples’ Friendship University of Russia (RUDN University) (e-mail: kulyabov-ds@rudn.ru, phone: +7(495)9520250, ORCID: <https://orcid.org/0000-0002-0877-7063>, ResearcherID: I-3183-2013, Scopus Author ID: 35194130800)

УДК 004.021:530.182.1

DOI: 10.22363/2658-4670-2019-27-4-365-377

## Численное моделирование стационарных псевдоспиновых волн на моноатомных плёнках графена

Ле Ань Ньат<sup>1</sup>, К. П. Ловецкий<sup>1</sup>, Л. А. Севастьянов<sup>1,2</sup>,  
Д. С. Кулябов<sup>1,3</sup>

<sup>1</sup> Кафедра прикладной информатики и теории вероятностей  
Российский университет дружбы народов  
ул. Миклухо-Маклая, д. 6, Москва, 117198, Россия

<sup>2</sup> Лаборатория теоретической физики  
Объединённый институт ядерных исследований  
ул. Жолио-Кюри, д. 6, г. Дубна, Московская область, 141980, Россия

<sup>3</sup> Лаборатория информационных технологий  
Объединённый институт ядерных исследований  
ул. Жолио-Кюри, д. 6, г. Дубна, Московская область, 141980, Россия

В экспериментах на однослойных графеновых плёнках наблюдается явление ферромагнетизма. При этом данный феномен не может порождаться ни одной из трёх распространённых причин: наличием примесей в графене, наличием дефектов в графене, влиянием границ однослойной графеновой плёнки. Авторы предполагают, что источником ферромагнетизма может служить спонтанное нарушение спиновой симметрии в графеновой плёнке. Классические полевые модели, описывающие спонтанное нарушение симметрии, являются нелинейными. Среди нелинейных моделей одной из простейших является широко известная  $\lambda\varphi^4$  модель. Предполагается, что в рамках данной модели можно описать большинство интересующих нас характеристик спиновых волн, а также феномен ферромагнетизма в графене. Эта модель допускает наличие кинковых и антикинковых точных решений, а также существование квазичастицы бризер. Авторами численно промоделировано квазичастичное решение бризер. Для этого численно получена энергия взаимодействия решений типа кинк-антикинк. Эта энергия используется для численного решения уравнения Шрёдингера для спиновых волн со структурой бризеров. Методом Ритца решения уравнения Шрёдингера приводятся к обобщённой задаче на собственные значения и собственные векторы. Эта задача исследуется в данной статье.

**Ключевые слова:** графен, солитоны, кинки, бризеры, нелинейные модели

PACS 07.05.Tp

DOI: 10.22363/2658-4670-2019-27-4-378-385

# Efficient computational scheme for ion dynamics in RF-field of Paul trap

Vladimir S. Melezhik<sup>1,2</sup><sup>1</sup> *Bogoliubov Laboratory of Theoretical Physics  
Joint Institute for Nuclear Research**6, Joliot-Curie St., Dubna, Moscow Region 141980, Russian Federation*<sup>2</sup> *Dubna State University**19, Universitetskaya St., Dubna, Moscow Region 141980, Russian Federation*

(received: December 23, 2019; accepted: December 30, 2019)

We have developed an efficient computational scheme for integration of the classical Hamilton equations describing the ion dynamics confined in the radio-frequency field of the Paul trap. It has permitted a quantitative treatment of cold atom-ion resonant collisions in hybrid atom-ion traps with taking into account unremovable ion micromotion caused by the radio-frequency fields (V.S. Melezhik et. al., Phys. Rev. A100, 063406 (2019)).

The important element of the hybrid atom-ion systems is the electromagnetic Paul trap confining the charged ion. The oscillating motion of the confined ion is defined by two frequencies of the Paul trap. It is the frequency of the order of 100 kHz due to the constant electric field and the radio-frequency of about 1–2 MHz defined by the alternating electromagnetic field of the ion trap. The necessity to accurately treat the ion motion in the combined field with two time scales defined by these two very different frequencies has demanded to develop the stable computational scheme for integration of the classical Hamilton equations for the ion motion. Moreover, the scheme must be stable on rather long time-interval of the ion collision with the cold atom  $\sim 10 \times 2\pi/\omega_a$  defined by the atomic trap frequency  $\omega_a \sim 10$  kHz and in the moment of the atom-ion collision when the Hamilton equations are strongly coupled. The developed numerical method takes into account all these features of the problem and makes it possible to integrate the system of coupled quantum-semiclassical equations with the necessary accuracy and quantitatively describes the processes of atomic-ion collisions in hybrid traps, including resonance effects.

**Key words and phrases:** cold atoms and ions, Paul trap, radio-frequency field, classical Hamilton equations, computational scheme

## 1. Introduction

In the last decade, there has been great interest in ultracold hybrid atomic-ion systems, which is due to the new opportunities that arise here for quantum

© Melezhik V. S., 2019



This work is licensed under a Creative Commons Attribution 4.0 International License

<http://creativecommons.org/licenses/by/4.0/>

simulation of various processes and effects from solid state physics to high-energy physics: electron-phonon coupling in solid state physics, critical phenomena in high-energy physics, quantum information processing etc. [1]. However, a realization of the hot proposals with cold atom and ions is impeded by the unremovable ion micromotion caused by the radio-frequency fields of the Paul traps used for confining ions in the hybrid confined atom-ion systems [1]. In the recent work [2] a quantum-semiclassical computational scheme for treating the collisional atom-ion dynamics in the confined geometry of the hybrid atom-ion traps was suggested where the ion micromotion caused by the radio-frequency fields of the ion trap was taken into account. In this work the following problem was considered: an ion confined in a time-dependent radio-frequency Paul trap with linear geometry, while the atom is constrained to move into a quasi-one-dimensional waveguide within the ion trap. In this approach the atom-ion dynamics was treated semiclassically, namely the atom dynamics is governed by the time-dependent Schrödinger equation, whereas the ion motion is described by the classical Hamilton equations of motion. Both equations were integrated simultaneously.

The quantum-semiclassical computational method [3]–[6] specifically designed for particle collisions such as the problem of ionisation of the helium ion colliding with protons [5] and antiprotons [6] has been employed and extended to the time-dependent domain, as the radio-frequency ionic confinement by the Paul trap requires. It has demanded to develop a new stable computational scheme for integration the classical Hamilton equations for the ion motion. Here, we describe the scheme and demonstrate its efficiency by using as an example of the specific Li/Yb<sup>+</sup> atom-ion pair, since it is the most promising atomic pair to reach the s-wave regime in Paul traps and it is currently under intense experimental investigations [7]–[9].

## 2. Method

A schematic view of the system under investigation is given in Figure 1. The ion is assumed to be confined in a linear Paul trap, whose electric fields read as [10]:

$$\begin{aligned}\mathbf{E}_s &= \frac{m_i}{2|e|} \omega_i^2 (x_i, y_i, -2z_i), \\ \mathbf{E}_{\text{rf}} &= \frac{m_i \Omega_{\text{rf}}^2 q}{2|e|} \cos(\Omega_{\text{rf}} t) (x_i, -y_i, 0).\end{aligned}\tag{1}$$

Here,  $m_i$  is the ion mass,  $\Omega_{\text{rf}}$  is the radio-frequency (rf),  $\omega_i = \Omega_{\text{rf}} \sqrt{a/2}$  is the secular frequency,  $q$  and  $a$  are dimensionless geometric parameters (i.e.  $q_z = 0$ ,  $q_y = -q_x \equiv q$ ,  $-a_z/2 = a_x = a_y \equiv a$ , and  $a \ll q^2 < 1$ ). We assume that the axis of the waveguide in which is travelling the colliding atom is precisely the  $z$ -axis of the Paul trap (see Figure 1). The corresponding ion-trap interaction potential is given by

$$U(\mathbf{r}_i, t) = \frac{m_i \omega_i^2}{2} \left( z_i^2 - \frac{x_i^2 + y_i^2}{2} \right) + \frac{m_i \Omega_{\text{rf}}^2 q}{2} \cos(\Omega_{\text{rf}} t) \left( \frac{y_i^2}{2} - \frac{x_i^2}{2} \right).\tag{2}$$

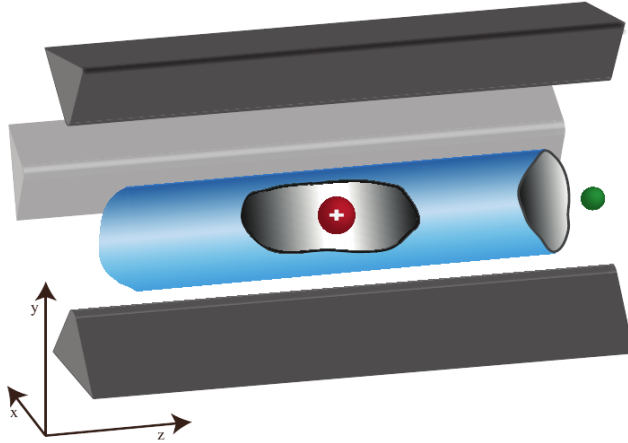


Figure 1. Pictorial illustration of the atom-ion system confined in hybrid trap. The light- and dark-grey electrodes (the big bars in the figure) of the Paul trap generate the time-dependent electric fields needed to confine the ion transversally, whereas longitudinally a static voltage is applied to ensure confinement (not shown). The atom is injected from the right to the left into a waveguide, whose centre hosts the ion. The waveguide is orientated along the longitudinal axis,  $z$ , of the linear Paul trap. In the transverse directions,  $x, y$ , the confining potential both for the atom and the ion is strong

Hence, the classical Hamiltonian describing an ion in a Paul trap is given by

$$H_i^{\text{trap}}(\mathbf{p}_i, \mathbf{r}_i, t) = \frac{\mathbf{p}_i^2}{2m_i} + U(\mathbf{r}_i, t). \quad (3)$$

When the atom is confined in the optical waveguide within the Paul trap, the ion experiences its presence via the atom-ion interaction  $V_{ai}(|\mathbf{r}_a - \mathbf{r}_i(t)|)$ , where  $\mathbf{r}_a$  defines the atom coordinates. The full classical ion Hamiltonian is therefore given by

$$H_i(\mathbf{p}_i, \mathbf{r}_i, t; \mathbf{r}_a) = H_i^{\text{trap}}(\mathbf{p}_i, \mathbf{r}_i, t) + \langle V_{ai}(|\mathbf{r}_a - \mathbf{r}_i(t)|) \rangle, \quad (4)$$

where

$$\langle V_{ai}(|\mathbf{r}_a - \mathbf{r}_i(t)|) \rangle = \langle \Psi(\mathbf{r}_a, t; \mathbf{r}_i) | V_{ai}(|\mathbf{r}_a - \mathbf{r}_i(t)|) | \Psi(\mathbf{r}_a, t; \mathbf{r}_i) \rangle \quad (5)$$

is the quantum mechanical average of the atom-ion interaction over the atomic density instantaneous distribution. We see that the ion Hamiltonian has parametric dependence on the atom position  $\mathbf{r}_a$ . It leads at the moment of the atom-ion collision to the strong non-separability of the Hamilton equations

$$\begin{aligned} \frac{d}{dt} \mathbf{p}_i &= -\frac{\partial}{\partial \mathbf{r}_i} H_i(\mathbf{p}_i, \mathbf{r}_i, t; \mathbf{r}_a), \\ \frac{d}{dt} \mathbf{r}_i &= \frac{\partial}{\partial \mathbf{p}_i} H_i(\mathbf{p}_i, \mathbf{r}_i, t; \mathbf{r}_a) \end{aligned} \quad (6)$$

describing the ion dynamics and, as a consequence, to the requirement of sufficient stability of the computational scheme to this strong perturbation.

The set of classical equations (6) together with the Schrödinger equation for the atomic wave function  $\Psi(\mathbf{r}_a, t, \mathbf{r}_i)$  form the complete set of dynamical equations for describing the confined atom-ion collision in hybrid traps [2]. In order to integrate simultaneously the equations we need proper initial conditions with physical significance. At the beginning of the collisional process, the atom and the ion are assumed to be far away from each other such that they do not interact ( $V_{ai} = 0$ ). In particular, the atom is initially in the ground state of the atomic trap with the longitudinal colliding energy, that is,  $E_{\text{coll}} \ll 2\hbar\omega_0$ , whereas the ion performs fast (with respect to atom motion) oscillations in the Paul trap with mean transversal  $\bar{E}_\perp$  and longitudinal  $\bar{E}_\parallel$  energies. Since the atom approaches the region of interaction with the ion very slowly ( $E_{\text{coll}}/\hbar \ll \omega_0 \ll \omega_i, \Omega_{\text{rf}}$ ), the initial position of the ion does not influence the scattering process itself, which depends only on  $\bar{E}_\perp$  and  $\bar{E}_\parallel$ . Specifically, the classical solution of the ion equations of motion (Mathieu equation) in the Paul trap (without the atom) are well approximated by  $A_j \cos(\omega_i t + \phi_j)[1 + q_j \cos(\Omega_{\text{rf}} t)/2]$ ,  $\forall j = x, y, z$  [11].

The associated kinetic energy depends on the amplitude  $A_j$ , but not on the phase  $\phi_j$ . Therefore, we choose, without loss of generality, the ion position at the initial time  $t = 0$  in the trap centre with transversal energy,  $E_\perp$ , and longitudinal energy,  $E_\parallel$ . This can be summarised with the following set of initial conditions:

$$\begin{aligned} \mathbf{r}_i(t = 0) &= (0, 0, 0), \\ p_{i,x}(t = 0) &= \sqrt{2m_i E_\perp}, \\ p_{i,y}(t = 0) &= 0, \\ p_{i,z}(t = 0) &= \sqrt{2m_i E_\parallel}. \end{aligned} \quad (7)$$

These initial conditions set the mean values of the ion transversal and longitudinal energies as  $\bar{E}_\perp = 1.64E_\perp$  (calculated numerically for our trap parameters  $\Omega_{\text{rf}} = 2\pi \times 2$  MHz,  $\omega_i = 2\pi \times 63$  kHz,  $a = 0.002$  and  $q = 0.08$ ) and  $\bar{E}_\parallel = E_\parallel/2$ , which is in qualitative agreement with the estimate

$$\bar{E}_\perp = \frac{E_\perp}{2} \left[ 1 + \left( \frac{q\Omega_{\text{rf}}}{2\omega_i} \right)^2 \right] \simeq 1.3E_\perp \quad (8)$$

from the first-order solution of the Mathieu equation [11], [12].

For the integration of the Hamilton equations of motion, which involve three considerably different scales of frequencies, namely  $\Omega_{\text{rf}}$ ,  $\omega_i$  as well as  $\omega_0$  in the quantum mechanical average  $\langle \Psi(\mathbf{r}_a, t; \mathbf{r}_i) | V_{ai}(|\hat{\mathbf{r}}_a - \mathbf{r}_i(t)|) | \Psi(\mathbf{r}_a, t; \mathbf{r}_i) \rangle$ , we employed the second-order Störmer–Verlet method [13].

Simultaneously to the forward in time propagation  $t_n \rightarrow t_{n+1} = t_n + \Delta t$  of the atom wave-packet  $\Psi_j(r_a, t_n) \rightarrow \Psi_j(r_a, t_{n+1})$  we integrate the Hamilton equations (6) with the initial conditions (7), which describe the dynamics of

the ion in the Paul trap. To this end, we have adapted the Störmer–Verlet method [13] to our problem

$$\begin{aligned} \mathbf{p}_i^{(n+1/2)} &= \mathbf{p}_i^{(n)} - \frac{\Delta t}{2} \frac{\partial}{\partial \mathbf{r}_i} H_i(\mathbf{p}_i^{(n+1/2)}, \mathbf{r}_i^{(n)}), \\ \mathbf{r}_i^{(n+1)} &= \mathbf{r}_i^{(n)} + \frac{\Delta t}{2} \left\{ \frac{\partial}{\partial \mathbf{r}_i} H_i(\mathbf{p}_i^{(n+1/2)}, \mathbf{r}_i^{(n)}) + \frac{\partial}{\partial \mathbf{r}_i} H_i(\mathbf{p}_i^{(n+1/2)}, \mathbf{r}_i^{(n+1)}) \right\}, \quad (9) \\ \mathbf{p}_i^{(n+1)} &= \mathbf{p}_i^{(n+1/2)} - \frac{\Delta t}{2} \frac{\partial}{\partial \mathbf{r}_i} H_i(\mathbf{p}_i^{(n+1/2)}, \mathbf{r}_i^{(n+1)}). \end{aligned}$$

Here,

$$\mathbf{p}_i^{(n)} = \mathbf{p}_i(t_n), \quad \mathbf{p}_i^{(n+1/2)} = \mathbf{p}_i\left(t_n + \frac{\Delta t}{2}\right), \quad \mathbf{p}_i^{(n+1)} = \mathbf{p}_i(t_n + \Delta t),$$

and the same definition for  $\mathbf{r}_i^{(n)}$ .

### 3. Numerical Example

The computational scheme (9) was successfully applied for numerical integration of the system of differential equations (6) with the initial conditions (7) for the Li/Yb<sup>+</sup> atom-ion systems confined in the hybrid traps with three absolutely different time-scales  $t_{\text{rf}} = 2\pi/\Omega_{\text{rf}} \ll t_i = 2\pi/\omega_i \ll t_0 = 2\pi/\omega_0$  defined by the frequencies of Paul trap ( $\Omega_{\text{rf}} = 2\pi \times 2$  MHz and  $\omega_i = 2\pi \times 63$  kHz) and atomic waveguide ( $\omega_0 = 2\pi \times 10$  kHz). These three time-scales define the demand to the computational scheme. The scheme must be stable in rather long time-interval (time of atom-ion collision)  $\sim 10t_0 = 10 \times 2\pi/\omega_0$  and, from the other side, it must accurately treats the fast oscillations defined by the frequency  $\Omega_{\text{rf}}$  of the rf-field.

In Figure 2 we present the calculated trajectory of the ion in the Paul trap ( $X_i$  variable) when there is no interaction with the atom:  $V_{ia} = 0$ . Here, the convergence over the step of integration on time  $\Delta t \rightarrow 0$  is demonstrated as well as the stability of the computational scheme over the entire integration interval  $0 \leq t \leq 10t_0$ . The efficiency of the computational scheme was confirmed by the calculation of the scattering parameters in the atom-ion resonant collisions confined in hybrid traps [2] and can be applied for other resonant low-dimensional atomic and atom-ion systems.

### Acknowledgments

The work was supported by the Grant of the Plenipotentiary Representative of the Republic of Kazakhstan to JINR.

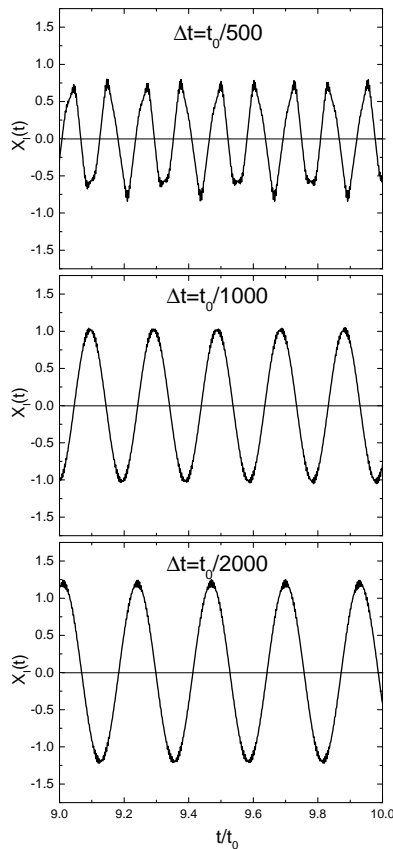


Figure 2. The calculated evolution in time of the ion trajectory ( $X_i(t)$ -variable), being initially at the state with  $E_{\perp}/k_B = E_{\parallel}/k_B = 4.25\mu\text{K}$ . The time scale is defined by the frequency  $t_0 = 2\pi/\omega_0$  of the atomic waveguide-like trap ( $\omega_0 = 2\pi \times 10$  kHz)

## References

- [1] M. Tomza, K. Jachymski, R. Gerritsma, A. Negretti, T. Calarco, Z. Idziaszek, and P. S. Julienne, “Cold hybrid ion-atom systems,” *Reviews of Modern Physics*, vol. 91, no. 3, p. 035 001, 2019. DOI: 10.1103/RevModPhys.91.035001.
- [2] V. S. Melezhik, Z. Idziaszek, and A. Negretti, “Impact of ion motion on atom-ion confinement-induced resonances in hybrid traps,” *Physical Review A*, vol. 100, no. 6, p. 063 406, 2019. DOI: 10.1103/PhysRevA.100.063406.
- [3] V. S. Melezhik and P. Schmelcher, “Quantum energy flow in atomic ions moving in magnetic fields,” *Physical Review Letters*, vol. 84, no. 9, pp. 1870–1873, 2000. DOI: 10.1103/physrevlett.84.1870.
- [4] V. S. Melezhik, “Recent progress in treatment of sticking and stripping with time-dependent approach,” *Hyperfine Interactions*, vol. 138, no. 1, pp. 351–354, 2001. DOI: 10.1023/A:1020833119205.

- [5] V. S. Melezhik, J. S. Cohen, and C.-Y. Hu, “Stripping and excitation in collisions between  $p$  and  $\text{He}^+(n \leq 3)$  calculated by a quantum time-dependent approach with semiclassical trajectories,” *Physical Review A*, vol. 69, no. 3, p. 032709, 2004. DOI: 10.1103/PhysRevA.69.032709.
- [6] V. S. Melezhik and L. A. Sevastianov, “Quantum-semiclassical calculation of transition probabilities in antiproton collisions with helium ions,” in *Analytical and Computational Methods in Probability Theory*, V. V. Rykov, N. D. Singpurwalla, and A. M. Zubkov, Eds., Cham: Springer International Publishing, 2017, pp. 449–460.
- [7] J. Joger, H. Frst, N. Ewald, T. Feldker, M. Tomza, and R. Gerritsma, “Observation of collisions between cold Li atoms and  $\text{Yb}^+$  ions,” *Physical Review A*, vol. 96, no. 3, 030703(R), 2017. DOI: 10.1103/physreva.96.030703.
- [8] H. Fürst, T. Feldker, N. V. Ewald, J. Joger, M. Tomza, and R. Gerritsma, “Dynamics of a single ion-spin impurity in a spin-polarized atomic bath,” *Physical Review A*, vol. 98, no. 1, p. 012713, 2018. DOI: 10.1103/physreva.98.012713.
- [9] T. Feldker, H. Fürst, H. Hirzler, N. V. Ewald, M. Mazzanti, D. Wiater, M. Tomza, and R. Gerritsma, “Buffer gas cooling of a trapped ion to the quantum regime,” 2019. arXiv: 1907.10926 [quant-ph].
- [10] D. Leibfried, R. Blatt, C. Monroe, and D. Wineland, “Quantum dynamics of single trapped ions,” *Reviews of Modern Physics*, vol. 75, pp. 281–324, 2003. DOI: 10.1103/RevModPhys.75.281.
- [11] D. J. Berkeland, J. D. Miller, J. C. Bergquist, W. M. Itano, and D. J. Wineland, “Minimization of ion micromotion in a Paul trap,” *Journal of Applied Physics*, vol. 83, no. 10, pp. 5025–5033, 1998. DOI: 10.1063/1.367318.
- [12] L. D. Landau and E. M. Lifshitz, *Mechanics*. New York: Pergamon, 1976, pp. 93–95, 93–95.
- [13] E. Hairer, C. Lubich, and G. Wanner, *Geometric numerical integration. Structure-preserving algorithms for ordinary differential equations*. Berlin, Heidelberg: Springer, 2006, ch. I.

#### For citation:

V. S. Melezhik, Efficient computational scheme for ion dynamics in RF-field of Paul trap, *Discrete and Continuous Models and Applied Computational Science* 27 (4) (2019) 378–385. DOI: 10.22363/2658-4670-2019-27-4-378-385.

#### Information about the authors:

**Vladimir S. Melezhik** — Doctor of Physical and Mathematical Sciences, Leading Researcher of Bogoliubov Laboratory of Theoretical Physics, Joint Institute for Nuclear Research; professor of Dubna State University (e-mail: melezhik@theor.jinr.ru, phone: +7 (49621)63615, ORCID: <https://orcid.org/0000-0002-1184-7544>, ResearcherID: F-6260-2012, Scopus Author ID: 7005803269)

PACS 07.05.Tr

DOI: 10.22363/2658-4670-2019-27-4-378-385

## Эффективная вычислительная схема для описания динамики иона в радиочастотном поле ловушки Пауля

В. С. Мележик<sup>1,2</sup>

<sup>1</sup> *Объединённый институт ядерных исследований*

*ул. Жолио Кюри, д. 6, г. Дубна, Московская область, 141980, Россия*

<sup>2</sup> *Государственный университет «Дубна»*

*ул. Университетская, д. 19, г. Дубна, Московская область, 141980, Россия*

В статье разработана эффективная вычислительная схема для интегрирования классических уравнений Гамильтона, описывающих динамику ионов пленённых радиочастотным полем ловушки Пауля. Она позволила провести количественные расчёты резонансных атомно-ионных столкновений в гибридных атомно-ионных ловушках с учётом неустранимого микродвижения ионов, вызванного радиочастотными полями (V.S. Melezhik et. al., Phys. Rev. A100, 063406 (2019)).

Важным элементом гибридных атомно-ионных систем является электромагнитная ловушка Пауля, удерживающая заряженный ион. Колебательное движение пленённого иона определяется двумя частотами ловушки Пауля. Это частота порядка 100 кГц из-за постоянного электрического поля и радиочастоты 1–2 МГц определяется переменным электромагнитным полем ионной ловушки. Необходимость точного описания движения ионов в комбинированном поле с двумя временными шкалами, задаваемыми двумя сильно различающимися частотами, потребовала разработки устойчивой вычислительной схемы для интегрирования классических уравнений (Гамильтона) движения ионов. Кроме того, требуется устойчивость схемы на достаточно большом интервале времени столкновения иона с холодным атомом  $\sim 10 \times 2\pi/\omega_a$ , определяемом частотой атомной ловушки  $\omega_a \sim 10$  кГц, и в сам момент столкновения атома с ионом при сильной связи уравнений Гамильтона. Разработанный численный метод учитывает все отмеченные особенности задачи и позволяет с необходимой точностью интегрировать систему связанных квантово-квазиклассических уравнений и количественно описывать процессы атомно-ионных столкновений в гибридных ловушках, включая резонансные эффекты.

**Ключевые слова:** холодные атомы и ионы, ловушка Пауля, радиочастотное поле, классические уравнения Гамильтона, вычислительная схема